

INVESTIGATIONS OF Pincer Iridium Complexes for Glycerol Deoxygenation  
and for Alkane Dehydrogenation

Byongjoo Bark

A DISSERTATION

in

Chemistry

Presented to the Faculties of the University of Pennsylvania

in

Partial Fulfillment of the Requirements for the

Degree of Doctor of Philosophy

2022

Supervisor of Dissertation

*Karen Goldberg*

Karen I. Goldberg

Vagelos Professor of Energy Research

Graduate Group Chairperson

*David Mindiola*

Daniel J. Mindiola, Brush Family Professor of Chemistry

Dissertation Committee

Eric J. Schelter, Professor of Chemistry

Daniel J. Mindiola, Brush Family Professor of Chemistry

Donald H. Berry, Professor of Chemistry

INVESTIGATIONS OF Pincer Iridium Complexes for Glycerol Deoxygenation  
and for Alkane Dehydrogenation

COPYRIGHT

2022

Byongjoo Bark

## ACKNOWLEDGEMENTS

I would like to thank everyone who helped me get to where I am today. Without your support and encouragement, I would not have made it this far. I am so blessed that I met you.

Thank you to my advisor, Karen Goldberg, for your guidance and wisdom over the past six years. Your enthusiasm for chemistry motivates me continuously. Your thought-provoking questions and attention to detail taught me to be a better scientist. I am glad that I joined your group.

I would like to thank Mike Heinekey for mentoring me with Karen at the University of Washington. I would also like to thank Jeffrey Johnson at Hope College and Nathaniel Szymczak at the University of Michigan for welcoming me to their labs and showing me exciting areas of chemistry.

To former and current members of the Goldberg and Heinekey groups, thank you so much for helping me. When I was stuck, you were always willing to discuss chemistry and suggest new ideas to me. Thank you to Jon Goldberg, Travis Lekich, and Louise Guard for training me when I first started in the group. To the Dawg Pound Gang, Sophie, Alex, and Hannah, from taking classes and joining the lab together to today, you made this journey so wonderful. It was so much fun to hang out with you in and outside the lab.

To Dale, Sarah, Abbie, and Anna, thank you for welcoming me into the family. You truly became my family. Even after I graduated from high school, you still welcomed me whenever I visited. Your support, encouragement, and prayers gave me comfort when I was stressed. I am so grateful for your family.

To my family, thank you for giving me an opportunity to study abroad. Thank you for supporting me throughout my education in the US. Your encouragement, belief, and prayers gave a strong foundation and made me a confident individual. Thank you and I love you.

“I can do everything through him who gives me strength.”

-Philippians 4:13

## ABSTRACT

### INVESTIGATIONS OF Pincer Iridium Complexes for Glycerol Deoxygenation and for Alkane Dehydrogenation

Byongjoo Bark

Karen I. Goldberg

Green chemistry is being paid increased attention with the growing awareness of the environmental impact of the chemical industry. Catalysis is important in the development of green processes as it reduces the waste that is generated and lowers the energy required. Abundant feedstocks such as natural gas or biomass can be catalytically converted to value-added chemicals. Catalysts are employed in a wide range of applications, and innovations in green catalysis are crucial to achieve sustainability. To reduce the dependency on the unsustainable petroleum feedstock, biodiesel has been recognized as an effective, sustainable alternative. During biodiesel production, by-product glycerol is generated in a large amount. Catalyst development for the deoxygenation of low-cost glycerol to value-added 1,3-propanediol is discussed in Chapter 2.

Alkane dehydrogenation to olefin is energy-intensive due to the endothermic nature of the reaction. A selective, energy-efficient catalyst is essential for sustainability. Immobilization of a homogeneous catalysts on heterogeneous supports can provide active, selective catalysts with robustness and recyclability. The immobilization enables the implementation of gas-phase continuous-flow reaction design. In the flow system, the by-product  $H_2$  can be effectively removed to achieve higher TON. Chapter 3 demonstrates catalytic dehydrogenation and hydrogenation reactions by an immobilized (POCOP)Ir complex on silica. Since homogeneous (Phebox)Ir and (CCC)Ir complexes have been demonstrated to activate C-H bonds, immobilization of those complexes on silica were attempted. The synthesis of Phebox and CCC ligands with functional groups to allow immobilization to silica are outlined in Chapter 4.

## Table of Contents

Acknowledgements .....	iii
Abstract .....	iv
Table of Contents .....	v
List of Tables .....	vi
List of Figures .....	vii
List of Schemes .....	viii
Chapter 1: Introduction .....	1
1.1 Introduction .....	1
1.2 References .....	4
Chapter 2: Glycerol Deoxygenation by (POCOP)Ir(CO) Complexes .....	5
2.1 Introduction .....	5
2.2 Synthesis and Reactivity of ( <sup>t</sup> BuPOCOP)Ir(CO) Complexes .....	11
2.3 Deoxygenation of Glycerol .....	15
2.4 Conclusions .....	24
2.5 Experimental .....	25
2.6 References .....	31
Chapter 3: Investigations of Immobilized ( <sup>t</sup> BuPOCOP)Ir(CO) as a Catalyst for Dehydrogenation and Hydrogenation Reactions .....	34
3.1 Introduction .....	34
3.2 (De)Hydrogenation Reactions by Immobilized ( <sup>t</sup> BuPOCOP)Ir(CO) .....	41
3.3 Conclusion .....	48
3.4 Experimental .....	50
3.5 References .....	53
Chapter 4: Functionalization of Phebox and CCC Ligands for Immobilization on Silica .....	57
4.1 Introduction .....	57
4.2 Synthesis and Functionalization of Phebox Ligands .....	62
4.3 Synthesis and Functionalization of CCC Ligands and CCC(Ir) Complexes .....	66
4.4 Conclusion .....	71
4.5 Experimental .....	72
4.6 References .....	79
Appendix A: Crystallographic Information .....	83
References .....	98
Bibliography .....	99

## List of Tables

Table 2-1. Glycerol deoxygenation reactions with different Ir complexes. <sup>a</sup> .....	15
Table 2-2. Glycerol deoxygenation with varying Ir complexes and acid concentrations. <sup>a</sup> .....	18
Table 2-3. Glycerol deoxygenation with varying solvent volumes and water concentrations. <sup>a</sup> .....	19
Table 2-4. Control reactions using the deoxygenated products as substrates. <sup>a</sup> .....	21
Table 2-5. Examination for possible Ir nanoparticles. <sup>a</sup> .....	22

## List of Figures

Figure 2-1. Polytrimethylene terephthalate (PTT).....	6
Figure 2-2. Ir complexes for electrocatalytic reduction of CO <sub>2</sub> . <sup>37</sup> .....	12
Figure 2-3. Stacked <sup>31</sup> P{ <sup>1</sup> H} NMR spectra of the protonation of <b>9</b> with sequential addition of acids in CD <sub>2</sub> Cl <sub>2</sub> . .....	14
Figure 2-4. Ir complexes with different alkyl groups used for alkane dehydrogenation.....	23
Figure 2-5. Proposed Ir complex for future study. ....	24
Figure 2-6. Photos of the HEL reactor assembly. A: reactor bottom, glass liner equipped with a spin vane, and gas-diffusing PTFE cap. B: gas-diffusing PTFE cap. C: reactor top. ....	28
Figure 2-7. Representative <sup>13</sup> C{ <sup>1</sup> H} NMR from deoxygenation of glycerol. ....	30
Figure 3-1. Ir Pincer complexes examined for (transfer) dehydrogenation of alkanes.....	35
Figure 3-2. Propane dehydrogenation by <b>23-SiO<sub>2</sub></b> with mesoporous silica (left) or amorphous silica (right). Conditions: V <sub>total</sub> = 20 mL/min <sup>-1</sup> , P <sub>propane</sub> = 0.25 atm, P <sub>He</sub> = 0.75 atm, P <sub>total</sub> = 1 atm, Temp = 280 – 520 °C (green line).....	43
Figure 3-3. Toluene hydrogenation by <b>23-SiO<sub>2</sub></b> (Red) and <b>IrO<sub>x</sub>-SiO<sub>2</sub></b> (Black). Conditions: 1 bar (3% toluene, 97% H <sub>2</sub> ); preheated under He flow at 340 °C prior to reaction. ....	44
Figure 3-4. MO hydrogenation by <b>23-SiO<sub>2</sub></b> and <b>IrO<sub>x</sub>-SiO<sub>2</sub></b> to MIBK. Conditions: 1 bar (5% MO, 95% H <sub>2</sub> ); preheated under He flow at 340 °C prior to reaction. ....	46
Figure 3-5. MO hydrogenation to MIBK with added water. Conditions: 1 bar (5% MO, 95% H <sub>2</sub> ), Pretreated at RT (No H <sub>2</sub> O); 1 bar (5% MO, 5% H <sub>2</sub> O, 90% H <sub>2</sub> ), Pretreated with 5% H <sub>2</sub> O at 150 °C (5% H <sub>2</sub> O); 1 bar (5% MO, 20% H <sub>2</sub> O, 75% H <sub>2</sub> ), Pretreated with 20% H <sub>2</sub> O at 150 °C (20% H <sub>2</sub> O). .	47
Figure 3-6. MO hydrogenation to MIBK catalyzed by neutral <b>23-SiO<sub>2</sub></b> (Light Blue) or acid-treated <b>23-SiO<sub>2</sub></b> (Dark Blue). Conditions: 1 bar (5% MO, 95% H <sub>2</sub> ), Pretreated at RT. ....	49
Figure 4-1. <sup>1</sup> H NMR spectrum of <sup>5</sup> -BrPhebox in CDCl <sub>3</sub> . ....	64
Figure 4-2. Desilylation reaction progress of <b>31</b> monitored by <sup>1</sup> H NMR. ....	70
Figure 4-3. <sup>1</sup> H NMR spectrum in CDCl <sub>3</sub> of white ppt from desilylation reaction. Residual TBAF denoted with *. ....	71

## List of Schemes

Scheme 2-1. Transesterification of triglyceride.....	5
Scheme 2-2. Potential commodity chemicals derived from glycerol via various transformations. ....	6
Scheme 2-3. Traditional production of 1,3-propanediol through hydration of acrolein (top) and hydroformylation of ethylene oxide (bottom).....	7
Scheme 2-4. Two-step process of conversion of glycerol to 1,3-propanediol.....	7
Scheme 2-5. 1,2-Propanediol deoxygenation reaction.....	9
Scheme 2-6. Proposed water-assisted hydrogen addition to complex <b>2</b> .....	9
Scheme 2-7. Glycerol deoxygenation reaction. ....	10
Scheme 2-8. Proposed mechanism of glycerol deoxygenation with $(^t\text{BuPOCOP})\text{Ir}(\text{CO})$ . ....	11
Scheme 2-9. Synthesis of complex <b>9</b> and <b>10</b> .....	12
Scheme 2-10. Sequential addition of acids to complex <b>9</b> . ....	14
Scheme 2-11. Glycerol deoxygenation reaction. ....	15
Scheme 2-12. Potential side products formed by dehydration, condensation, and hydrogenation. Reproduced from Ref. 20 with permission from the Royal Society of Chemistry. ....	16
Scheme 2-13. Hydrogen addition to pincer-ligated Ir complexes. ....	24
Scheme 3-1. Catalytic transfer dehydrogenation of cyclooctane. ....	35
Scheme 3-2. Acceptorless dehydrogenation of cyclodecane. ....	36
Scheme 3-3. Pd-catalyzed allylation of ethyl acetoacetate with DBU. ....	39
Scheme 3-4. Cu-catalyzed cyclohexane oxidation. ....	39
Scheme 3-5. Immobilization of $(^t\text{BuPOCOP})\text{Ir}$ via the ligand backbone (Top) or the metal center (Bottom). ....	41
Scheme 3-6. Immobilization of $(^t\text{BuPOCOP})\text{Ir}(\text{CO})$ by oxidative addition of surface silanol.....	42
Scheme 3-7. Selective hydrogenation of MO. ....	45
Scheme 3-8 A: Outer-sphere ionic hydrogenation mechanism; B: Inner-sphere oxidative addition mechanism.....	46
Scheme 3-9. Hydrogenation of carbonyl substrates.....	48
Scheme 4-1. Transfer or acceptorless alkane dehydrogenation via oxidative addition mechanism. ....	58
Scheme 4-2. Stepwise <i>n</i> -octane dehydrogenation with O <sub>2</sub> as the hydrogen acceptor.....	59
Scheme 4-3. Transfer and acceptorless dehydrogenation of cyclooctane by $(\text{CCC}^{\text{Mes}})\text{Ir}(\text{H})(\text{Cl})$ ( <b>27</b> ).....	60
Scheme 4-4. <i>n</i> -Octane activation by $(\text{CCC})\text{Ir}(\text{OAc})_2$ and $(\text{Phebox})\text{Ir}(\text{OAc})_2$ .....	61
Scheme 4-5. Silylation of 2-( <i>o</i> -tolyl)oxazoline. <sup>108, 109</sup> .....	62
Scheme 4-6. Proposed synthetic plan to functionalize <sup>dm</sup> Phebox with trialkoxysilane. ....	62

Scheme 4-7. Reactivity of Phebox with different lithium reagents. <sup>113</sup> .....	63
Scheme 4-8. Substitution of <sup>4</sup> -BrPhebox. <sup>114</sup> .....	63
Scheme 4-9. Synthesis of bromine-substituted Phebox ligands. ....	64
Scheme 4-10. Functionalization of <sup>Br</sup> Phebox with trimethoxysilane. ....	65
Scheme 4-11. Potential dehydrohalogenation of 3-iodopropyltrimethoxysilane.....	66
Scheme 4-12. Synthesis of <sup>Br</sup> CCC precursor. <sup>121, 122</sup> .....	67
Scheme 4-13. Synthesis of alkyne-functionalized CCC <sup>Me</sup> ligands.....	68
Scheme 4-14. Metalation of <sup>alkyne</sup> CCC <sup>Me</sup> ligand with [Ir( $\mu$ -OMe)(COD)] <sub>2</sub> and synthesis of Ir(OAc) <sub>2</sub> complex.....	69

# Chapter 1: Introduction

## 1.1 Introduction

The modern world has undoubtedly benefited from the growth and advancement of the chemical industry. Chemical products can be found in many different areas of life from clothing to food additives, to electronic devices. The expansion of the chemical industry has also resulted in negative impacts on humans and the environment. Some chemical processes generate toxic waste and leave soil, water, and air polluted. In response to the negative consequences of such chemical processes, the chemistry field has accepted the idea of Green Chemistry. Green chemistry focuses on the prevention of any hazardous impact on human health and the environment by carefully planning, with the goal of sustainability.<sup>1</sup> The following are the twelve principles of green chemistry, introduced by Anastas and Werner in 1998, as design criteria or guidelines, to provide a framework for green chemistry design:<sup>1</sup>

1. Waste prevention
2. Atom economy
3. Less hazardous chemical synthesis
4. Designing safer chemicals
5. Safer solvents and auxiliaries
6. Design for energy efficiency
7. Use of renewable feedstocks
8. Reduce derivatives
9. Catalysis
10. Design for degradation
11. Real-time analysis for pollution prevention
12. Inherently safer chemistry for accident prevention

The design of a process that fulfills all twelve criteria is not trivial. However, a catalytic process may meet several criteria by avoiding the use of stoichiometric amounts of reagents, restricting the waste generated, and lowering the energy required for a transformation. A selective catalyst may avoid sequential reaction steps, minimizing derivatization. Moreover, catalysis may be key in promoting some very challenging chemical transformations such as the partial oxidation of methane or the selective reduction of carbon dioxide. Innovations in catalysis are essential to achieve sustainability.

As a society, we are highly dependent on fossil feedstocks for energy, with 79% of total US energy production in 2020 being derived from fossil fuels.<sup>2</sup> To reduce the dependency on unsustainable petroleum feedstock, biodiesel has been recognized as an effective alternative. Biodiesel is made from renewable feedstocks such as vegetable oil and animal fat.<sup>3</sup> The use of renewable feedstock is in accordance with green chemistry principles, but a major concern for biodiesel industry is the major byproduct of biodiesel production, glycerol, generated in 10 wt%.<sup>4</sup> The increase in biodiesel production provides enough glycerol to saturate the market demand.<sup>5</sup> The excess glycerol is now considered waste and becomes a financial and environmental burden. It is critical to develop new technologies to utilize the excess glycerol for sustainability and economic viability of the biodiesel industry. One of the attractive chemical transformations of glycerol is a selective deoxygenation to 1,3-propanediol. 1,3-propanediol is mainly used in the production of polytrimethylene terephthalate polymer, and the market for 1,3-propanediol is expected to reach over \$600 million by 2021.<sup>6</sup> Chapter 2 describes the synthesis and characterization of a new pincer (POCOP)Ir(CO) catalyst that can be used to convert glycerol to 1,3-propanediol. The activity of this catalyst is compared to related known catalysts, and investigations to understand and improve the observed poor mass balance in glycerol deoxygenation reactions are presented.

Olefins are essential chemical building blocks used to make a wide variety of commodity chemicals. The development of shale fracking has made light alkanes (C<sub>1</sub>-C<sub>4</sub>) more available. Catalytic dehydrogenation processes of these alkanes have been implemented industrially to make

light olefins.<sup>7</sup> Due to the inert nature of alkanes, these cracking processes are carried out at high temperatures. At those temperatures, unwanted coke formation is favored and leads to catalyst deactivation and low selectivities.<sup>8</sup> A selective, energy-efficient catalytic system is desired to make olefin production greener and more sustainable.

Promising alkane dehydrogenations have been demonstrated with homogeneous, transition-metal catalysts at milder temperatures,<sup>9</sup> but their activities were too low to be industrially relevant.<sup>10</sup> Homogeneous catalysts generally exhibit better activity and selectivity, whereas product separation and catalyst recycle are advantageous aspects of heterogeneous catalysis. Homogeneous and heterogeneous catalysis each fulfill some green chemistry criteria, but a combination of the advantageous features of both homogeneous and heterogeneous catalysis has the potential to result in a novel catalytic system that better accommodates the principles of green chemistry. This new catalyst system may be achieved by immobilizing a homogeneous catalyst on a heterogeneous support. The immobilization enables the implementation of gas-phase continuous-flow reaction design. In the flow system, the by-product H<sub>2</sub> can be effectively removed to achieve higher TON. Chapter 3 describes the investigations of the immobilized (POCOP)Ir(CO) complex as a catalyst for dehydrogenation and hydrogenation reactions in gas-phase flow conditions.

Alkane dehydrogenation is not thermodynamically favored due to the endothermic nature of the reaction. The utilization of a hydrogen acceptor such as a sacrificial olefin may overcome the unfavorable thermodynamics, but this action results in poor atom economy and waste. Instead of sacrificial olefins, cofeeding of molecular oxygen as a hydrogen acceptor makes the reaction thermodynamically favorable, reduces coke deposition, and generates environmentally benign H<sub>2</sub>O as the byproduct. Our group has demonstrated the activation of the C-H bond of alkanes by (Phebox)Ir(OAc)<sub>2</sub>(OH<sub>2</sub>) and (CCC)Ir(OAc)<sub>2</sub>(OH<sub>2</sub>) via a concerted metalation deprotonation mechanism. A β-hydride elimination reaction then releases olefin and forms an Ir-hydride complex. Stoichiometric reaction of the Ir-hydride with O<sub>2</sub> and acetic acid regenerates the Ir-bisacetate complex that activates alkane, suggesting that there is the potential to use molecular oxygen as a

hydrogen acceptor in a catalytic system. Chapter 4 discusses the attempted functionalization of Phebox and CCC ligand and their Ir complexes to allow for their immobilization on a solid support.

## 1.2 References

1. Anastas, P.; Eghbali, N., Green Chemistry: Principles and Practice. *Chem. Soc. Rev.* **2010**, 39 (1), 301-312.
2. Energy Information Administration U.S. energy facts explained. <https://www.eia.gov/energyexplained/us-energy-facts/> (accessed Dec 19, 2021).
3. Quispe, C. A. G.; Coronado, C. J. R.; Carvalho Jr, J. A., Glycerol: Production, consumption, prices, characterization and new trends in combustion. *Renew. Sustain. Energy Rev.* **2013**, 27, 475-493.
4. Johnson, D. T.; Taconi, K. A., The glycerin glut: Options for the value-added conversion of crude glycerol resulting from biodiesel production. *Environ. Prog.* **2007**, 26 (4), 338-348.
5. Anitha, M.; Kamarudin, S. K.; Kofli, N. T., The potential of glycerol as a value-added commodity. *Chem. Eng. J.* **2016**, 295, 119-130.
6. Vivek, N.; Pandey, A.; Binod, P., Production and Applications of 1,3-Propanediol. In *Curr. Dev. Biotechnol. Bioeng.: Prod., Isol. Purif. Ind. Prod.*, 2017; pp 719-738.
7. Sattler, J. J. H. B.; Ruiz-Martinez, J.; Santillan-Jimenez, E.; Weckhuysen, B. M., Catalytic Dehydrogenation of Light Alkanes on Metals and Metal Oxides. *Chem. Rev.* **2014**, 114 (20), 10613-10653.
8. Dong, S.; Altvater, N. R.; Mark, L. O.; Hermans, I., Assessment and comparison of ordered & non-ordered supported metal oxide catalysts for upgrading propane to propylene. *Appl. Catal. A* **2021**, 617, 118121.
9. Kumar, A.; Bhatti, T. M.; Goldman, A. S., Dehydrogenation of Alkanes and Aliphatic Groups by Pincer-Ligated Metal Complexes. *Chem. Rev.* **2017**, 117 (19), 12357-12384.
10. Kozuch, S.; Martin, J. M. L., "Turning Over" Definitions in Catalytic Cycles. *ACS Catal.* **2012**, 2 (12), 2787-2794.

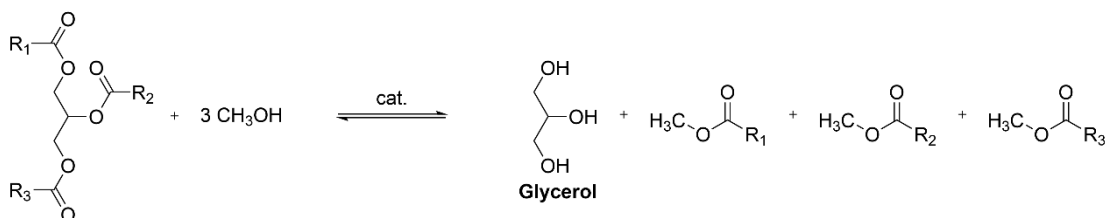
# Chapter 2: Glycerol Deoxygenation by (POCOP)Ir(CO) Complexes

## 2.1 Introduction

### 2.1.1 Glycerol as Chemical Feedstock

Alternative energy sources are being sought to replace traditional petroleum fuels. Biodiesel is an attractive alternate fuel because it can be easily obtained through transesterification of triglycerides (Scheme 2-1), which themselves can be obtained from various feedstocks such as vegetable oil and animal fat.<sup>3</sup> Biodiesel can also be directly used in conventional diesel engines with limited modifications and without loss in engine performance.<sup>4</sup> The biodiesel industry has grown rapidly over the last decade with an anticipated worldwide production of 40 billion liters annually.<sup>11</sup> One major concern in the biodiesel industry is the by-product, glycerol, generated in 10 wt% during biodiesel production. Although glycerol is used in cosmetics, food additives, and pharmaceuticals, the increasing supply has saturated the market demand and caused a significant drop in the price of crude glycerol.<sup>5</sup> For the biodiesel industry to be both sustainable *and* economically viable, it is critical to develop new technologies to use or functionalize glycerol.

**Scheme 2-1. Transesterification of triglyceride.**

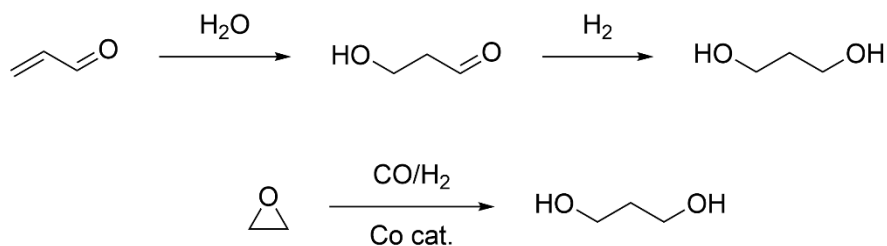


### 2.1.2 Glycerol to 1,3-Propanediol

Numerous chemicals can be derived from glycerol and used in a wide range of applications. In fact, glycerol has been identified as one of the top twelve platform chemicals



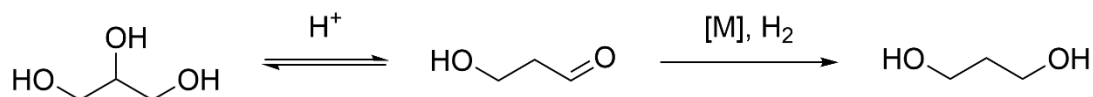
**Scheme 2-3. Traditional production of 1,3-propanediol through hydration of acrolein (top) and hydroformylation of ethylene oxide (bottom).**



(Scheme 2-3).<sup>13</sup> Since these two processes are both based on petroleum feedstocks, an alternative pathway was sought using renewable resources. Dupont and Genencor International, Inc. genetically modified *E. coli* to produce 1,3-PD through fermentation of glucose and successfully commercialized this process.<sup>14</sup> Glycerol can be an alternative renewable feedstock for 1,3-PD. In addition, the utilization of surplus glycerol from the biodiesel industry for 1,3-PD production would increase the economic incentive for biodiesel production.

While the conversion of glycerol to 1,3-PD using natural or modified bacterial species has been developed, this process suffers from several major drawbacks including: the formation of byproducts, inhibition at high substrates/products concentration, the requirement of expensive coenzyme vitamin B<sub>12</sub>, and potential pathogenicity.<sup>15-19</sup> We are interested in homogeneous transition-metal catalysts for this transformation due to their robust nature and their ability to be easily modified to achieve optimal rates and selectivities. Schlaf envisioned that the selective deoxygenation of glycerol can be achieved via a dehydration-hydrogenation process. An acid-catalyzed dehydration of glycerol is followed by transition-metal catalyzed hydrogenation to produce 1,3-PD (Scheme 2-4).<sup>20</sup> This strategy requires an efficient, selective hydrogenation catalyst that is stable to water and acid.

**Scheme 2-4. Two-step process of conversion of glycerol to 1,3-propanediol.**

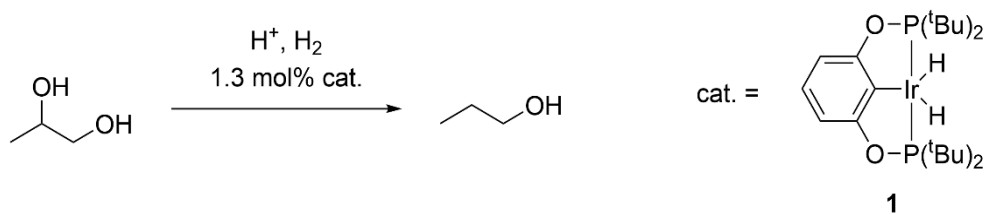


### 2.1.3 Catalytic Conversion of Glycerol to 1,3-Propanediol

The catalytic conversion of glycerol to 1,3-PD has been achieved using both heterogeneous and homogeneous catalysts. There are many heterogeneous catalysts with transition metals such as Pt, Pd, Ir, Ru, Cu, and Ni (both monometallic and bimetallic) which have been used for the conversion of glycerol to 1,3-PD.<sup>21</sup> The most active and selective heterogeneous systems for 1,3-PD production use Pt nanoparticles supported on  $WO_x$  boehmite materials and achieved 66% yield of 1,3-PD along with the formation of 1,2-propanediol (1,2-PD, 2%), 1-propanol (1-PO, 11%), and 2-propanol (6%).<sup>22</sup>

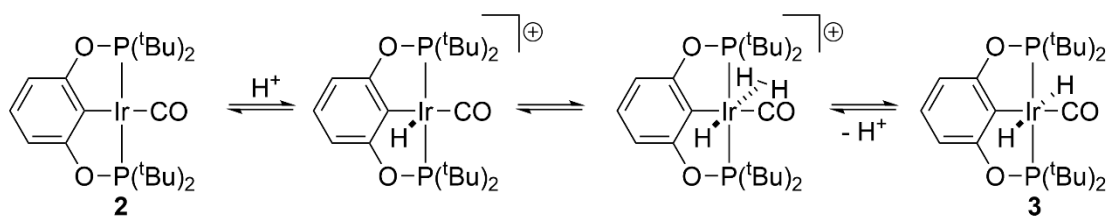
There are also several examples of homogeneous systems that catalyze the deoxygenation of glycerol or 1,2-PD, a model substrate for glycerol. Che reported an early example of glycerol deoxygenation yielding 21% 1,3-PD along with 23% 1,2-PD and 3.6% 1-PO using  $Rh(CO)_2(acac)_2$  and  $H_2WO_4$  as the catalysts.<sup>23</sup> This study achieved a moderate yield and selectivity for 1,3-PD. Drent and Jager used  $Pd(OAc)_2$ , 1,2-bis(1,5-cyclooctylenephosphino)ethane, and methanesulfonic acid for glycerol deoxygenation and converted 7.4% of the glycerol with product selectivity of 31% 1,3-PD, 22% 1,2-PD, and 47% of 1-PO using  $Pd(OAc)_2$ , 1,2-bis(1,5-cyclooctylenephosphino)ethane, and methanesulfonic acid.<sup>24</sup> Braca reported a system using  $Ru(CO)_4I_2$  and HI to deoxygenate neat glycerol producing 1,3-PD in 9.8% selectivity while 1-PO and its ether derivatives were produced with high selectivity (70%). Diluting glycerol with water increased selectivity for 1-PO and its ether derivatives to >90%.<sup>25</sup> Furthermore, Schlaf examined several Ru complexes for glycerol deoxygenation reactions, but analysis of the reaction mixture revealed no 1,3-PD formation under various conditions investigated.<sup>26-28</sup> While these examples provide insight into the glycerol deoxygenation reactions, catalysts that enable high selectivity for 1,3-PD remain elusive.

**Scheme 2-5. 1,2-Propanediol deoxygenation reaction.**



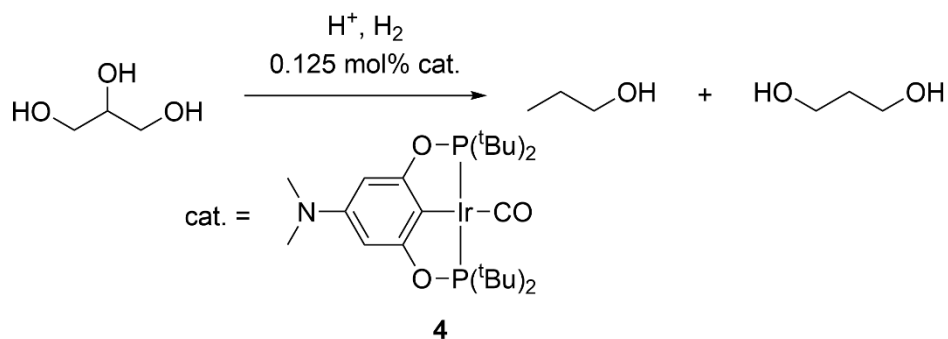
Previously, the Goldberg and Heinekey groups examined iridium pincer complexes for the deoxygenation of glycerol. First the deoxygenation of 1,2-PD, a model substrate for glycerol, was examined using  $(\text{tBuPOCOP})\text{Ir}(\text{H})_2$  (**1**) ( $\text{R}^{\text{tBuPOCOP}} = \kappa^3\text{-C}_6\text{H}_3\text{-2,6-(OPR}_2)_2$ ) and triflic acid (Scheme 2-5).<sup>29</sup> This iridium pincer complex is thermally stable<sup>30</sup> and known to be active for transfer dehydrogenation of cyclooctane.<sup>31</sup> Using **1** as the catalyst, 1,2-PD was successfully converted to 1-PO and its ether derivative in 95% yield using aqueous *p*-dioxane as solvent at low acid concentrations. After the reaction, two Ir species were identified:  $(\text{tBuPOCOP})\text{Ir}(\text{CO})$  (**2**) and  $(\text{tBuPOCOP})\text{Ir}(\text{CO})(\text{H})_2$  (**3**). Complex **2** is also active for deoxygenation and is air- and water-stable, while complex **1** decomposes in air. Complex **2** was proposed to be generated by decarbonylation of the aldehyde intermediate. A water-assisted oxidative addition of hydrogen to complex **2** then generates complex **3** (Scheme 2-6). Separate experiments verified that acid addition to **2** led to the formation of **3** under  $\text{H}_2$  atmosphere.

**Scheme 2-6. Proposed water-assisted hydrogen addition to complex 2.**



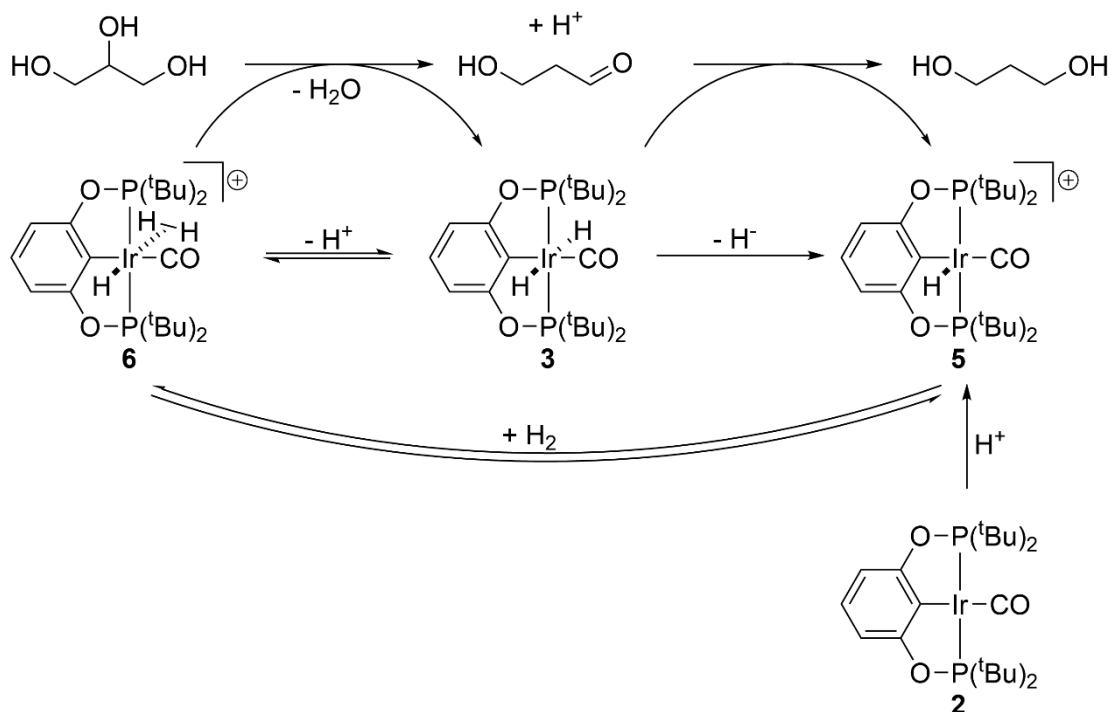
Subsequent work from Goldberg and Heinekey demonstrated that the same catalyst system converted glycerol to 1-PO and 1,3-PD (Scheme 2-7).<sup>32</sup> A dimethylamino group was introduced into the *para* position of the aryl backbone of  $(\text{tBuPOCOP})\text{Ir}(\text{CO})$  complex (**4**) to increase the solubility in the aqueous dioxane media. Using 1 mol% sulfuric acid (relative to glycerol) and

**Scheme 2-7. Glycerol deoxygenation reaction.**



complex **4**, 45% conversion to 1-PO and 1,3-PD in 4:1 ratio was observed after 48 h. To study the effect of acid, the glycerol deoxygenation reactions were carried out with **4** and increasing acid concentration from 0.25% to 4.0% (relative to glycerol), and the results after 24 h showed that ratio of 1-PO: 1,3-PD increased from 1:2 to 4:1 with the increased conversion from 8% to 38%. Interestingly, 1,2-PD was observed in the product mixture at the lowest acid concentration (0.25% relative to glycerol) in the same amount as 1-PO while no 1,2-PD was observed at higher acid concentrations. Generally, decreasing acid concentration lowers the glycerol conversion but increases the 1,3-PD selectivity. Post-reaction analysis of the catalyst revealed the presence of **4** and the dimethylamino-substituted  $(^t\text{BuPOCOP})\text{Ir}(\text{CO})(\text{H})_2$ , likely formed by the same mechanism as **3**. Based on knowledge of  $(^t\text{BuPOCOP})\text{Ir}$  chemistry and the observations above, the mechanism for the glycerol deoxygenation as shown in Scheme 2-8 was proposed. Initially, protonation of  $(^t\text{BuPOCOP})\text{Ir}(\text{CO})$  (**2**) occurs, leading to the five-coordinate species  $[(^t\text{BuPOCOP})\text{Ir}(\text{CO})(\text{H})]^+$  (**5**). Under a hydrogen atmosphere, dihydrogen binds to **5**, forming the dihydrogen complex **6**. The dihydrogen of complex **6** or an external acid can then protonate glycerol, leading to formation of the aldehyde intermediate and **3**. The aldehyde can be easily protonated, and subsequent hydride transfer by species **3** forms 1,3-PD and regenerates **5**. The acid-assisted hydrogen addition to form **3** was previously reported and the protonated species **5** has been characterized.<sup>33</sup> The dihydrogen species is not observed at room temperature, but at low temperature (-80 °C) under 40 atm  $\text{H}_2$  it was detected by  $^1\text{H}$  NMR spectroscopy with distinct signals for metal-bound dihydrogen and a

**Scheme 2-8. Proposed mechanism of glycerol deoxygenation with  $(^t\text{BuPOCOP})\text{Ir}(\text{CO})$ .**



hydride.<sup>34</sup> In the same study, isotope exchange between  $\text{H}_2$  and  $\text{CD}_3\text{OD}$  was observed with complex **2** or **4**, further supporting the protonation of glycerol by **6**.

## 2.2 Synthesis and Reactivity of $(^t\text{BuPOCOP})\text{Ir}(\text{CO})$ Complexes

### 2.2.1 Synthesis and Characterization of $(^t\text{BuPOCOP})\text{Ir}(\text{CO})$ Complexes

Crude glycerol from the biodiesel production contains water, and glycerol itself is highly hygroscopic. Additionally, water is produced as a byproduct in the glycerol deoxygenation via dehydration-hydrogenation pathway. Thus, it is desirable to carry out the glycerol deoxygenation reaction in aqueous media to be economically viable and environmentally friendly. For a homogeneous system, in which the metal complex needs to be soluble in polar solvents, it is often functionalized with groups such as sulfonate<sup>35, 36</sup> or ammonium.<sup>37</sup> For example, a water-soluble pincer Ir complex has been synthesized by Brookhart and coworkers for electrocatalytic reduction of carbon dioxide. In their prior work, an iridium complex (**7**, Figure 2-2) with the  $^t\text{BuPOCOP}$  ligand

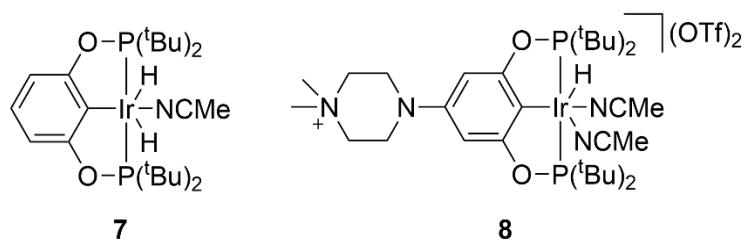
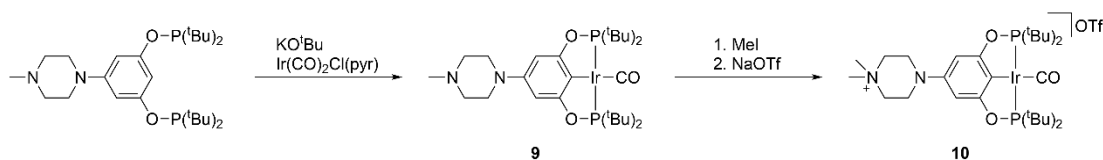


**Figure 2-2.** Ir complexes for electrocatalytic reduction of CO<sub>2</sub>.<sup>37</sup>

was shown to be an effective catalyst in organic solvents, but this complex is not soluble in water.<sup>38</sup> Subsequently, a new (<sup>t</sup>BuPOCOP)Ir complex (**8**, Figure 2-2) was prepared with an ammonium functional group in the ligand backbone, enabling dissolution of this complex in aqueous media. It is also shown that the triflate counterions are important for solubility in water as the complexes with iodide or PF<sub>6</sub> anions are poorly soluble in water.<sup>37</sup>

Inspired by Brookhart and coworkers, we sought to prepare a complex analogous to complex **2** with an ammonium moiety. The piperazine-substituted <sup>t</sup>BuPOCOP ligand was synthesized, following the reported procedure,<sup>37</sup> and was metalated with Ir(CO)<sub>2</sub>(Cl)(pyr) (pyr = pyridine) in presence of base to prepare the Ir complex (**9**) as yellow solid (first reaction of Scheme 2-9). Complex **9** has <sup>31</sup>P{<sup>1</sup>H} NMR signal at 200 ppm (singlet), comparable to that of complex **4** (at 200 ppm). <sup>1</sup>H NMR spectrum shows a virtual triplet at 1.34 ppm assigned to the *tert*-butyl groups coupled to two magnetically inequivalent phosphorus and two multiplets at 2.47 and 3.15 ppm and a singlet at 2.27 ppm, assigned to the methylene protons and the methyl group on the piperazinyl moiety, respectively. The virtual triplet signal for *tert*-butyl groups of complex **4** shows up at 1.36 ppm. The CO stretching frequencies in pentane are 1949 cm<sup>-1</sup> for **2**,<sup>39</sup> 1941 cm<sup>-1</sup> for **4**,<sup>32</sup> and 1943 cm<sup>-1</sup> for **9**. These IR data show that the piperazinyl group is an electron-donating group like the

**Scheme 2-9. Synthesis of complex 9 and 10.**



dimethylamino group. The similarities in  $^{31}\text{P}\{^1\text{H}\}$  NMR signals, virtual triplet  $^1\text{H}$  NMR signals, and CO stretching frequencies indicate that Ir centers of complex **4** and **9** are in similar chemical environments. Another complex with a triflate anion (**10**), analogous to complex **8**, was prepared by reacting complex **9** with methyl iodide, followed by salt metathesis using NaOTf to exchange the anion from the iodide precursor (second reaction of Scheme 2-9). This complex **10** has a  $^{31}\text{P}\{^1\text{H}\}$  NMR signal at 201 ppm, very close to the parent complex **9**. The  $^1\text{H}$  NMR signals from the piperazinyl group shifted from 2.47, 3.15, and 2.27 ppm to 3.50, 3.76 and 3.52 ppm, respectively. The singlet signal at 3.52 ppm is assigned to the two methyl groups on the nitrogen atom (6H). There was no change in  $^1\text{H}$  NMR spectrum noted for salt metathesis reaction (exchange of iodide for triflate), but  $^{19}\text{F}\{^1\text{H}\}$  NMR of **10** showed one singlet at -79.1 ppm assigned to the triflate anion.

### 2.2.2 Protonation of Complex **9** with $[\text{H}(\text{OEt}_2)]\text{BF}_4$

Because complex **9** contained multiple basic sites, protonation studies in  $\text{CD}_2\text{Cl}_2$  were undertaken by titrating with  $[\text{H}(\text{OEt}_2)]\text{BF}_4$  to understand the nature of the protonated species. As shown in Figure 2-3, the reaction of **9** with 1 equiv.  $[\text{H}(\text{OEt}_2)]\text{BF}_4$  resulted in a narrow signal at 201 ppm in the  $^{31}\text{P}\{^1\text{H}\}$  NMR spectrum, replacing the signal for complex **9** (200 ppm). This species was assigned as complex **11** with the protonation at the nitrogen atom distal to the aryl ring since the  $^{31}\text{P}\{^1\text{H}\}$  NMR signal is comparable to complex **10** (Scheme 2-10). When 2 equiv.  $[\text{H}(\text{OEt}_2)]\text{BF}_4$  were added, two signals at 203 and 194 ppm appeared. Upon the addition of the third equivalent of  $[\text{H}(\text{OEt}_2)]\text{BF}_4$ , the signal at 203 became sharper and shifted to 205 ppm. The resonance at 205 ppm was assigned as complex **12** (Scheme 2-10) with the protonation at both nitrogen atoms, supported by the chemical shift of the complex **4** with *N*-protonation (205 ppm).<sup>34</sup> The broad signal at 194 ppm became narrow and shifted to 196 ppm with the addition of >3 equiv. of the acid,

**Scheme 2-10. Sequential addition of acids to complex 9.**

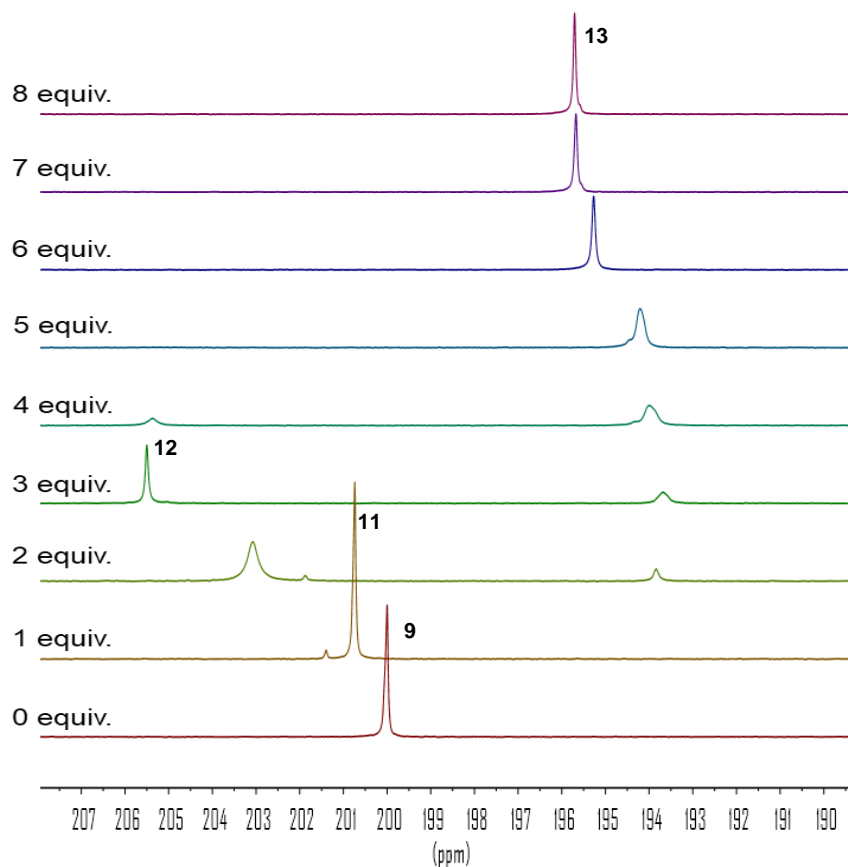
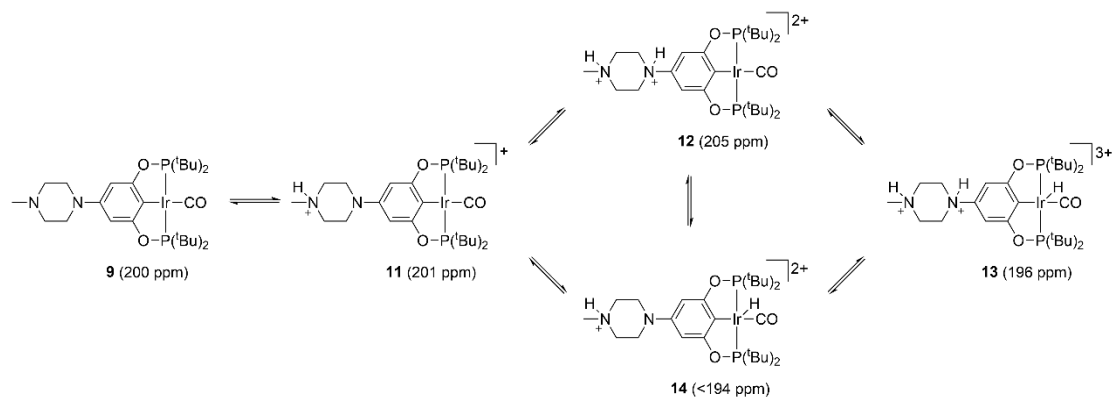


**Figure 2-3.** Stacked  $^{31}\text{P}\{^1\text{H}\}$  NMR spectra of the protonation of **9** with sequential addition of acids in  $\text{CD}_2\text{Cl}_2$ .

indicative of tri-cationic species **13**. Since  $[(^t\text{BuPOCOP})\text{Ir}(\text{CO})(\text{H})]\text{BArF}_{20}$  has a  $^{31}\text{P}\{^1\text{H}\}$  NMR signal reported at 191.8 ppm and complex **9** has a signal at 196 ppm, we propose another species is present to account for the broad signal at 194 ppm. This species is proposed to be a di-cationic Ir-

hydride species (**14**), where the second protonation occurred at the Ir center instead of the nitrogen atom proximal to the aryl ring, also supported by the presence of a Ir-H  $^1\text{H}$  NMR signal at -34.3 ppm. This Ir-H signal shifted to -35.2 ppm and narrowed to form a triplet signal of complex **13** with 8 equiv. of acid. Based on the observation that **4** and **9** were not soluble in neutral aqueous media, these complexes may form the protonated species *in situ* and dissolve in acidic aqueous media, but no solubility of **4** and **9** were observed in acidic aqueous media.

## 2.3 Deoxygenation of Glycerol

### 2.3.1 Deoxygenation of Glycerol with ( $^t\text{BuPOCOP}$ )Ir(CO) Complexes

A typical catalytic experiment was conducted in acidic aqueous *p*-dioxane solution with glycerol (3.61M), 0.125 mol% Ir cat. (relative to glycerol), and 1 mol%  $\text{H}_2\text{SO}_4$  (relative to glycerol) at 200 °C under 80 bar  $\text{H}_2$  (Scheme 2-11). The reaction mixture was added to a glass liner, capped by a Teflon lid with a small hole, allowing gas to diffuse into the reaction mixture. The liner was inserted into a pressure reactor, which was heated in an aluminum block for 24 h. After heating, an aliquot was taken from the reaction mixture, diluted with  $\text{D}_2\text{O}$ , and filtered to remove precipitates, mainly Ir complex. The conversion of glycerol and the yields of 1-PO and 1,3-PD were analyzed by quantitative  $^{13}\text{C}\{^1\text{H}\}$  NMR spectroscopy of reaction mixture aliquots in  $\text{D}_2\text{O}$  (see experimental

**Scheme 2-11. Glycerol deoxygenation reaction.**

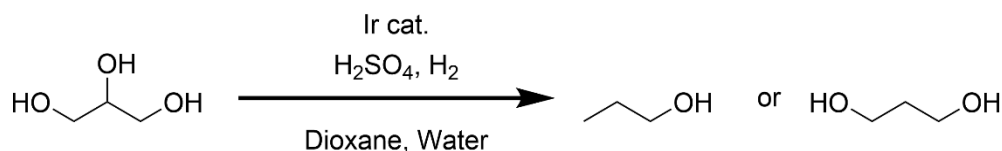


**Table 2-1. Glycerol deoxygenation reactions with different Ir complexes.<sup>a</sup>**

Ir Cat.	Conv. (%)	1-PO Yield (%)	1,3-PD Yield (%)	Mass Balance (%) <sup>b</sup>
<b>2</b>	76.9	15.0	1.1	21
<b>4</b>	74.3	15.9	1.4	23
<b>9</b>	73.4	15.4	1.3	23

<sup>a</sup> Reaction conditions: 0.0065 mmol Ir complex, 5.2 mmol glycerol, and 0.052 mmol  $\text{H}_2\text{SO}_4$  in water (0.249 mL) and *p*-dioxane (1.19 mL) under 80 bar  $\text{H}_2$ . Heated to 200 °C. <sup>b</sup> Mass balance = (Sum of product yields) / (Conversion of glycerol).



pathways. Another explanation for mass balance issue is that the deoxygenated products (1,3-PD and 1-PO) may undergo further reactions, lowering the yields of products and selectivities (discussed in section 2.3.3).

Despite the poor mass balance, the deoxygenation reaction results were similar between Ir complexes. The substitution on the <sup>t</sup>BuPOCOP ligand was done to increase the solubility in polar media, but it would also have an effect on the electronics of these complexes. The dimethylamino group is electron-donating ( $\sigma_p = -0.83$ ), and the protonation causes a drastic change for the dimethylamino group to become electron-withdrawing ( $\sigma_p \approx 0.60-0.83$ ).<sup>40</sup> The CO stretching frequency of complex **9** (1943 cm<sup>-1</sup>), compared to that of complex **2** (1949 cm<sup>-1</sup>), suggests that the piperazinyl group is an electron-donating group and expected to go through similar change in electronics as complex **4** (1941 cm<sup>-1</sup>) upon protonation. The incorporation of these electron-withdrawing protonated groups should make the iridium center less basic. The altered electronics at the metal center should affect the activity of hydrogenation reaction. However, the similar results of the deoxygenation reactions with different Ir complexes may suggest that the change in the rate of hydrogenation is less influential in determining the overall reactivity and that understanding and controlling acid-catalyzed pathways is more important.

Additionally, weaker acids such as acetic acid (pK<sub>a</sub><sup>H<sub>2</sub>O</sup> = 4.76), formic acid (pK<sub>a</sub><sup>H<sub>2</sub>O</sup> = 3.77), or phosphoric acid (pK<sub>a1</sub><sup>H<sub>2</sub>O</sup> = 2.12) were explored, but no reaction occurred. <sup>13</sup>C NMR spectra after the samples were heated to 200 °C under 80 bar H<sub>2</sub> showed only signals for *p*-dioxane and glycerol. These results suggests that the added acid must be sufficiently strong to initiate deoxygenation.

### 2.3.2 Improving Mass Balance of Glycerol Deoxygenation

To minimize undesired side pathways of condensation or dehydration, we tested three conditions: 1) lowering the acid concentrations, 2) lowering the concentrations of all reagents by diluting the reaction mixture, and 3) increasing water concentrations. Both condensation and dehydration steps are catalyzed by acid, and lowering its concentration should slow down both

these steps. However, decreasing acid concentration is known to lead to lower glycerol conversion.<sup>32</sup> Diluting the reaction mixture by adding more solvents would lower the concentrations of glycerol, Ir complex, and the acid, and thus also reduce overall reactivity, but it could change selectivity. Water is formed as a byproduct from condensation or dehydration, and adding water to the reaction mixture would limit the equilibrium position of those reactions.

Glycerol deoxygenation reactions were carried out with complex **2**, **4**, and **9** and with varying equivalents of acid. Generally, glycerol conversion and 1-PO yield increased with higher acid concentrations, but the yield of 1,3-PD had an inverse relationship to the acid concentration. Interestingly, 1,2-PD was observed at low acid concentration, and 1,2-PD yield also increased with decreasing acid concentration (Table 2-2, entry 2 vs. 3, 5 vs. 6). Decreasing glycerol conversion at lower concentration of acid is expected because there was less acid available to catalyze the dehydration step. Simultaneously, the rate of hydrogenation to form the deoxygenated products became more competitive with the rate of acid-catalyzed side pathways. This effect is seen by the improved mass balance of up to 48% with **4** and 1 equivalent of acid (Table 2-2, entry 6). It is interesting that the result of glycerol deoxygenation with **2** and 1 equivalent of acid (Table 2-2, entry

**Table 2-2. Glycerol deoxygenation with varying Ir complexes and acid concentrations.<sup>a</sup>**

Entry	Ir Cat.	Acid Equiv. <sup>b</sup>	Conv. (%)	1-PO Yield (%)	1,3-PD Yield (%)	1,2-PD Yield (%)	Mass Balance <sup>c</sup> (%)
1	<b>2</b>	8	76.9	15.0	1.1	0	21
2	<b>2</b>	2	53.5	11.5	1.8	0.7	26
3	<b>2</b>	1	39.0	7.4	2.5	0.8	27
4	<b>4</b>	8	74.3	15.9	1.4	0	23
5	<b>4</b>	2	37.0	9.4	2.1	0.7	33
6	<b>4</b>	1	14.3	3.8	2.2	0.8	48
7	<b>9</b>	8	73.4	15.4	1.3	0	23
8	<b>9</b>	2	40.1	8.9	2.1	0.8	29

<sup>a</sup> Reaction conditions: 0.0065 mmol Ir complex, 5.2 mmol glycerol, and H<sub>2</sub>SO<sub>4</sub> in water (0.249 mL) and *p*-dioxane (1.19 mL) under 80 bar H<sub>2</sub>. Heated to 200 °C. <sup>b</sup> Acid Equivalents per Ir atom. <sup>c</sup> Mass balance = (Sum of product yields) / (Conversion of glycerol).

3) is comparable to the results with **4** or **9** and 2 equivalents of acid (Table 2-2, entry 5, 8). Higher conversion of glycerol and higher 1-PO yield and lower 1,3-PD yield were observed with **2** and 2 equivalents of acid (Table 2-2, entry 2). Complex **4** or **9** has basic sites (one or two, respectively) on the ligand backbone, unlike complex **2**. Due to the interaction of the acid with the basic sites, there may be less acid available to catalyze the dehydration.

Glycerol deoxygenation reactions were carried out with more solvent to reduce the concentrations of reagents by half and to slow down the catalysis. The decline in both glycerol conversion and product yields demonstrates the diminished overall reactivity (Table 2-3, entries 1, 2). As observed with low acid concentrations, 1,2-PD also appeared. While the concentrations of reagents were lowered, the concentration of hydrogen remained the same in the reaction mixture. This steady concentration of hydrogen may have led to a better rate of hydrogenation relative to competing condensation pathways and the slightly improved mass balance.

Glycerol deoxygenation reactions were also carried out varying the water concentration. Previously, deoxygenation of 1,2-PD was reported with a selectivity up to 95% of 1-PO and *n*-propyl ether when the acid loading was reduced and the water concentration increased.<sup>29</sup> The effect of

**Table 2-3. Glycerol deoxygenation with varying solvent volumes and water concentrations.<sup>a</sup>**

Entry	Ir Cat.	<i>p</i> -Dioxane:H <sub>2</sub> O (% v/v)	Conv. (%)	1-PO Yield (%)	1,3-PD Yield (%)	1,2-PD Yield (%)	Mass Balance <sup>b</sup> (%)
1	<b>4</b>	83:17	74.3	15.9	1.4	0	23
2 <sup>c</sup>	<b>4</b>	83:17	51.7	12.2	0.8	0.3	26
3	<b>9</b>	83:17	73.4	15.4	1.3	0	23
4	<b>9</b>	65:35	69.9	17.8	2.4	0.4	29
5	<b>9</b>	48:52	56.8	17.7	2.8	0.4	37
6 <sup>c,d</sup>	<b>4</b>	48:52	9.1	4.1	0.6	0	51
7 <sup>c,d</sup>	<b>9</b>	48:52	7.3	3.2	0.7	0	53

<sup>a</sup>Reaction conditions: 0.0065 mmol Ir complex, 5.2 mmol glycerol, and 0.052 mmol H<sub>2</sub>SO<sub>4</sub> in aqueous dioxane solution under 80 bar H<sub>2</sub>. The total volume of solvent mixture was 1.439 mL. Heated to 200 °C. <sup>b</sup>Mass balance = (Sum of product yields) / (Conversion of glycerol). <sup>c</sup>The total volume of solvents doubled. <sup>d</sup>Amount of H<sub>2</sub>SO<sub>4</sub> changed to 0.013 mmol.

water concentration was not yet studied with glycerol as substrate. At high water concentration (52% v/v) (Table 2-3, entry 5), the conversion of glycerol decreased to 56.8% and 1-PO yield slightly increased to 17.7%. The yield of 1,3-PD doubled from 1.3% to 2.8% as more water was added. A concurrent decrease in glycerol conversion and increased product yields led to an improvement in mass balance to 37%. The added water not only inhibited the first dehydration of glycerol, leading to lower catalytic activity and conversion, but also suppressed other dehydration and condensation pathways. Schlaf observed the concentration of glycerol was the same before and after the deoxygenation reaction at 150 °C with at least 20% water, indicating that the condensation pathways are suppressed when the water concentration is sufficiently high.<sup>28</sup> Increasing water concentration made the hydrogenation step relatively faster and improved the overall product yield and mass balance. Interestingly, 1,3-PD yield increased monotonically with the increasing % water, but unfortunately a deoxygenation of glycerol in pure water was not feasible due to insolubility of Ir complexes in water.

Lastly, we examined the deoxygenation reaction under the combined modified reaction conditions (lower acid conc., dilute conditions, high water conc.). The conversion of glycerol drastically dropped to 7-9% because the low concentration of acid and high concentration of water inhibited dehydration of glycerol. Notably, the mass balance improved to over 50% (Table 2-3, entries 6, 7). The rate of deoxygenation of glycerol is dependent on the dehydration of glycerol, but increasing the rate of dehydration is detrimental to mass balance and 1,3-PD selectivity. Slowing down the dehydration improves the yield and selectivity of 1,3-PD by making the rate of hydrogenation more competitive than condensation or dehydration reactions.

### 2.3.3 Control Reactions

To further understand the mass balance issue, we examined whether the deoxygenated products are stable to the reaction conditions. Deoxygenation reactions with 1-PO, 1,2-PD, and 1,3-PD were carried out with complex **4** at 200 °C under 80 bar H<sub>2</sub> in acidic aqueous dioxane

solution. At high acid concentration, 1-PO was recovered in only 45% yield and 1,3-PD in only 51% yield (Table 2-4, entry 1, 2). Thus the deoxygenated products are undergoing further reactions to form other products, worsening the mass balance. When the acid concentration was lowered, the % recovery for 1-PO improved to 51% and to 72% for 1,3-PD (Table 2-4, entry 3, 4). With 1,2-PD as substrate, almost full conversion (95%) was observed with the formation of 1-PO in 56% yield. However, 1-PO was not observed when 1,3-PD was a substrate, and this observation is consistent with previous reports.<sup>28, 32</sup> Based on the successful deoxygenation of 1,2-PD to 1-PO and no observation of 1-PO from 1,3-PD, it is reasonable to suggest that, if the initial dehydration of glycerol occurs at the primary OH group, then it forms 1,2-PD, followed by an activation of the secondary OH group, eventually leading to the formation of 1-PO. On the other hand, if the initial dehydration occurs at the secondary OH group, then it leads to the formation of 1,3-PD.

Furthermore, another set of control reactions were carried out to examine whether poor mass balance was due to any mechanical loss of the deoxygenated products. Glycerol and 1,3-PD were recovered quantitatively, but 1-PO was only accounted for 76% when these substrates were subjected to the reaction conditions without Ir complex and acid. Based on the observation of liquid between outside of the glass liner and inside the reactor well when 1-PO was a substrate, it suggests that 1-PO, which is more volatile than glycerol or 1,3-PD, vapourizes out of the glass liner and condenses inside the reactor well. In this control reaction, the initial amount of 1-PO was much greater than the amount formed in the glycerol deoxygenation reactions, so the % recovery value

**Table 2-4. Control reactions using the deoxygenated products as substrates.<sup>a</sup>**

Entry	Substrate	Acid Equiv. <sup>b</sup>	% Recovery
1	1-PO	8	45
2	1-PO	2	51
3	1,3-PD	8	40
4	1,3-PD	2	72

<sup>a</sup> Reaction conditions: 0.0065 mmol Ir complex **4**, 2.6 mmol substrate, and H<sub>2</sub>SO<sub>4</sub> in water (0.249 mL) and *p*-dioxane (1.19 mL) under 80 bar H<sub>2</sub>. Heated to 200 °C. <sup>b</sup> Acid equivalents per Ir atom.

(76%) could not be directly applied to account for the mass balance from glycerol reactions. Nonetheless, it is likely that some 1-PO escapes the glass liner during the glycerol deoxygenation reactions.

#### 2.3.4 Examination for Nanoparticle Formation

Recently, the *in-situ* generation of nanoparticles from **1** during the deoxygenation of 1,2-octanediol was reported.<sup>41</sup> Nanoparticles, isolated by centrifugation, revealed a diffraction pattern that resembles metallic iridium. The nanoparticles adhered to the liner surface in the reactor or the surface of the stirbar were active for the deoxygenation of 1,2-octanediol, although this reactivity faded over the repeated experiments. While such particles were not obvious in the reaction mixture for our system, dark deposits were observed on the PTFE stirbars. We examined the possibility of nanoparticle formation in the glycerol deoxygenation reactions. For each experiment, the reactor was charged with 5.2 mmol glycerol and 0.013 mmol (0.250 mol% relative to glycerol) H<sub>2</sub>SO<sub>4</sub> in aqueous *p*-dioxane. In Run 1 (Table 2-5), with a brand new glass liner and stirbar and *without any iridium complex*, the conversion of glycerol was 54.1% with the total product yield of 0.5% (1-PO and 1,3-PD) at 200 °C after 24 h. The initially colorless reaction mixture appeared dark brown with some visible particles after the reaction. In Run 2 (Table 2-5), using the same liner and stirbar, now with **4** added, the conversion of glycerol dropped to 35.0% and 1-PO was observed in 8.0% and 1,3-PD in 2.2%. The same reactions were repeated twice again with the same liner and stirbar

**Table 2-5. Examination for possible Ir nanoparticles.<sup>a</sup>**

Run	Conv. (%)	1-PO Yield (%)	1,3-PD Yield (%)	Total Yield (%)
1	54.1	0.4	0.1	0.5
2 <sup>b</sup>	35.0	8.0	2.2	10.2
3	50.3	5.3	0.3	5.6
4	60.8	1.2	0.1	1.3

<sup>a</sup> Reaction conditions: 5.2 mmol substrate, and 0.013 mmol H<sub>2</sub>SO<sub>4</sub> in water (0.249 mL) and *p*-dioxane (1.19 mL) under 80 bar H<sub>2</sub>. Heated to 200 °C. <sup>b</sup> 0.0065 mmol Ir complex **4** added.

(Table 2-5, run 3-4) and without any Ir catalyst added. The conversion of glycerol returned to above 50%, and the yields of 1-PO and 1,3-PD decreased significantly.

Total yield of the products (1-PO and 1,3-PD) in Run 3 (Table 2-5) was reduced by about half from Run 2, and this reduction is comparable to the results reported for the 1,2-octanediol deoxygenation.<sup>41</sup> The continued, albeit decreased, reactivity suggests the presence of nanoparticles participating in the catalysis. Intriguingly, the % yield difference between Run 2 and 3 is much greater for 1,3-PD than 1-PO, where the difference between two runs is the presence of molecular Ir complex. The nanoparticles may favor activation of terminal OH groups since they are sterically more accessible and lead to the formation of 1,2-PD, which turns into 1-PO as observed in the control reaction. Because the post-reaction analysis by NMR spectroscopy confirms the presence of molecular Ir complex, the *in-situ* generated nanoparticles and molecular complex must coexist in the reaction mixture, and it cannot be conclusively determined which is catalyzing the reaction. Rather than one or the other being responsible for all the catalysis, it is possible that heterogeneous nanoparticles favor the activation of terminal OH groups leading to 1,2-PD and later 1-PO while the homogeneous complex is the catalyst to produce 1,3-PD. This possibility is intriguing and in need of further investigation as it implies that a more robust homogeneous catalyst may allow for greater selectivity in the production of 1,3-PD from glycerol.

Previously, to improve the robustness of pincer complex, *tert*-butyl groups on phosphorus atoms of  $(^t\text{BuPCP})\text{Ir}(\text{H})_2$  ( $^{\text{R}}\text{PCP} = \kappa^3\text{-C}_6\text{H}_3\text{-2,6-(CH}_2\text{PR}_2)_2$ ) (**17**, Figure 2-4) were substituted with adamantyl groups (**18**, Figure 2-4), and this substitution increased thermal robustness to 250 °C while providing a similar steric and electronic environment around Ir center and a comparable

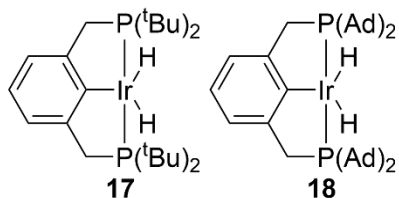


**Figure 2-4.** Ir complexes with different alkyl groups used for alkane dehydrogenation.

**Scheme 2-13. Hydrogen addition to pincer-ligated Ir complexes.**

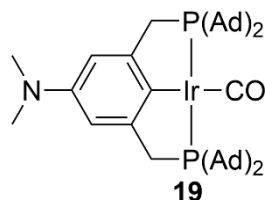
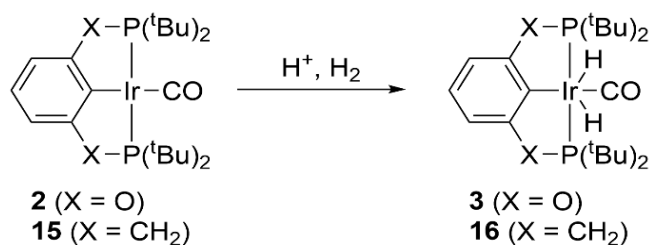


**Figure 2-5.** Proposed Ir complex for future study.

catalytic activity for alkane dehydrogenation.<sup>42</sup> In addition to the increased robustness of the catalyst, a faster rate of hydrogenation is desired because the faster incorporation of hydrogen to the catalyst would enhance the rate of the hydrogenation and improve 1,3-PD selectivity. In the study of hydrogen addition to pincer complexes, (<sup>t</sup>BuPOCOP)Ir(CO) (**2**) converted to (<sup>t</sup>BuPOCOP)Ir(CO)(H)<sub>2</sub> (**3**) only in 14% over 6 days in presence of acid under hydrogen atmosphere. However, (<sup>t</sup>BuPCP)Ir(CO) (**15**) resulted in (<sup>t</sup>BuPCP)Ir(CO)(H)<sub>2</sub> (**16**) immediately and quantitative yield under the same conditions as **2** (Scheme 2-13).<sup>43</sup> Based on the prompt hydrogen addition of a PCP ligand and the thermal stability of adamantyl groups, it's possible that new complex (**19**) can be prepared to increase 1,3-PD yield and minimize catalyst decomposition to nanoparticles.

## 2.4 Conclusions

A new derivative of (<sup>t</sup>BuPOCOP)Ir(CO) complex (**9**) was synthesized with a piperazinyll group at *para* position of ligand backbone. A protonation study revealed the sequential addition of protons and eventual formation of tri-cationic species. While it was anticipated that the protonation of complex **9** would enhance its solubility in aqueous solution, it was found that complex **9** was not soluble in neutral or acidic aqueous media. The results from glycerol deoxygenation reactions with

three Ir complexes with different substituents on the ligand backbone were similar affording only a very small yield of 1,3-PD. They also showed poor mass balance of 20%. The poor mass balance and low 1,3-PD yield are similar to the results reported by Schlaf with Ru catalysts, where no 1,3-PD was observed and incomplete mass balance was recorded.<sup>27, 28</sup> The mass balance improved when (1) the acid concentration was lowered, (2) the entire reaction mixture was diluted, or (3) the water concentration increased. These modifications to the reaction conditions also confirmed that the conversion of glycerol is related directly to the acid concentration and inversely to the water concentration while 1,3-PD yield has the opposite relationships to them. The inverse relationship of 1,3-PD and water contradicts the observation by Braca using Ru(CO)<sub>4</sub>l<sub>2</sub>, where the addition of water shifted the product distribution away from 1,3-PD towards 1-PO.<sup>25</sup> The lowest conversion and the best mass balance were observed when all three modified conditions were applied together. Control reactions revealed the formation of 1-PO from 1,2-PD, not 1,3-PD. Control reactions also showed that 1-PO and 1,3-PD were not fully recovered, indicating that they react further under the reaction conditions. In order to determine whether nanoparticles had formed in the reaction mixture, a series of experiments were performed using the same glass liner and stirbar. The continued reactivity in absence of molecular Ir complex suggests the formation of Ir nanoparticles. A more drastic drop in 1,3-PD yield than 1-PO yield without any molecular catalyst after nanoparticle formation seems that a molecular catalyst is required for selective formation of 1,3-PD. To increase 1,3-PD production, a more robust homogeneous catalyst is likely required.

## 2.5 Experimental

All experiments and manipulations were performed using standard Schlenk techniques under an argon atmosphere or in a nitrogen-filled glovebox unless otherwise specified. CH<sub>2</sub>Cl<sub>2</sub> (DCM), benzene, pentane, CH<sub>3</sub>CN and toluene were passed through columns containing activated alumina and molecular sieves. *p*-Dioxane (stabilized with BHT) and all other reagents were used as received. CD<sub>2</sub>Cl<sub>2</sub> was dried over CaH<sub>2</sub>. <sup>1</sup>H, <sup>31</sup>P{<sup>1</sup>H}, <sup>19</sup>F{<sup>1</sup>H}, and <sup>13</sup>C{<sup>1</sup>H} NMR spectra were recorded on Bruker AV300, AV500, DRX500 or NEO600 instruments at ambient temperature and

referenced to the residual solvent peak ( $^1\text{H}$ ,  $^{13}\text{C}\{^1\text{H}\}$ ).<sup>44</sup>  $^{31}\text{P}\{^1\text{H}\}$  NMR shifts were referenced to 85%  $\text{D}_3\text{PO}_4$  (0 ppm).  $^{19}\text{F}\{^1\text{H}\}$  NMR shifts were not referenced. Elemental analyses were performed by the CENTC Elemental Analysis Facility at the University of Rochester. Samples were weighed with a PerkinElmer Model AD6000 Autobalance and their compositions were determined with a PerkinElmer 2400 Series II Analyzer. IR spectra were recorded on a Bruker Tensor 27 FT-IR spectrometer. X-ray crystal structures were collected at  $-173\text{ }^\circ\text{C}$  on a Bruker APEX II single crystal X-ray diffractometer, Mo-radiation.

### 2.5.1 Synthesis

$(^t\text{BuPOCOP})\text{Ir}(\text{CO})$ ,<sup>39</sup>  $(p\text{-NMe}_2\text{-}^t\text{BuPOCOP})\text{Ir}(\text{CO})$ ,<sup>32</sup>  $[\text{Ir}(\text{CO})_2\text{Cl}(\text{pyr})]$ ,<sup>45</sup> and  $(5\text{-}(1\text{-methylpiperaziny})\text{-}^t\text{BuPOCOP})$ <sup>37</sup> were synthesized according to literature procedures.

#### *Synthesis of $(p\text{-}(1\text{-methylpiperaziny})\text{-}^t\text{BuPOCOP})\text{Ir}(\text{CO})$ (**9**)*

In a nitrogen-atmosphere glovebox, a flask with a Teflon stopcock was charged with 0.490 g (0.99 mmol) of  $5\text{-}(1\text{-methylpiperaziny})\text{-}^t\text{BuPOCOP}$ , 0.362 g (1.0 mmol) of  $\text{Ir}(\text{CO})_2\text{Cl}(\text{pyr})$ , and 0.113g (1.0 mmol) of KO<sup>t</sup>Bu in 30 mL of toluene. Bubbling was observed upon mixing of these reagents, due to CO dissociation. The flask was sealed with a Teflon stopcock, removed from the glovebox, and heated to  $130\text{ }^\circ\text{C}$  in an oil bath for 18 h. After cooling the mixture, toluene was evaporated under vacuum. The residue was dissolved in pentane and filtered to yield a yellow filtrate. The pentane was evaporated from the filtrate to isolate **9** as a yellow solid. Yield: 0.591 g (84% yield). Crystals suitable for X-ray diffraction were grown by slow evaporation of a DCM solution at room temperature.

$^1\text{H}$  NMR( $\text{CD}_2\text{Cl}_2$ , 600 MHz):  $\delta$  6.20 (s, 2H; Ar-H), 3.15 (m, 4H;  $\text{N}(\text{CH}_2\text{CH}_2)_2\text{N-}$ ), 2.47 (m, 4H;  $\text{CH}_3\text{N}(\text{CH}_2\text{CH}_2)_2\text{N-}$ ), 2.27 (s, 3H;  $\text{NCH}_3$ ), 1.34 (vt,  $^3J_{\text{PH}} + ^5J_{\text{PH}} = 7.2\text{ Hz}$ , 36H; <sup>t</sup>Bu).

$^{31}\text{P}\{^1\text{H}\}$  NMR ( $\text{CD}_2\text{Cl}_2$ , 202 MHz):  $\delta$  200 (s)

$^{13}\text{C}\{^1\text{H}\}$  NMR ( $\text{CD}_2\text{Cl}_2$ , 150 MHz):  $\delta$  199.7 (t,  $^2J_{\text{PC}} = 5\text{ Hz}$ ), 170.6 (vt,  $J_{\text{PC}} = 8\text{ Hz}$ ), 153.5 (s),

139.8 (t,  $^2J_{PC} = 9$  Hz), 91.6 (vt,  $J_{PC} = 6$  Hz), 55.4 (s), 48.9 (s), 46.0 (s), 40.8 (vt,  $J_{PC} = 12.3$  Hz), 28.2 (vt,  $J_{PC} = 3.3$  Hz)

IR (solution,  $\text{cm}^{-1}$ ):  $\nu(\text{CO})$  1943 (pentane)

Elemental Analysis (calculated): C 47.26 (46.98), H 6.77 (6.90), N 3.83 (3.91)

#### *Synthesis of [(p-(1,1-dimethylpiperaziny)-<sup>t</sup>BuPOCOP)Ir(CO)][OTf] (10)*

In a nitrogen-atmosphere glovebox, **9** (26 mg, 0.036 mmol) was dissolved in benzene (2 mL). MeI (40  $\mu\text{L}$ , 0.64 mmol) was added to the benzene solution of **9** with a micropipettor in the dark. After stirring for 46 h at room temperature, a yellow precipitate was collected by filtering through a pad of celite. The yellow solid was dissolved in DCM, and the DCM was evaporated under reduced pressure to yield a yellow solid. This solid was dissolved in  $\text{CH}_3\text{CN}$  (2 mL). After addition of NaOTf (15.4 mg, 0.090 mmol), the solution was allowed to stir for 17 h at room temperature. After stirring, the  $\text{CH}_3\text{CN}$  was evaporated under vacuum, and the product was extracted with DCM, filtered through a pad of Celite, and dried under vacuum to give a yellow solid (27 mg, 88% yield).

$^1\text{H}$  NMR( $\text{CD}_2\text{Cl}_2$ , 300 MHz):  $\delta$  6.25 (s, 2H; Ar-H), 3.76 (m, 4H; N- $\text{CH}_2$ ), 3.50 (m, 4H; N- $\text{CH}_2$ ), 3.52 (s, 6H; N( $\text{CH}_3$ ) $_2$ ), 1.35 (vt,  $^3J_{\text{PH}} + ^5J_{\text{PH}} = 7.2\text{Hz}$ , 36H; <sup>t</sup>Bu)

$^{31}\text{P}\{^1\text{H}\}$  NMR ( $\text{CD}_2\text{Cl}_2$ , 121 MHz):  $\delta$  201 (s)

$^{19}\text{F}\{^1\text{H}\}$  NMR ( $\text{CD}_2\text{Cl}_2$ , 470 MHz):  $\delta$  -79.1

#### 2.5.2 Protonation Studies of Complex **9**

In a nitrogen-atmosphere glovebox, a J. Young NMR tube was charged with complex **9** (20.6 mg, 0.029 mmol) and  $\text{CD}_2\text{Cl}_2$  (0.5 mL). Then, 8 equivalents of  $[\text{HEt}_2\text{O}][\text{BF}_4]$  were added successively one equiv. at a time with a micropipettor. The reaction progress was monitored using  $^1\text{H}$  and  $^{31}\text{P}\{^1\text{H}\}$  NMR spectroscopy after each addition.

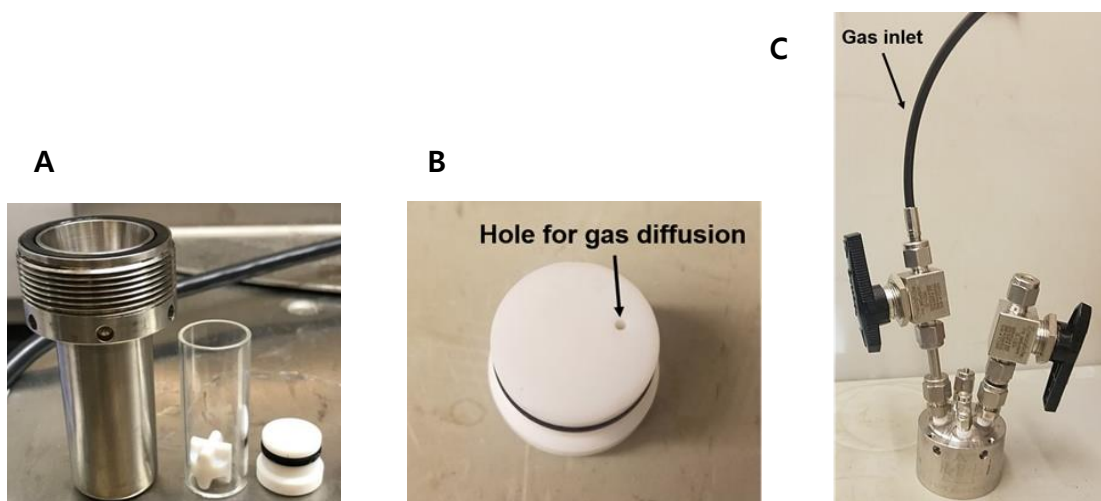


**Figure 2-6.** Photos of the HEL reactor assembly. A: reactor bottom, glass liner equipped with a spin vane, and gas-diffusing PTFE cap. B: gas-diffusing PTFE cap. C: reactor top.

### 2.5.3 General Procedures for Glycerol Deoxygenation Reactions

All deoxygenation reactions were conducted in a custom-made HEL DigiCAT high pressure system in 16 mL Hastelloy autoclaves equipped with glass liners, PTFE spin vanes and gas-diffusing PTFE caps (Figure 2-6). The reaction temperatures and stirring speed (300 rpm) were controlled using the HEL software interface. H<sub>2</sub> (Research 6.0 grade) was purchased from Airgas and used as received. Catalytic solutions were prepared on benchtop and sealed in Hastelloy reactors before connecting to the HEL DigiCAT system. Reactions were analyzed by quantitative <sup>13</sup>C{<sup>1</sup>H} NMR spectroscopy using reaction aliquots diluted with D<sub>2</sub>O.

In a typical reaction, glycerol (5.2 mmol), Ir catalyst (0.0065 mmol), and H<sub>2</sub>SO<sub>4</sub> (1M in H<sub>2</sub>O, 0.052 mmol) were added to a glass liner, followed by water (0.249 mL) and *p*-dioxane (1.19 mL). The glass liner was equipped with a spin vane, stopped with PTFE cap, sealed inside a Hastelloy reactor, and connected to the HEL DigiCAT system. The reactor was pressurized with N<sub>2</sub> (20 psi) and purged three times, then with H<sub>2</sub> (500 psi) and purged three times, and finally pressurized with H<sub>2</sub> (1160 psi). The reactor was heated to 200 °C in an aluminum block while stirring. After 24 h, the reactor was cooled to warm temperature (30-35 °C), further cooled in an ice bath for 40 min, and

depressurized while cold to minimize loss of material in the vapor phase. The reactor was then opened, and dimethylsulfone (45-50 mg) was added as an internal standard. Once dimethylsulfone was dissolved in the reaction mixture, an aliquot was taken out for quantitative  $^{13}\text{C}\{^1\text{H}\}$  NMR. Specific reaction conditions were listed under Table 1-3. After each experiment, the used reactors and stirbars were washed with acetone and air-dried.

The aliquot (300  $\mu\text{L}$ ) from the reaction mixture was diluted with  $\text{D}_2\text{O}$  (400  $\mu\text{L}$ ), usually resulting in cloudy mixture. This mixture was filtered through PTFE syringe filter, and the filtrate was added to a NMR tube with  $\text{GdCl}_3$  (7.5 mg/mL in  $\text{D}_2\text{O}$ , 20  $\mu\text{L}$ ) as a relaxation agent. A quantitative  $^{13}\text{C}\{^1\text{H}\}$  spectrum was obtained by collecting inverse-gated decoupled NMR spectrum to avoid NOE enhancement. For reactions with larger volume of solvents, an aliquot (400  $\mu\text{L}$ ) was diluted with  $\text{D}_2\text{O}$  (300  $\mu\text{L}$ ). All spectra were referenced to *p*-dioxane (67.19 ppm) in  $\text{D}_2\text{O}$ .<sup>44</sup> Figure 2-7 shows a representative  $^{13}\text{C}\{^1\text{H}\}$  NMR spectrum. The following are the  $^{13}\text{C}\{^1\text{H}\}$  NMR signals used for quantification:

Glycerol:  $\delta$  63.19 (2C)

1-PO:  $\delta$  10.34 (1C)

1,3-PD:  $\delta$  59.19 (2C)

1,2-PD:  $\delta$  18.82 (1C)

Dimethylsulfone (internal standard):  $\delta$  42.24 (2C)

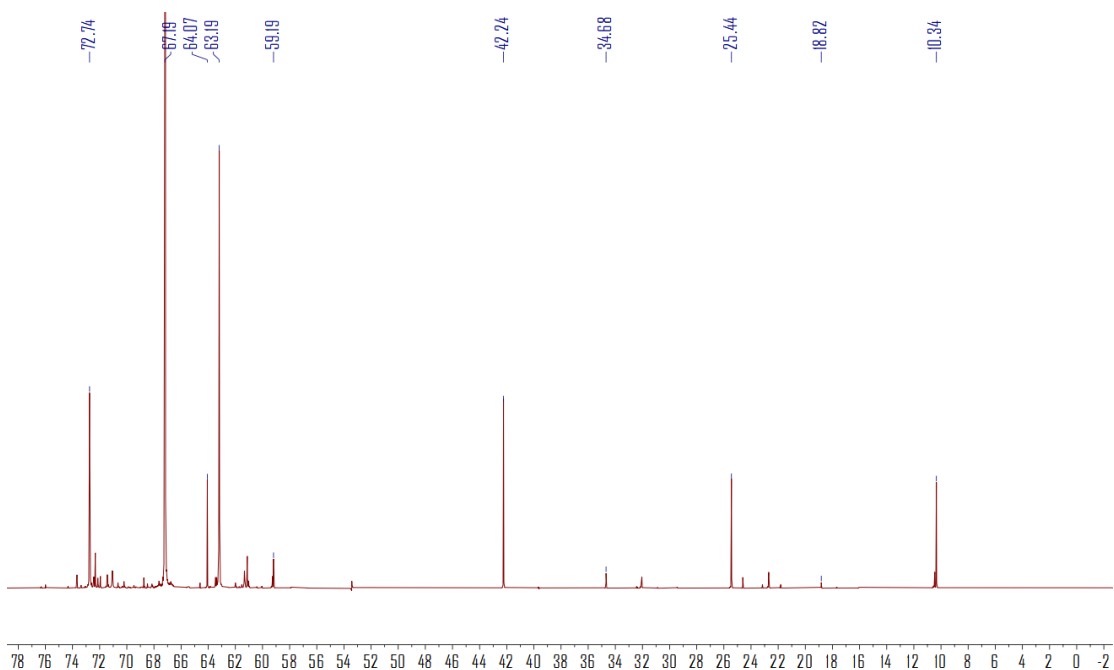


**Figure 2-7.** Representative  $^{13}\text{C}\{^1\text{H}\}$  NMR from deoxygenation of glycerol.

#### 2.5.4 Control Reactions

Following a similar procedure for deoxygenation of glycerol, control reactions were performed with 1-PO or 1,3-PD instead of glycerol. Specific reaction conditions are listed under Table 4. Aliquots were taken out for quantitative  $^{13}\text{C}\{^1\text{H}\}$  NMR in  $\text{D}_2\text{O}$ .

#### 2.5.5 Examination for Potential Nanoparticle Formation

Following a similar procedure for deoxygenation of glycerol, Run 1 was carried out with a brand new PTFE stirbar and glass liner but without any Ir catalyst. After Run 1, the PTFE stirbar and glass liner were washed with acetone, then water, then acetone again, and dried in the oven for at least 24 h. Run 2 was performed with complex **4** added following a similar procedure for deoxygenation of glycerol. Before each run after Run 2, the same washing and drying of the stirbar and glass liner was done. Run 3 and 4 were continued using the same stirbar and glass liner as in Run 1 or 2 but no Ir catalyst was added. A similar procedure for deoxygenation of glycerol was followed. Specific reaction conditions are listed under Table 5. Aliquots were taken out for

quantitative  $^{13}\text{C}\{^1\text{H}\}$  NMR in  $\text{D}_2\text{O}$ .

## 2.6 References

3. Quispe, C. A. G.; Coronado, C. J. R.; Carvalho Jr, J. A., Glycerol: Production, consumption, prices, characterization and new trends in combustion. *Renew. Sustain. Energy Rev.* **2013**, *27*, 475-493.
4. Johnson, D. T.; Taconi, K. A., The glycerin glut: Options for the value-added conversion of crude glycerol resulting from biodiesel production. *Environ. Prog.* **2007**, *26* (4), 338-348.
5. Anitha, M.; Kamarudin, S. K.; Kofli, N. T., The potential of glycerol as a value-added commodity. *Chem. Eng. J.* **2016**, *295*, 119-130.
6. Vivek, N.; Pandey, A.; Binod, P., Production and Applications of 1,3-Propanediol. In *Curr. Dev. Biotechnol. Bioeng.: Prod., Isol. Purif. Ind. Prod.*, 2017; pp 719-738.
11. OECD/FAO, *OECD-FAO Agricultural Outlook (Edition 2020)*, <https://www.oecd-ilibrary.org/content/data/4919645f-en> (accessed 2021-09-19).
12. *Top Value Added Chemicals from Biomass: Volume I -- Results of Screening for Potential Candidates from Sugars and Synthesis Gas*, U.S. Department of Energy: Energy Efficiency and Renewable Energy, United States, 2004.
13. Zhou, C. H.; Beltrami, J. N.; Fan, Y. X.; Lu, G. Q., Chemoselective catalytic conversion of glycerol as a biorenewable source to valuable commodity chemicals. *Chem. Soc. Rev.* **2008**, *37* (3), 527-49.
14. Nakamura, C. E.; Whited, G. M., Metabolic engineering for the microbial production of 1,3-propanediol. *Curr. Opin. Biotechnol.* **2003**, *14* (5), 454-459.
15. Saxena, R. K.; Anand, P.; Saran, S.; Isar, J., Microbial production of 1,3-propanediol: Recent developments and emerging opportunities. *Biotechnol. Adv.* **2009**, *27* (6), 895-913.
16. Celinska, E., Debottlenecking the 1,3-propanediol pathway by metabolic engineering. *Biotechnol. Adv.* **2010**, *28* (4), 519-30.
17. Maervoet, V. E. T.; De Mey, M.; Beauprez, J.; De Maeseneire, S.; Soetaert, W. K., Enhancing the Microbial Conversion of Glycerol to 1,3-Propanediol Using Metabolic Engineering. *Org. Process Res. Dev.* **2011**, *15* (1), 189-202.
18. Frazao, C. J. R.; Trichez, D.; Serrano-Bataille, H.; Dagkesamanskaia, A.; Topham, C. M.; Walther, T.; Francois, J. M., Construction of a synthetic pathway for the production of 1,3-propanediol from glucose. *Sci. Rep.* **2019**, *9* (1), 11576.
19. Ju, J. H.; Wang, D.; Heo, S. Y.; Kim, M. S.; Seo, J. W.; Kim, Y. M.; Kim, D. H.; Kang, S. A.; Kim, C. H.; Oh, B. R., Enhancement of 1,3-propanediol production from industrial by-product by *Lactobacillus reuteri* CH53. *Microb. Cell Fact.* **2020**, *19* (1), 6.
20. Schlaf, M., Selective deoxygenation of sugar polyols to alpha,omega-diols and other oxygen content reduced materials--a new challenge to homogeneous ionic hydrogenation and hydrogenolysis catalysis. *Dalton Trans.* **2006**, (39), 4645-53.

21. Bhowmik, S.; Darbha, S., Advances in solid catalysts for selective hydrogenolysis of glycerol to 1,3-propanediol. *Catal. Rev.* **2020**, 1-65.
22. Arundhathi, R.; Mizugaki, T.; Mitsudome, T.; Jitsukawa, K.; Kaneda, K., Highly Selective Hydrogenolysis of Glycerol to 1,3-Propanediol over a Boehmite-Supported Platinum/Tungsten Catalyst. *ChemSusChem* **2013**, 6 (8), 1345-1347.
23. Che, T. M. Production of propanediols. US4642394A, 1987.
24. Drent, E.; Jager, W. w. Hydrogenolysis of glycerol. US6080898A, 2000.
25. Braca, G.; Raspolli Galletti, A. M.; Sbrana, G., Anionic ruthenium iodocarbonyl complexes as selective dehydroxylation catalysts in aqueous solution. *J. Organomet. Chem.* **1991**, 417 (1-2), 41-49.
26. Dykeman, R. R.; Luska, K. L.; Thibault, M. E.; Jones, M. D.; Schlaf, M.; Khanfar, M.; Taylor, N. J.; Britten, J. F.; Harrington, L., Catalytic deoxygenation of terminal-diols under acidic aqueous conditions by the ruthenium complexes  $[(\eta^6\text{-arene})\text{Ru}(\text{X})(\text{N}\cap\text{N})](\text{OTf})_n$ , X=H<sub>2</sub>O, H,  $\eta^6\text{-arene}=\text{p-Me-iPr-C}_6\text{H}_4$ , C<sub>6</sub>Me<sub>6</sub>, N $\cap$ N=bipy, phen, 6,6'-diamino-bipy, 2,9-diamino-phen, n=1, 2). *J. Mol. Catal. A: Chem.* **2007**, 277 (1-2), 233-251.
27. Taher, D.; Thibault, M. E.; Di Mondo, D.; Jennings, M.; Schlaf, M., Acid-, water- and high-temperature-stable ruthenium complexes for the total catalytic deoxygenation of glycerol to propane. *Chem. Eur. J.* **2009**, 15 (39), 10132-43.
28. Thibault, M. E.; DiMondo, D. V.; Jennings, M.; Abdelnur, P. V.; Eberlin, M. N.; Schlaf, M., Cyclopentadienyl and pentamethylcyclopentadienyl ruthenium complexes as catalysts for the total deoxygenation of 1,2-hexanediol and glycerol. *Green Chem.* **2011**, 13 (2), 357-366.
29. Ahmed Foskey, T. J.; Heinekey, D. M.; Goldberg, K. I., Partial Deoxygenation of 1,2-Propanediol Catalyzed by Iridium Pincer Complexes. *ACS Catal.* **2012**, 2 (6), 1285-1289.
30. Choi, J.; MacArthur, A. H.; Brookhart, M.; Goldman, A. S., Dehydrogenation and related reactions catalyzed by iridium pincer complexes. *Chem. Rev.* **2011**, 111 (3), 1761-79.
31. Göttker-Schnetmann, I.; White, P.; Brookhart, M., Iridium Bis(phosphinite)p-XPCP Pincer Complexes: Highly Active Catalysts for the Transfer Dehydrogenation of Alkanes. *J. Am. Chem. Soc.* **2004**, 126 (6), 1804-1811.
32. Lao, D. B.; Owens, A. C. E.; Heinekey, D. M.; Goldberg, K. I., Partial Deoxygenation of Glycerol Catalyzed by Iridium Pincer Complexes. *ACS Catal.* **2013**, 3 (10), 2391-2396.
33. Goldberg, J. M.; Wong, G. W.; Brastow, K. E.; Kaminsky, W.; Goldberg, K. I.; Heinekey, D. M., The Importance of Steric Factors in Iridium Pincer Complexes. *Organometallics* **2015**, 34 (4), 753-762.
34. Goldberg, J. M.; Goldberg, K. I.; Heinekey, D. M.; Burgess, S. A.; Lao, D. B.; Linehan, J. C., Detection of an Iridium-Dihydrogen Complex: A Proposed Intermediate in Ionic Hydrogenation. *J. Am. Chem. Soc.* **2017**, 139 (36), 12638-12646.
35. Finn, M.; Ridenour, J. A.; Heltzel, J.; Cahill, C.; Voutchkova-Kostal, A., Next-Generation Water-Soluble Homogeneous Catalysts for Conversion of Glycerol to Lactic Acid. *Organometallics* **2018**, 37 (9), 1400-1409.
36. Walsh, J. J.; Neri, G.; Smith, C. L.; Cowan, A. J., Water-Soluble Manganese Complex for Selective Electrocatalytic CO<sub>2</sub> Reduction to CO. *Organometallics* **2018**, 38 (6),

1224-1229.

37. Kang, P.; Meyer, T. J.; Brookhart, M., Selective electrocatalytic reduction of carbon dioxide to formate by a water-soluble iridium pincer catalyst. *Chem. Sci.* **2013**, *4* (9), 3497-3502.
38. Kang, P.; Cheng, C.; Chen, Z.; Schauer, C. K.; Meyer, T. J.; Brookhart, M., Selective electrocatalytic reduction of CO<sub>2</sub> to formate by water-stable iridium dihydride pincer complexes. *J. Am. Chem. Soc.* **2012**, *134* (12), 5500-3.
39. Göttker-Schnetmann, I.; White, P. S.; Brookhart, M., Synthesis and Properties of Iridium Bis(phosphinite) Pincer Complexes (p-XPCP)IrH<sub>2</sub>, (p-XPCP)Ir(CO), (p-XPCP)Ir(H)(aryl), and {(p-XPCP)Ir}<sub>2</sub>{μ-N<sub>2</sub>} and Their Relevance in Alkane Transfer Dehydrogenation. *Organometallics* **2004**, *23* (8), 1766-1776.
40. Hansch, C.; Leo, A.; Taft, R. W., A Survey of Hammett Substituent Constants and Resonance and Field Parameters. *Chem. Rev.* **1991**, *91* (2), 165-195.
41. Gitnes, R. M.; Wang, M.; Bao, Y.; Scheuermann, M. L., In Situ Generation of Catalytically Relevant Nanoparticles from a Molecular Pincer Iridium Precatalyst during Polyol Deoxygenation. *ACS Catal.* **2021**, *11* (2), 495-501.
42. Punji, B.; Emge, T. J.; Goldman, A. S., A Highly Stable Adamantyl-Substituted Pincer-Ligated Iridium Catalyst for Alkane Dehydrogenation. *Organometallics* **2010**, *29* (12), 2702-2709.
43. Goldberg, J. M.; Cherry, S. D. T.; Guard, L. M.; Kaminsky, W.; Goldberg, K. I.; Heinekey, D. M., Hydrogen Addition to (pincer)Ir(CO) Complexes: The Importance of Steric and Electronic Factors. *Organometallics* **2016**, *35* (20), 3546-3556.
44. Fulmer, G. R.; Miller, A. J. M.; Sherden, N. H.; Gottlieb, H. E.; Nudelman, A.; Stoltz, B. M.; Bercaw, J. E.; Goldberg, K. I., NMR Chemical Shifts of Trace Impurities: Common Laboratory Solvents, Organics, and Gases in Deuterated Solvents Relevant to the Organometallic Chemist. *Organometallics* **2010**, *29* (9), 2176-2179.
45. Roberto, D.; Cariati, E.; Psaro, R.; Ugo, R., Formation of [Ir(CO)<sub>2</sub>Cl]<sub>x</sub> (x = 2, n) Species by Mild Carbonylation of [Ir(cyclooctene)<sub>2</sub>Cl]<sub>2</sub> Supported on Silica or in Solution: A New Convenient Material for the Synthesis of Iridium(I) Carbonyl Complexes. *Organometallics* **1994**, *13* (11), 4227-4231.

## Chapter 3: Investigations of Immobilized (<sup>t</sup>BuPOCOP)Ir(CO) as a Catalyst for Dehydrogenation and Hydrogenation Reactions

### 3.1 Introduction

#### 3.1.1 Production of Light Olefins

Light olefins (C<sub>2</sub>-C<sub>4</sub>) are versatile building block chemicals used to produce a wide range of chemicals, including polymers (polyethylene, polypropylene) and oxygenates (ethylene glycol, propylene oxide).<sup>7, 46, 47</sup> Annual global demand of light olefins exceeds hundreds of millions of tons.<sup>46, 48-51</sup> The leading technology for light olefin production is steam cracking of naphtha, a flammable hydrocarbon mixture that originates from distillation of crude oil. In the steam cracking process, naphtha feedstock, mixed with steam, is cracked, or broken down, at high temperature (775 – 950 °C).<sup>52</sup> Steam cracking of a typical naphtha mix produces approximately 18% methane, 34% ethylene, 14% propylene, and 8% C<sub>4</sub> gases, and C<sub>5</sub>+ hydrocarbons constitute the rest. Product separation increases the overall cost of the process. Recent developments in shale fracking and the large availability of natural gas drove a feedstock change for many new crackers from naphtha to ethane, the second largest component of natural gas.<sup>7, 50</sup> The steam cracking of ethane yields ethylene with 80% selectivity, while other olefins are produced in low amounts.<sup>8, 48, 53</sup> The chemical industry is searching for new methods to produce propylene and several highly selective (90%) catalytic propane dehydrogenation processes have recently been implemented industrially: Catofin by Lummus, Oleflex by UOP, STAR by Uhde, and Fluidized Bed Dehydrogenation (FBD) by Yarsintez-Snamprogetti.<sup>7, 8, 49, 50, 54</sup> Because dehydrogenation of alkanes is an endothermic and equilibrium-limited reaction, these processes require high temperature operation (500 – 700 °C). Coke formation is favored at high temperatures, and this leads to catalyst deactivation and low selectivities. Catalyst regeneration, to remove unwanted coke, necessitates significant down time of the reactors. Therefore, a selective, low temperature,

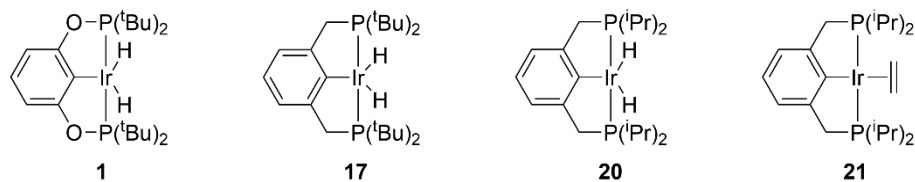


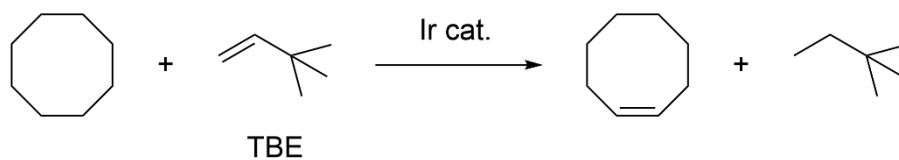
**Figure 3-1.** Ir Pincer complexes examined for (transfer) dehydrogenation of alkanes.

energy-efficient catalytic system for alkane dehydrogenation is sought.

### 3.1.2 Pincer Complexes as Dehydrogenation Catalysts

In the search for selective catalytic dehydrogenation systems, homogeneous, transition-metal complexes have shown significant promise. An initial report by Crabtree demonstrated that cyclopentane and cyclooctane were dehydrogenated by  $[\text{IrH}_2(\text{acetone})_2(\text{PPh}_3)_2][\text{BF}_4]$  to yield the corresponding cyclic olefin bound Ir species in the presence of 3,3-dimethyl-1-butene (*tert*-butylethylene, TBE) as a sacrificial hydrogen acceptor.<sup>55</sup> This reaction represents a transfer dehydrogenation reaction wherein the  $\text{H}_2$  produced from dehydrogenation of an alkane substrate hydrogenates a sacrificial olefin. Following this work by Crabtree, catalytic transfer dehydrogenation by monodentate phosphine-ligated Re or Ir complexes were reported with low activity by Felkin and Crabtree.<sup>56, 57</sup> Remarkable progress was made with the discovery of  $(^{\text{tBu}}\text{PCP})\text{Ir}(\text{H})_2$  ( $^{\text{R}}\text{PCP} = \kappa^3\text{-C}_6\text{H}_3\text{-2,6-(CH}_2\text{PR}_2)_2$ ) (**17**) as a catalyst for transfer dehydrogenation of cyclooctane by Kaska and Jensen (Scheme 3-1).<sup>58</sup> In the presence of TBE, a TOF of  $12 \text{ min}^{-1}$  was achieved at  $200^\circ\text{C}$  and the catalyst was stable for up to one week at this temperature. The catalytic activity was limited by the hydrogen acceptor TBE, and incremental additions of TBE during the reaction enabled up to 1000 TON to be realized. Brookhart found that, when the ligand was changed to phosphinite-based  $(^{\text{tBu}}\text{POCOP})\text{Ir}(\text{H})_2$  ( $^{\text{R}}\text{POCOP} = \kappa^3\text{-C}_6\text{H}_3\text{-2,6-(OPR}_2)_2$ ) (**1**), in the

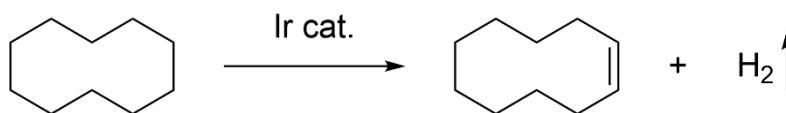
**Scheme 3-1.** Catalytic transfer dehydrogenation of cyclooctane.



presence of TBE, the catalytic transfer dehydrogenation of cyclooctane occurred with an initial TOF of  $115 \text{ min}^{-1}$  and TON of up to 3000.<sup>59</sup>

The thermal stability of pincer complexes also allowed the catalytic dehydrogenation of alkane without any sacrificial olefin. This acceptorless dehydrogenation requires high reaction temperatures due to the unfavorable thermodynamics. For efficient acceptorless dehydrogenation,  $\text{H}_2$  is removed from the reaction mixture to drive the reaction forward. Jensen and Goldman reported the dehydrogenation of cyclodecane (Scheme 3-2) catalyzed by **17** with TON of 170 and 360 after 4 and 24 h, respectively, at refluxing temperature ( $201 \text{ }^\circ\text{C}$ ).<sup>60</sup> Goldman discovered that the less sterically bulky *iso*-propyl derivative of PCP complex,  $(i\text{PrPCP})\text{Ir}(\text{H})_2$  (**20**), was more active for the acceptorless dehydrogenation of cyclodecane. After 1 h, 406 TONs were observed, and the TOF increased by an order of magnitude compared to **17**.<sup>61</sup> In the same report, an acceptorless dehydrogenation of *n*-undecane catalyzed by **20** was observed for the first time.<sup>61</sup> Interestingly, Krogh-Jespersen and Goldman demonstrated that  $(i\text{PrPCP})\text{Ir}(\text{C}_2\text{H}_4)$  (**21**) is an active heterogeneous catalyst for gas-phase pentane/propene transfer dehydrogenation with an initial TOF of  $3780 \text{ h}^{-1}$  at  $240 \text{ }^\circ\text{C}$  and that heterogeneous dehydrogenation yielded greater  $\alpha$ -olefin selectivity compared to the homogeneous solution-phase system.<sup>62</sup> While the pincer-ligated Ir complexes are catalytically active for alkane dehydrogenation reactions under milder conditions than current industrial processes, their activities are too low ( $\text{TON} \leq 1000$ ) to be useful in industrial applications.<sup>10</sup>

**Scheme 3-2. Acceptorless dehydrogenation of cyclodecane.**



### 3.1.3 Immobilization of Homogeneous Catalysts

Despite the advances in homogeneous catalysts, industrial catalytic processes mostly use heterogeneous catalysts (80%).<sup>63</sup> Heterogeneous catalysts have a significant advantage in that they, by definition, are easily separated from the reaction mixture and can be recycled or used in continuous systems. Another advantage of heterogeneous catalysts is that they often are

more robust and can be utilized under forcing conditions (high temperature, high pressure). Although these advantages enable their use in industrial settings, drawbacks to heterogeneous catalysts also exist. Because the reaction occurs at the reagent/catalyst interface (usually gas/solid or liquid/solid), only a fraction of metals near the surface are actively involved in catalysis. Furthermore, the presence of multiple active sites both leads to unselective reactions and complicates mechanistic studies.

Homogeneous catalysts, on the other hand, hold some advantages over heterogeneous ones. They can be highly active and selective under mild reaction conditions and can be systematically tuned to improve activity and selectivity. Catalyst optimization typically occurs through modifications to the ligand framework. Since homogeneous catalysts can be characterized by solution-phase techniques such as NMR, IR, or UV-Vis spectroscopies, along with other methods, their structures can be well-defined and we can develop good understanding of the active species. Based on the understanding of the active species and mechanisms, the ligand can be finely tuned to achieve the desired activity and selectivity. The major drawbacks of homogeneous catalysts are their inefficient separation from reaction mixtures and difficulty of catalyst recycling.

A new approach has been taken to develop a supported catalyst, which leverages the advantages of both homogeneous and heterogeneous catalysts. These supported catalysts are prepared by immobilizing homogeneous catalysts on heterogeneous support materials, with the aim to achieve highly selective, robust, *and* easily separated catalysts.

#### 3.1.4 Complicating Issues of Immobilization

There are consistently questions regarding the nature of immobilized catalysts. One key issue is that the molecular complex can detach from the support and leach into the reaction mixture. For an active catalytic system, it must be considered whether the active catalytic species is on the support (heterogeneous) or is detached from the support (homogeneous). In examples of immobilized catalysts for cross-coupling reactions, Pd complexes frequently leach from the

support and became homogeneous, catalytically active Pd species.<sup>64</sup> Specifically, Richardson and Jones prepared a mercaptopropyl-modified mesoporous silica, and they found that this modified silica can be used as not only the support material for immobilization but also a poison for any detached Pd species during catalysis.<sup>65</sup> Hot filtration and poisoning tests suggest that the cross-coupling reaction is not catalyzed by the immobilized Pd complex, but instead by soluble Pd species homogeneously. Additionally, leaching can cause deactivation of the catalysis through intermolecular interactions between homogeneous metal species.

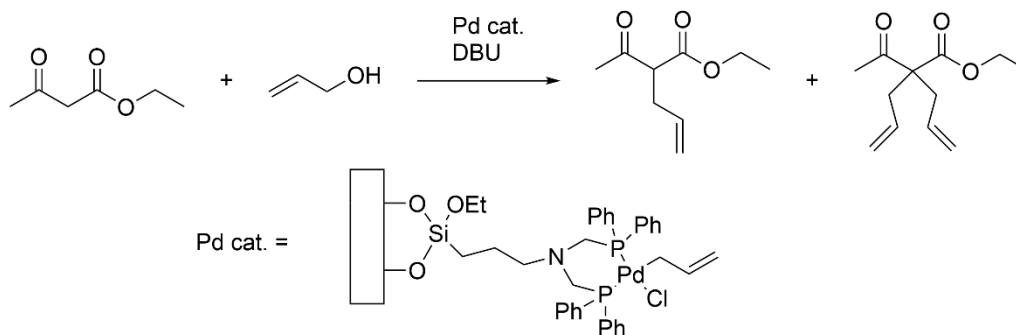
Although leaching is against the initial purpose of immobilization, some groups decided to take advantage of leaching, especially for olefin metathesis reactions.<sup>66-68</sup> In a proposed 'release-return' mechanism, the immobilized complex is a precatalyst or a reservoir of the active species, which are released during the reaction and re-captured by the support. This type of release and recapture provides efficient homogeneous catalysis with the ability to recover and re-use the catalyst. While this approach is quite interesting, much of the focus in the field is on the minimization of catalyst leaching.

Another key issue to consider in supported catalysis is how the support itself affects the overall reactivity. Despite some examples exhibiting improved activities over their homogeneous counterparts,<sup>69-71</sup> immobilization often lowers the catalytic activity, rendering the immobilized catalyst difficult to be adopted industrially.<sup>72</sup> Other reports have demonstrated that the support material offers significant benefits in catalysis. For example, when the homogeneous catalysts are site-isolated on the surface of the support, reactive or coordinatively unsaturated species are physically separated and this separation prevents some deactivation pathways such as dimerization.<sup>73-75</sup> In addition, multiple functionalities can co-exist, even if they may not be compatible with each other in solution. For example, sulfonic acid groups and amine groups have been co-immobilized on silica by Davis.<sup>76</sup> In solution, sulfonic acids would protonate the amine leading to precipitation out of solution; the physical separation imparted by immobilization enables these functional groups to be used in the same reaction. Metal complexes can also be co-

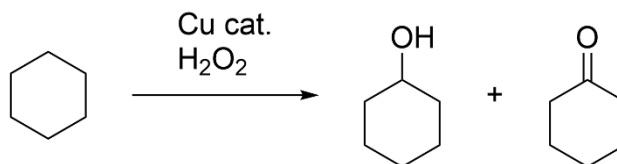
immobilized with acid<sup>77, 78</sup> or base.<sup>79, 80</sup>

Immobilization in the pores of the support often affects the activity, selectivity, or stereoselectivity due to confinement effects. Mesoporous silica-supported Pd catalysts were prepared with various pore sizes by Motokura.<sup>81</sup> During Pd-catalyzed allylation (Scheme 3-3), optimal catalytic activity was achieved using a pore size of 23 Å, while smaller or larger pore sizes led to decreased activity. Additionally, Fan and Li demonstrated that encapsulation of a homogeneous complex can have a beneficial impact on catalysis and that the uniform pore size provided size-selectivity.<sup>82</sup> When tris(1,10-phenanthroline) Cu complex encapsulated in MIL-100(Al) materials was subjected to cyclohexane oxidation reactions (Scheme 3-4), the catalytic activity of the confined catalyst was higher than its free homogeneous counterpart or the Cu precursor alone. Encapsulation was achieved by assembling the Cu complex inside the pores of the support material. Once assembled, this complex became too large to escape and was trapped inside the pore (encapsulation). Interestingly, the catalytic activity decreased with increasing substrate size from cyclohexane to cycloheptane and cyclooctane, while the

**Scheme 3-3. Pd-catalyzed allylation of ethyl acetoacetate with DBU.**



**Scheme 3-4. Cu-catalyzed cyclohexane oxidation.**



homogeneous complex gave comparable results for all three substrates.

To develop a robust immobilized catalyst, a sufficiently strong interaction between the homogeneous catalyst and the support material is required to minimize leaching of metal species. This interaction/attachment may be accomplished by including chelating ligands and/or utilizing a covalent tethering method. Additionally, a good understanding of both the homogeneous catalyst and support material is helpful in selecting the combination of the catalyst and the support for a specific reaction.

### 3.1.5 Immobilized Pincer Complexes

The immobilization of transition-metal pincer complexes has been attempted previously and these attempts were reviewed in detail.<sup>83</sup> For transfer dehydrogenation of cyclooctane, (tBu<sub>2</sub>PO-<sup>t</sup>BuPOCOP)Ir(C<sub>2</sub>H<sub>4</sub>) (**22**) was immobilized on  $\gamma$ -Al<sub>2</sub>O<sub>3</sub>. At 200 °C with TBE as hydrogen acceptor, a TON over 4000 was achieved, which was higher than that using the homogeneous counterpart (2660 TON).<sup>84</sup> This immobilized catalyst was recycled once but with diminished TON of 1520. The alumina support catalyzed the isomerization of TBE to 2,3-dimethyl-2-butene (DM2B) and 2,3-dimethyl-1-butene (DM1B), which are both poor hydrogen acceptors compared to TBE. When the alumina was modified with Na<sub>2</sub>O, the isomerization was reduced to 1-2%. Minimal leaching (0.007%) was observed during the reaction. A follow-up study confirmed that **22** was immobilized with a simultaneous loss of phosphine oxide and the covalent tethering at the ligand backbone (Scheme 3-5, top).<sup>85</sup> In contrast, Mezzetti observed that unfunctionalized **1** was bound to the surface through the Ir atom when reacted with surface hydroxyl group (Scheme 3-5, bottom).<sup>86</sup>

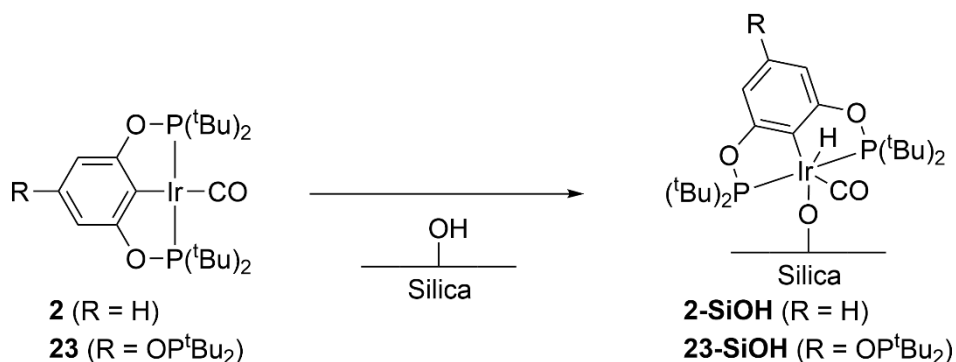
To improve the atom economy and lower the cost of dehydrogenation, acceptorless dehydrogenation is desired instead of using sacrificial olefins. However, acceptorless dehydrogenation reactions in sealed vessels, similar to the gas-phase transfer dehydrogenation of pentane reported by Krogh-Jespersen and Goldman,<sup>62</sup> are limited by thermodynamics.



Ir-bound P(<sup>t</sup>Bu)<sub>2</sub> groups and a doublet signal at 1.08 ppm is from the free P(<sup>t</sup>Bu)<sub>2</sub> group in the ligand backbone. In the <sup>31</sup>P{<sup>1</sup>H} NMR spectrum, two signals were observed in a 2:1 ratio from these two types of P(<sup>t</sup>Bu)<sub>2</sub> groups. A CO stretching frequency of **23** was observed at 1928 cm<sup>-1</sup> (ATR), consistent with the reported values at 1932 cm<sup>-1</sup> (ATR)<sup>87</sup> or 1934 cm<sup>-1</sup> (nujol).<sup>84</sup>

Immobilization was performed by dissolving **23** in benzene, toluene, or pentane and stirring vigorously with silica. The silica turned from white to yellow upon immobilization. The initial attempt of immobilization by stirring for two hours in benzene resulted in two signals in CO stretching frequency region: 1955 and 2050 cm<sup>-1</sup> by Diffuse Reflectance Infrared Fourier-Transform Spectroscopy (DRIFTS). When the stirring period was extended to at least 16 hours, the signal at 2050 cm<sup>-1</sup> disappeared and only the signal at 1955 cm<sup>-1</sup> remained. The signal at 1955 cm<sup>-1</sup> corresponds to **23** anchored through the ligand backbone (**23-SiO<sub>2</sub>**), (the reported IR stretching frequency is 1945 cm<sup>-1</sup>).<sup>87</sup> A possible species for the signal at 2050 cm<sup>-1</sup> is **23** grafted on the silica through the metal center (**23-SiOH**) by oxidatively adding a surface hydroxyl group (Scheme 3-6). When the unsubstituted variant, (<sup>t</sup>Bu<sub>2</sub>POCOP)Ir(CO) (**2**) was grafted on silica through the metal center, **2-SiOH** had a CO stretching frequency at 2026 cm<sup>-1</sup> (Scheme 3-6) and could return to the molecular complex **2** by reductive elimination, indicated by solid-state <sup>1</sup>H and <sup>31</sup>P NMR and IR spectroscopies.<sup>86</sup> The grafted complex **23-SiOH** may be an intermediate that eventually converts to the anchored complex **23-SiO<sub>2</sub>**. The immobilization was also analyzed with ICP-OES, and the Ir

**Scheme 3-6. Immobilization of (<sup>t</sup>Bu<sub>2</sub>POCOP)Ir(CO) by oxidative addition of surface silanol.**



loading of **23-SiO<sub>2</sub>** was determined to be  $0.77 \pm 0.02$  wt%. The theoretical loading of Ir is 0.8 wt% based on the amount of **23** (50 mg) used for immobilization on silica (150 mg).

To assess the reactivity of **23-SiO<sub>2</sub>**, it was screened for propane dehydrogenation at elevated temperatures (left graph in Figure 3-2). Propane was dehydrogenated above 320 °C, and the activity was stable up to 400 °C for two hours with rates as high as  $363 \text{ h}^{-1}$ . Above 400 °C, the activity started to decline, although the initial rate was faster at higher temperatures. The initial rate was  $636 \text{ h}^{-1}$  at 440 °C and  $927 \text{ h}^{-1}$  at 480°C, and then the rates after two hours at the same temperature dropped by 10 %. The color of the catalyst was yellow initially but turned grey after the reaction at elevated temperatures, indicating the decomposition of **23-SiO<sub>2</sub>**. Goldman and Celik determined the catalyst was stable up to 340 °C and noted a similar color change and decomposition of the catalyst above 340 °C.<sup>87</sup> The origin of the enhanced stability observed for **23-SiO<sub>2</sub>** in our system may be due to a discrepancy in the location of the thermocouple. The recorded temperature for our system was the temperature reading of the heating unit whereas the temperature was measured directly at the catalyst bed in Goldman and Celik's system. When the mesoporous silica was replaced by amorphous silica (right graph in Figure 3-2), the reaction rates were comparable to those with mesoporous silica, and a decline in catalyst activity was also observed above 400 °C. These data revealed that the dehydrogenation of propane is not dependent on the morphology of the support, verifying that the support does not influence the

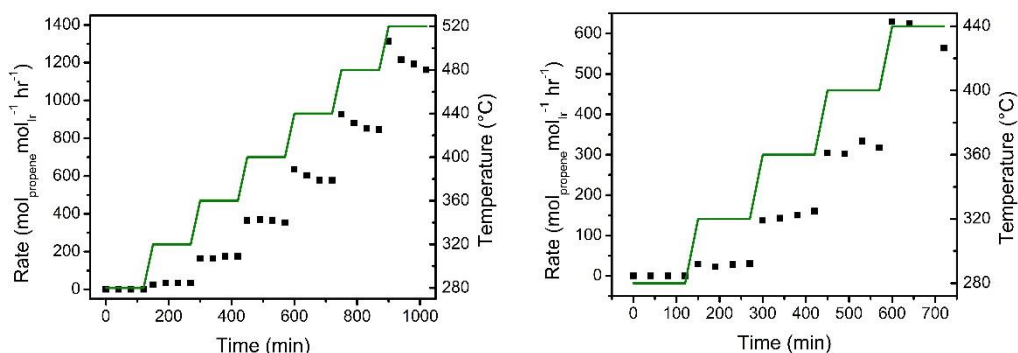


**Figure 3-2.** Propane dehydrogenation by **23-SiO<sub>2</sub>** with mesoporous silica (left) or amorphous silica (right). Conditions:  $V_{\text{total}} = 20 \text{ mL/min}^{-1}$ ,  $P_{\text{propane}} = 0.25 \text{ atm}$ ,  $P_{\text{He}} = 0.75 \text{ atm}$ ,  $P_{\text{total}} = 1 \text{ atm}$ , Temp = 280 – 520 °C (green line).

activity of the catalyst. Analysis of **23-SiO<sub>2</sub>** by DRIFTS at varying temperature revealed that the CO stretching frequency at 1955 cm<sup>-1</sup> disappeared at 250 °C or higher. The loss of the CO stretching frequency is consistent with the formation of the three-coordinate, open-site (t<sup>Bu</sup>POCOP)Ir species, formed after the dissociation of CO ligand proposed to be the active catalyst in dehydrogenation reactions.<sup>87</sup>

The immobilized complex **23-SiO<sub>2</sub>** was examined for the hydrogenation of toluene, a commonly studied reaction in heterogeneous catalysis (Figure 3-3). While Ir nanoparticles supported on silica catalyzed the complete hydrogenation of toluene to methylcyclohexane at 200 °C, **23-SiO<sub>2</sub>** showed no catalytic activity at the same temperature based on GC-MS analysis. Based on the observation that the molecular catalyst **2** is also not active for toluene hydrogenation, this result demonstrates the reactivity of **23-SiO<sub>2</sub>** more closely resembles that of the homogeneous complex.

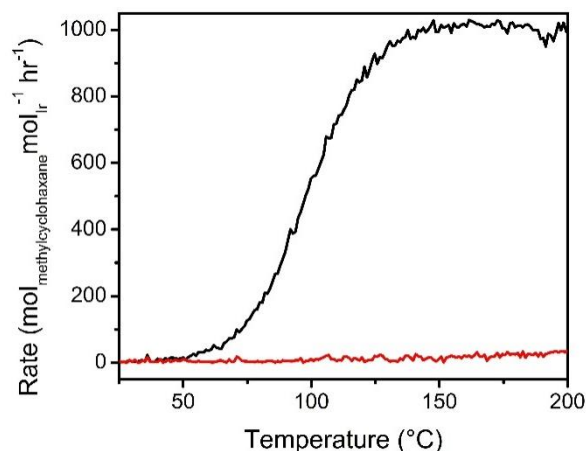


**Figure 3-3.** Toluene hydrogenation by **23-SiO<sub>2</sub>** (Red) and **IrO<sub>x</sub>-SiO<sub>2</sub>** (Black). Conditions: 1 bar (3% toluene, 97% H<sub>2</sub>); preheated under He flow at 340 °C prior to reaction.

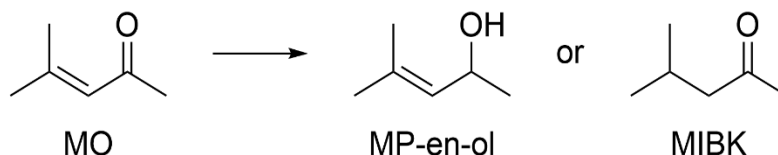
### 3.2.2 Selective Hydrogenation of Mesityl Oxide

We explored the feasibility of selective hydrogenation of unsaturated carbonyl compounds to unsaturated alcohols by **23-SiO<sub>2</sub>**. Unsaturated alcohols are used as fragrances and pharmaceuticals, and green approaches to synthesis of these compounds are desired.<sup>88</sup> Instead of using stoichiometric amounts of hydride-donor reagents such as LiAlH<sub>4</sub> or NaBH<sub>4</sub>, a catalytic

system is desired for greener process. The selective hydrogenation of C=O bond in an  $\alpha,\beta$ -unsaturated ketone is difficult because the C=C bond could be hydrogenated instead or both C=O and C=C bond can be hydrogenated to yield a saturated alcohol.<sup>89</sup>

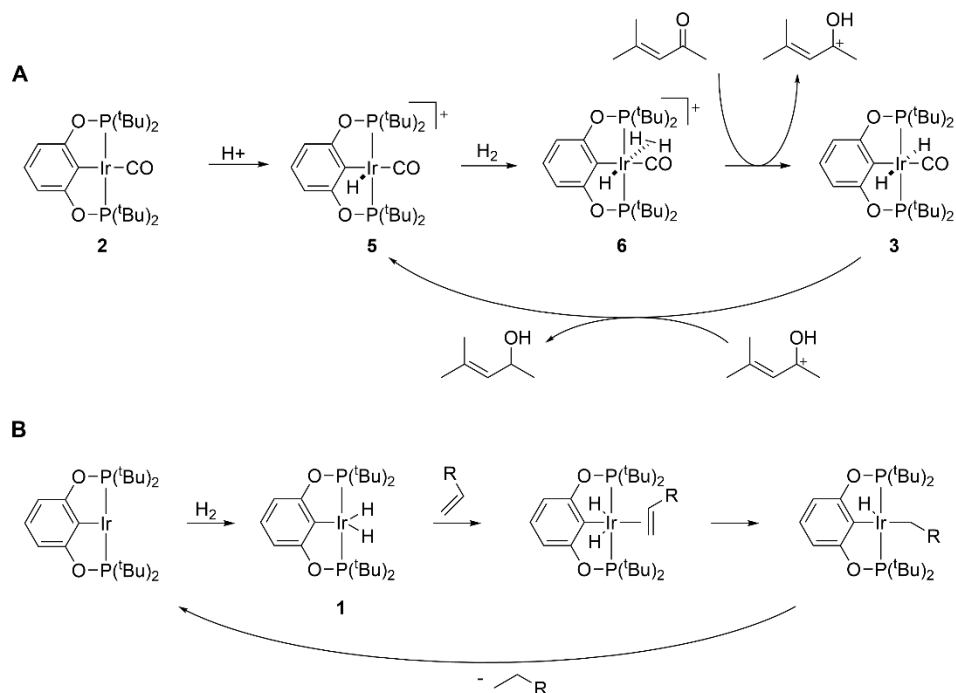
To investigate the reactivity of our supported Ir catalyst for hydrogenation, we chose a simple unsaturated ketone, mesityl oxide (MO), as a substrate (Scheme 3-7). First, the homogeneous complex **2** was tested for hydrogenation of MO in solution-phase and found to hydrogenate the C=O bond selectively to yield 4-methyl-3-penten-2-ol (MP-en-ol) with 2.9% conversion after 20 h at 60 °C. The slow rate of MP-en-ol formation may be attributed to the slow reaction of hydrogen with **2** to form the active species (POCOP)Ir(CO)(H)<sub>2</sub> (**3** in Scheme 3-8A), presumably assisted by adventitious HCl or H<sub>2</sub>O present in CDCl<sub>3</sub>. In a continuous-flow system, the hydrogenation of MO was catalyzed by **23-SiO<sub>2</sub>** to yield methyl isobutyl ketone (MIBK) exclusively. The switch in selectivity from MP-en-ol to MIBK likely results from different operative mechanisms in the homogeneous vs heterogeneous systems.

**Scheme 3-7. Selective hydrogenation of MO.**



The homogeneous catalyst **2** is proposed to operate via mechanism **A** (Scheme 3-8) demonstrated by the CO ligand remaining intact throughout the reaction. The complex is protonated in solution and the cationic Ir center binds H<sub>2</sub>. A proton and hydride are then transferred to the substrate sequentially. For the heterogeneous catalyst **23-SiO<sub>2</sub>**, mechanism **B** (Scheme 3-8) is proposed. Before the reaction, **23-SiO<sub>2</sub>** was pretreated at high temperatures (340 °C) where CO ligand dissociation occurs to generate the reactive three-coordinate, open-site Ir(I) species. This three-coordinate, 14-electron intermediate readily undergoes oxidative addition with H<sub>2</sub>. The Ir(H)<sub>2</sub> species then binds alkene, and subsequent insertion and reductive elimination yield the

**Scheme 3-8 A: Outer-sphere ionic hydrogenation mechanism; B: Inner-sphere oxidative addition mechanism.**



hydrogenated product. The hydrogenation of MO was also examined with heterogeneous catalyst  $\text{IrO}_x\text{-SiO}_2$ , resulting in MIBK exclusively but at a faster rate than with  $\text{23-SiO}_2$  (Figure 3-4).

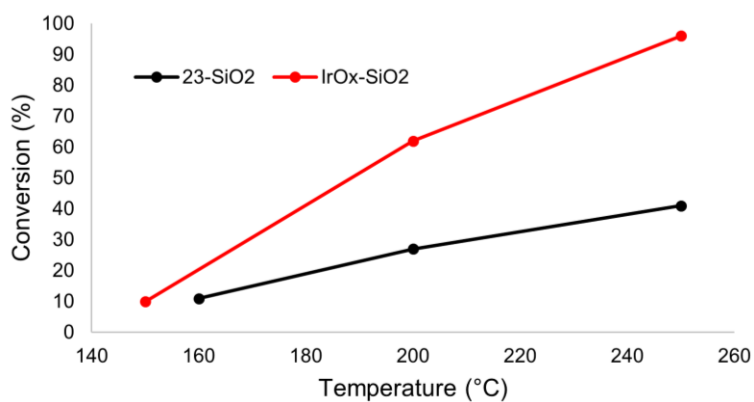


**Figure 3-4.** MO hydrogenation by  $\text{23-SiO}_2$  and  $\text{IrO}_x\text{-SiO}_2$  to MIBK. Conditions: 1 bar (5% MO, 95%  $\text{H}_2$ ); preheated under He flow at 340 °C prior to reaction.

We chose to implement two major changes to the catalyst preparation and reaction conditions in an attempt to enable mechanism **A** with the supported catalyst **23-SiO<sub>2</sub>**. First was to pretreat **23-SiO<sub>2</sub>** either at room temperature or at 150 °C to retain CO bound to Ir during the reaction. The bound CO ligand should inhibit the mechanism **B** as the reactive, open-site Ir(I) species would not be accessible. A second change was to add water to the reaction mixture. Previously, water has been proposed to promote the formation of (t<sup>Bu</sup>POCOP)Ir(CO)(H)<sub>2</sub> (**3**) in the presence of H<sub>2</sub> by acting as a proton source.<sup>29</sup> With these changes, the hydrogenation reactions were conducted, and water was introduced at two different concentrations. There was no effect of water addition on activity and selectivity, and MIBK was still the only observed product (Figure 3-5). The activity increased significantly above 200 °C as the dissociation of CO ligand occurs more readily at higher temperatures. To determine if **23-SiO<sub>2</sub>** can hydrogenate C=O bonds at all, other carbonyl compounds were hydrogenated. 5-methyl furfural resulted in 5-methyl furfuryl alcohol selectively (Scheme 3-9, top). Sulcatone (6-methyl-5-hepten-2-one) gave a mixture of products with 37% selectivity of the C=O hydrogenated product (Scheme 3-9, bottom). These results suggest that **23-SiO<sub>2</sub>** is capable of hydrogenating C=O bonds and that the tautomerization of MP-

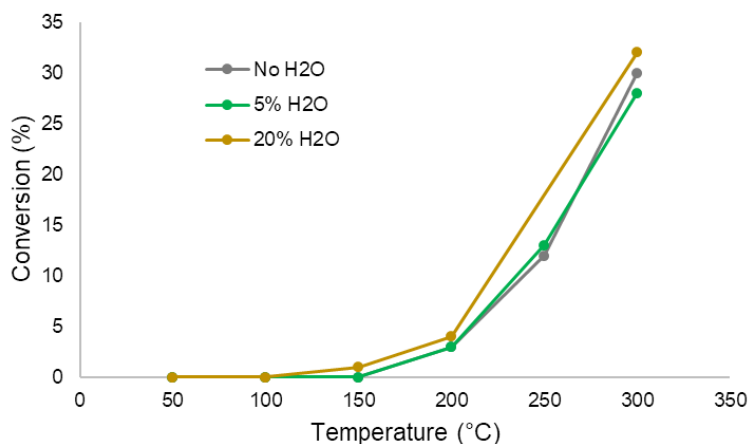
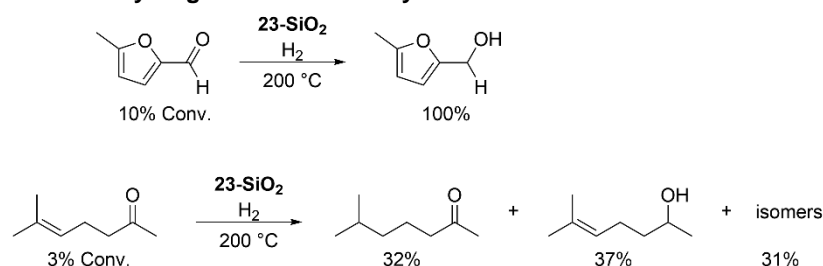


**Figure 3-5.** MO hydrogenation to MIBK with added water. Conditions: 1 bar (5% MO, 95% H<sub>2</sub>), Pretreated at RT (No H<sub>2</sub>O); 1 bar (5% MO, 5% H<sub>2</sub>O, 90% H<sub>2</sub>), Pretreated with 5% H<sub>2</sub>O at 150 °C (5% H<sub>2</sub>O); 1 bar (5% MO, 20% H<sub>2</sub>O, 75% H<sub>2</sub>), Pretreated with 20% H<sub>2</sub>O at 150 °C (20% H<sub>2</sub>O).

### Scheme 3-9. Hydrogenation of carbonyl substrates.



en-ol to MIBK may occur after the initial hydrogenation of the C=O bond in MO. The tautomerization, or isomerization, of enol to ketone is well documented.<sup>90</sup>

Additionally, we explored the possibility of increasing the rate of hydrogenation. It is known that  $(\text{tBuPOCOP})\text{Ir}(\text{CO})(\text{H})_2$  (**3**) cannot be formed from  $(\text{tBuPOCOP})\text{Ir}(\text{CO})$  (**2**) without an acid, indicating that the formation of **3** is more facile from  $(\text{tBuPOCOP})\text{Ir}(\text{CO})(\text{H})^+$  (**5**).<sup>43</sup> Similarly, an immobilized, cationic  $\text{Ir}(\text{CO})(\text{H})$  species (analogous to **5** in Scheme 3-8) may incorporate  $\text{H}_2$  faster, leading to the improved rate of hydrogenation. This immobilized, cationic species can be prepared either by protonating **23** and then supporting on the silica or by protonating already-immobilized **23-SiO<sub>2</sub>**. In a preliminary study,  $\text{HNTf}_2$  (1 or 2 equiv.) was added to the suspension of **23-SiO<sub>2</sub>** in pentane. Although  $\text{HNTf}_2$  was not soluble in pentane, the color change from yellow to light orange was observed, consistent with the color change of **2** upon protonation, while no change was observed based on IR spectroscopy. Based on the spectroscopic observation, the protonation of **23-SiO<sub>2</sub>** by  $\text{HNTf}_2$  was inconclusive. When this acid-treated **23-SiO<sub>2</sub>** was tested for the hydrogenation of MO, 87% conversion to MIBK was achieved at 300 °C while neutral **23-SiO<sub>2</sub>** gave 30% conversion (Figure 3-6). The origin of the accelerated rate with the acid-treated **23-SiO<sub>2</sub>** was not understood yet.

### 3.3 Conclusion

Synthesis and immobilization of **23** on silica were successfully reproduced. Propane was catalytically dehydrogenated by **23-SiO<sub>2</sub>** at the rate of 363  $\text{h}^{-1}$  at 400 °C. Comparable rates were observed when the support material was changed from mesoporous silica to amorphous silica, demonstrating no dependence on the morphology of silica. Toluene hydrogenation was examined

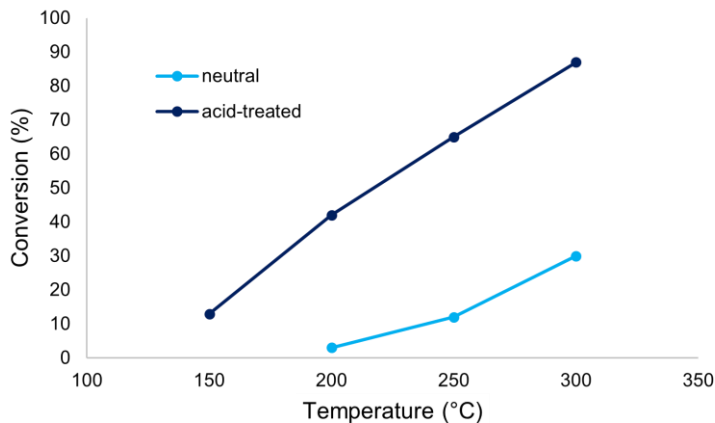


**Figure 3-6.** MO hydrogenation to MIBK catalyzed by neutral **23-SiO<sub>2</sub>** (Light Blue) or acid-treated **23-SiO<sub>2</sub>** (Dark Blue). Conditions: 1 bar (5% MO, 95% H<sub>2</sub>), Pretreated at RT.

with molecular catalyst **2**, immobilized catalyst **23-SiO<sub>2</sub>**, and Ir nanoparticle catalyst **IrO<sub>x</sub>-SiO<sub>2</sub>**. No activity was observed with **2** and **23-SiO<sub>2</sub>** while toluene was fully hydrogenated to methylcyclohexane with **IrO<sub>x</sub>-SiO<sub>2</sub>**, indicating that **23-SiO<sub>2</sub>** is more akin to the homogeneous form of the catalyst.

The feasibility of selective hydrogenation by **23-SiO<sub>2</sub>** was examined with mesityl oxide (MO) as a substrate. In a homogeneous system with **2**, mesityl oxide was hydrogenated at the C=O bond, resulting in 4-methyl-3-penten-2-ol (MP-en-ol) exclusively. In a continuous-flow system with **23-SiO<sub>2</sub>**, the only observed product was methyl isobutyl ketone (MIBK). The selectivity switch was attributed to different active species and different mechanisms. The pretreatment of **23-SiO<sub>2</sub>** at 340 °C promoted dissociation of the CO ligand, leading to the three-coordinate, open-site Ir(I) species. To direct the selectivity towards to MP-en-ol, pretreatment at low temperature and cofeeding of water were implemented. However, MIBK was still the sole observed product. Unfortunately, MO was hydrogenated to MIBK with **IrO<sub>x</sub>-SiO<sub>2</sub>** at a faster rate than with **23-SiO<sub>2</sub>**. To test whether **23-SiO<sub>2</sub>** is capable of the hydrogenation of C=O bonds, 5-methyl furfural and sulcatone were employed as a substrate. With the furfural substrate, 5-methyl furfuryl alcohol was observed as the only product, and sulcatone was hydrogenated at the C=O bond at 37% selectivity. Because the ketone product is generally more thermodynamically favorable than the unsaturated alcohol obtained upon hydrogenation of the carbonyl, it is possible that isomerization of MP-en-ol to MIBK occurs under

the reaction conditions eroding any potential selectivity of this reaction, though this remains to be tested.

### 3.4 Experimental

All experiments and manipulations were performed using standard Schlenk techniques under an argon atmosphere or in a nitrogen-filled glovebox unless otherwise specified. Benzene, pentane, and toluene were passed through columns containing activated alumina and molecular sieves. C<sub>6</sub>D<sub>6</sub> was dried over Na<sup>0</sup>/benzophenone. <sup>1</sup>H, <sup>31</sup>P{<sup>1</sup>H} NMR spectra were recorded on Bruker UNI400 instrument at ambient temperature and referenced to the residual solvent peak (<sup>1</sup>H).<sup>44</sup> <sup>31</sup>P{<sup>1</sup>H} NMR shifts were referenced to 85% D<sub>3</sub>PO<sub>4</sub> (0 ppm). IR measurements were recorded on Mattson Galaxy 2020 with DiffusIR (Pike Technologies) accessory (DRIFTS), Perkinelmer Spectrum Two (ATR), and Perkinelmer Spectrum 2000 with a Perkinelmer IR NaCl liquid cell (pentane solution). Ir loading on the silica was measured with Spectro Genesis ICP-OES.

#### 3.4.1 Synthesis

(tBu<sub>2</sub>PO-<sup>t</sup>BuPOCOP)Ir(H)(Cl)<sup>87</sup> was synthesized according to literature procedures.

##### *Synthesis of (tBu<sub>2</sub>PO-<sup>t</sup>BuPOCOP)Ir(CO) (**23**)<sup>87</sup>*

In a nitrogen-atmosphere glovebox, a flask with a Teflon stopcock was charged with 750.8 mg (0.95 mmol) of (tBu<sub>2</sub>PO-<sup>t</sup>BuPOCOP)Ir(H)(Cl) in 50 mL of toluene. The flask was sealed with a Teflon stopcock, and removed from the glovebox. The flask was cycled and charged with CO (1 atm) and shaken vigorously. The toluene solution rapidly changed color from deep red to golden yellow. After the color change, the flask was degassed (freeze, pump, thaw x 3) and brought into a nitrogen-atmosphere glovebox where K<sup>t</sup>OBU (110 mg, 0.98 mmol) was added. The flask was then sealed, removed from the glovebox, and the toluene solution was heated to reflux (120 °C) for 16 h. After cooling the mixture, toluene was evaporated under vacuum. The product was extracted with pentane and filtered through a pad of celite to yield a yellow filtrate. The pentane was evaporated to isolate **23** as a yellow solid. Yield: 608 mg (82% yield).

$^1\text{H}$  NMR( $\text{C}_6\text{D}_6$ , 400 MHz):  $\delta$  7.00 (s, 2H; Ar-H), 1.31 (vt,  $^3J_{\text{PH}}+^5J_{\text{PH}} = 7.1\text{Hz}$ , 36H, 4x  $^t\text{Bu}$ ), 1.08 (d,  $^3J_{\text{PH}} = 11.8\text{ Hz}$ , 18H, OP $^t\text{Bu}$ ).

$^{31}\text{P}\{^1\text{H}\}$  NMR ( $\text{C}_6\text{D}_6$ , 162 MHz):  $\delta$  200 (s), 152 (s)

IR ( $\text{cm}^{-1}$ ):  $\nu(\text{CO})$  1928 (ATR), 1946 (pentane)

### 3.4.2 Preparation of Immobilized Complex **23-SiO<sub>2</sub>**

Mesoporous silica (Sigma-Aldrich) and amorphous silica (Degussa) were obtained commercially. Silica was packed between glass wool plugs in a quartz tube with 0.25-in. ID. Calcination was carried out with dry air ( $100\text{ mL min}^{-1}$ ) using a  $2\text{ }^\circ\text{C min}^{-1}$  temperature ramp to  $550\text{ }^\circ\text{C}$ , held for 3 h, and cooled to room temperature at  $2\text{ }^\circ\text{C min}^{-1}$ .

To prepare **23-SiO<sub>2</sub>**, 5 mg of catalyst **23** was immobilized onto 150 mg of silica by dissolving the catalyst in benzene or toluene (2 mL), or pentane (5 mL) and stirring vigorously. The theoretical catalyst loading supported on silica is approximately 0.8 wt % based on iridium from the amount of metal complex immobilized on the support. After stirring for at least 16 h, yellow solid was dried under vacuum and stored in the glovebox prior to packing in the gas-phase flow reactor.

To prepare the heterogeneous **IrOx-SiO<sub>2</sub>**, Ir metal was deposited onto silica surface by incipient wetness impregnation. Aqueous solution of iridium trichloride hydrate was added to the silica powder to prepare the catalyst with Ir metal loading of 5 wt%. After impregnation of the Ir salt, the solid was dried overnight at  $60\text{ }^\circ\text{C}$  and calcined under air at  $500\text{ }^\circ\text{C}$  for 1 h.

Dispersion measurements can provide estimations on metal particle sizes. Metal dispersions were estimated using CO chemisorption at room temperature, assuming a stoichiometry of one CO per metal. Within the adsorption system, the samples were reduced in 400 Torr  $\text{H}_2$  for 30 min at 473 K to remove any oxide formed. Dispersion measurement indicated Ir particle size to be 5 nm.

### 3.4.3 Propane Dehydrogenation

Reactions were carried out in 0.25-in. ID quartz, tubular-flow reactor. The reactor was packed with the supported catalyst **23-SiO<sub>2</sub>** (50 mg) with glass wool plugs on both ends. The reactor was placed inside a furnace with external temperature control. Propane (Airgas, 99.99%) and helium (Airgas, 99.99%) were used as received. The reaction product was analyzed using a GC (SRI 8610C) with a thermal conductivity detector (TCD). The total gas flow rate was maintained at 20 mL min<sup>-1</sup>, and the total pressure was kept at 1 atm with 25% propane and 75% helium.

### 3.4.4 Toluene Hydrogenation

Reactions were carried out in 0.25-in. ID quartz, tubular-flow reactor. The reactor was packed with the supported catalyst **23-SiO<sub>2</sub>** (50 mg) with glass wool plugs on both ends. The reactor was placed inside a furnace with external temperature control. Toluene and hydrogen (Airgas, 99.999%) were used as received. The reaction product was analyzed using a GC with a quadrupole mass spectrometer (SRS RGA-100). The total gas flow rate was maintained at 20 mL min<sup>-1</sup>, and the total pressure was kept at 1 atm with 3% toluene and 97% hydrogen.

### 3.4.5 Hydrogenation of Mesityl Oxide

The reactor was a 200-mm long stainless-steel tube with a 4.6-mm ID. The reactor was packed with the supported catalyst **23-SiO<sub>2</sub>** (50 mg) or **IrO<sub>x</sub>-SiO<sub>2</sub>** (50 mg) with glass wool plugs on both ends, and the catalyst bed was held in place by inserting a solid stainless-steel rod into the end of the tube. The rod also reduced the empty volume in the reactor, decreasing the hold-up of products. The substrate was fed to the reactor using syringe pumps (PHD 2000 Infusion, Harvard Apparatus) with hydrogen as a carrier. Mesityl oxide was used as received. All the reaction lines were wrapped with heating tape and held at a temperature at least 50 °C higher than the condensation temperature of the substrate. The products were measured using an on-line GC-MS (QP5000, Shimadzu) equipped with a capillary column (HP-INNOWAX, Agilent Technologies). The

total gas flow rate was maintained at 20 mL min<sup>-1</sup>, and the total pressure was kept at 1 atm. The specific conditions for catalyst pretreatment and gas mixtures are listed under Figure 4-6.

### 3.4.6 Hydrogenation of 5-Methyl Furfural and Sulcatone

Following a similar procedure for hydrogenation of mesityl oxide, the reactor was packed with the supported catalyst **23-SiO<sub>2</sub>** (50 mg). 5-methyl furfural and sulcatone (6-methyl-5-hepten-2-one) were used as received. The products were measured using an on-line GC-MS (QP5000, Shimadzu) equipped with a capillary column (HP-INNOWAX, Agilent Technologies). The total gas flow rate was maintained at 20 mL min<sup>-1</sup>, and the total pressure was kept at 1 atm with 2% substrate and 98% hydrogen.

## 3.5 References

7. Sattler, J. J. H. B.; Ruiz-Martinez, J.; Santillan-Jimenez, E.; Weckhuysen, B. M., Catalytic Dehydrogenation of Light Alkanes on Metals and Metal Oxides. *Chem. Rev.* **2014**, *114* (20), 10613-10653.
8. Dong, S.; Altvater, N. R.; Mark, L. O.; Hermans, I., Assessment and comparison of ordered & non-ordered supported metal oxide catalysts for upgrading propane to propylene. *Appl. Catal. A* **2021**, *617*, 118121.
10. Kozuch, S.; Martin, J. M. L., "Turning Over" Definitions in Catalytic Cycles. *ACS Catal.* **2012**, *2* (12), 2787-2794.
29. Ahmed Foskey, T. J.; Heinekey, D. M.; Goldberg, K. I., Partial Deoxygenation of 1,2-Propanediol Catalyzed by Iridium Pincer Complexes. *ACS Catal.* **2012**, *2* (6), 1285-1289.
30. Choi, J.; MacArthur, A. H.; Brookhart, M.; Goldman, A. S., Dehydrogenation and related reactions catalyzed by iridium pincer complexes. *Chem. Rev.* **2011**, *111* (3), 1761-79.
39. Göttker-Schnetmann, I.; White, P. S.; Brookhart, M., Synthesis and Properties of Iridium Bis(phosphinite) Pincer Complexes (p-XPCP)IrH<sub>2</sub>, (p-XPCP)Ir(CO), (p-XPCP)Ir(H)(aryl), and {(p-XPCP)Ir}<sub>2</sub>{μ-N<sub>2</sub>} and Their Relevance in Alkane Transfer Dehydrogenation. *Organometallics* **2004**, *23* (8), 1766-1776.
43. Goldberg, J. M.; Cherry, S. D. T.; Guard, L. M.; Kaminsky, W.; Goldberg, K. I.; Heinekey, D. M., Hydrogen Addition to (pincer)IrI(CO) Complexes: The Importance of Steric and Electronic Factors. *Organometallics* **2016**, *35* (20), 3546-3556.
44. Fulmer, G. R.; Miller, A. J. M.; Sherden, N. H.; Gottlieb, H. E.; Nudelman, A.; Stoltz, B. M.; Bercaw, J. E.; Goldberg, K. I., NMR Chemical Shifts of Trace Impurities: Common Laboratory Solvents, Organics, and Gases in Deuterated Solvents Relevant to the Organometallic Chemist. *Organometallics* **2010**, *29* (9), 2176-2179.

46. Najari, S.; Saeidi, S.; Concepcion, P.; Dionysiou, D. D.; Bhargava, S. K.; Lee, A. F.; Wilson, K., Oxidative dehydrogenation of ethane: catalytic and mechanistic aspects and future trends. *Chem. Soc. Rev.* **2021**, *50* (7), 4564-4605.
47. Zhang, Z.; Jimenez-Izal, E.; Hermans, I.; Alexandrova, A. N., Dynamic Phase Diagram of Catalytic Surface of Hexagonal Boron Nitride under Conditions of Oxidative Dehydrogenation of Propane. *J. Phys. Chem. Lett.* **2019**, *10* (1), 20-25.
48. Venegas, J. M.; McDermott, W. P.; Hermans, I., Serendipity in Catalysis Research: Boron-Based Materials for Alkane Oxidative Dehydrogenation. *Acc. Chem. Res.* **2018**, *51* (10), 2556-2564.
49. Van Goethem, M. W. M.; Barendregt, S.; Grievink, J.; Moulijn, J. A.; Verheijen, P. J. T., Ideal Chemical Conversion Concept for the Industrial Production of Ethene from Hydrocarbons. *Ind. Eng. Chem. Res.* **2007**, *46* (12), 4045-4062.
50. Amghizar, I.; Vandewalle, L. A.; Van Geem, K. M.; Marin, G. B., New Trends in Olefin Production. *Engineering* **2017**, *3* (2), 171-178.
51. Grant, J. T.; Venegas, J. M.; McDermott, W. P.; Hermans, I., Aerobic Oxidations of Light Alkanes over Solid Metal Oxide Catalysts. *Chem. Rev.* **2018**, *118* (5), 2769-2815.
52. Sundaram, K. M.; Shreehan, M. M.; Olszewski, E. F., Ethylene. In *Kirk-Othmer Encyclopedia of Chemical Technology*, John Wiley & Sons, Inc.: 2010.
53. Grant, J. T.; Love, A. M.; Carrero, C. A.; Huang, F.; Panger, J.; Verel, R.; Hermans, I., Improved Supported Metal Oxides for the Oxidative Dehydrogenation of Propane. *Top. Catal.* **2016**, *59* (17-18), 1545-1553.
54. Nawaz, Z., Light alkane dehydrogenation to light olefin technologies: a comprehensive review. *Rev. Chem. Eng.* **2015**, *31* (5), 413-436.
55. Crabtree, R. H.; Mihelcic, J. M.; Quirk, J. M., Iridium complexes in alkane dehydrogenation. *J. Am. Chem. Soc.* **1979**, *101* (26), 7738-7740.
56. Baudry, D.; Ephritikhine, M.; Felkin, H.; Holmes-Smith, R., The selective catalytic conversion of cycloalkanes into cycloalkenes using a soluble rhenium polyhydride system. *J. Chem. Soc., Chem. Commun.* **1983**, (14), 788-789.
57. Burk, M. J.; Crabtree, R. H.; Parnell, C. P.; Uriarte, R. J., Selective stoichiometric and catalytic carbon-hydrogen bond cleavage reactions in hydrocarbons by iridium complexes. *Organometallics* **1984**, *3* (5), 816-817.
58. Gupta, M.; Hagen, C.; Flesher, R. J.; Kaska, W. C.; Jensen, C. M., A highly active alkane dehydrogenation catalyst: stabilization of dihydrido rhodium and iridium complexes by a P-C-P pincer ligand. *Chem. Commun.* **1996**, (17), 2083-2084.
59. Göttker-Schnetmann, I.; White, P.; Brookhart, M., Iridium Bis(phosphinite) p-XPCP Pincer Complexes: Highly Active Catalysts for the Transfer Dehydrogenation of Alkanes. *J. Am. Chem. Soc.* **2004**, *126* (6), 1804-1811.
60. Xu, W.-W.; Rosini, G. P.; Krogh-Jespersen, K.; Goldman, A. S.; Gupta, M.; Jensen, C. M.; Kaska, W. C., Thermochemical alkane dehydrogenation catalyzed in solution without the use of a hydrogen acceptor. *Chem. Commun.* **1997**, (23), 2273-2274.
61. Liu, F.; Goldman, A. S., Efficient thermochemical alkane dehydrogenation and isomerization catalyzed by an iridium pincer complex. *Chem. Commun.* **1999**, (7), 655-656.

62. Kumar, A.; Zhou, T.; Emge, T. J.; Mironov, O.; Saxton, R. J.; Krogh-Jespersen, K.; Goldman, A. S., Dehydrogenation of n-Alkanes by Solid-Phase Molecular Pincer-Iridium Catalysts. High Yields of  $\alpha$ -Olefin Product. *J. Am. Chem. Soc.* **2015**, *137* (31), 9894-9911.
63. Védrine, J. C., Metal Oxides in Heterogeneous Oxidation Catalysis: State of the Art and Challenges for a More Sustainable World. *ChemSusChem* **2019**, *12* (3), 577-588.
64. Phan, N. T. S.; Van Der Sluys, M.; Jones, C. W., On the Nature of the Active Species in Palladium Catalyzed Mizoroki–Heck and Suzuki–Miyaura Couplings – Homogeneous or Heterogeneous Catalysis, A Critical Review. *Adv. Synth. Catal.* **2006**, *348* (6), 609-679.
65. Richardson, J.; Jones, C., Strong evidence of solution-phase catalysis associated with palladium leaching from immobilized thiols during Heck and Suzuki coupling of aryl iodides, bromides, and chlorides. *J. Catal.* **2007**, *251* (1), 80-93.
66. Kingsbury, J. S.; Hoveyda, A. H., Regarding the Mechanism of Olefin Metathesis with Sol–Gel-Supported Ru-Based Complexes Bearing a Bidentate Carbene Ligand. Spectroscopic Evidence for Return of the Propagating Ru Carbene. *J. Am. Chem. Soc.* **2005**, *127* (12), 4510-4517.
67. Bieniek, M.; Michrowska, A.; Usanov, D. L.; Grela, K., In an Attempt to Provide a User's Guide to the Galaxy of Benzylidene, Alkoxybenzylidene, and Indenylidene Ruthenium Olefin Metathesis Catalysts. *Chem. Eur. J.* **2008**, *14* (3), 806-818.
68. Bates, J. M.; Lummiss, J. A. M.; Bailey, G. A.; Fogg, D. E., Operation of the Boomerang Mechanism in Olefin Metathesis Reactions Promoted by the Second-Generation Hoveyda Catalyst. *ACS Catal.* **2014**, *4* (7), 2387-2394.
69. Rimoldi, M.; Nakamura, A.; Vermeulen, N. A.; Henkelis, J. J.; Blackburn, A. K.; Hupp, J. T.; Stoddart, J. F.; Farha, O. K., A metal-organic framework immobilised iridium pincer complex. *Chem. Sci.* **2016**, *7* (8), 4980-4984.
70. Burgess, S. A.; Kassie, A.; Baranowski, S. A.; Fritzsching, K. J.; Schmidt-Rohr, K.; Brown, C. M.; Wade, C. R., Improved Catalytic Activity and Stability of a Palladium Pincer Complex by Incorporation into a Metal–Organic Framework. *J. Am. Chem. Soc.* **2016**, *138* (6), 1780-1783.
71. Syed, Z. H.; Kaphan, D. M.; Perras, F. A.; Pruski, M.; Ferrandon, M. S.; Wegener, E. C.; Celik, G.; Wen, J.; Liu, C.; Dogan, F.; Goldberg, K. I.; Delferro, M., Electrophilic Organoiridium(III) Pincer Complexes on Sulfated Zirconia for Hydrocarbon Activation and Functionalization. *J. Am. Chem. Soc.* **2019**, *141* (15), 6325-6337.
72. Hübner, S.; de Vries, J. G.; Farina, V., Why Does Industry Not Use Immobilized Transition Metal Complexes as Catalysts? *Adv. Synth. Catal.* **2016**, *358* (1), 3-25.
73. Wang, P.-W.; Fox, M. A., A Polymer-Bound Bidentate-Phosphine-Palladium Complex as a Catalyst in the Heck Arylation. *J. Org. Chem.* **1994**, *59* (18), 5358-5364.
74. Allen, D. P.; Van Wingerden, M. M.; Grubbs, R. H., Well-Defined Silica-Supported Olefin Metathesis Catalysts. *Org. Lett.* **2009**, *11* (6), 1261-1264.
75. Waki, M.; Maegawa, Y.; Hara, K.; Goto, Y.; Shirai, S.; Yamada, Y.; Mizoshita, N.; Tani, T.; Chun, W.-J.; Muratsugu, S.; Tada, M.; Fukuoka, A.; Inagaki, S., A Solid Chelating Ligand: Periodic Mesoporous Organosilica Containing 2,2'-Bipyridine within the Pore Walls. *J. Am. Chem. Soc.* **2014**, *136* (10), 4003-4011.
76. Zeidan, R. K.; Hwang, S.-J.; Davis, M. E., Multifunctional Heterogeneous Catalysts:

- SBA-15-Containing Primary Amines and Sulfonic Acids. *Angew. Chem. Int. Ed.* **2006**, *45* (38), 6332-6335.
77. Wang, Y.; Gu, Z.; Liu, W.; Yao, Y.; Wang, H.; Xia, X.-F.; Li, W., Conversion of glucose into 5-hydroxymethylfurfural catalyzed by chromium(III) Schiff base complexes and acidic ionic liquids immobilized on mesoporous silica. *RSC Adv.* **2015**, *5* (75), 60736-60744.
78. Yuan, W.; Huang, Y.; Wu, C.; Liu, X.; Xia, Y.; Wang, H., MCM-41 Immobilized Acidic Functional Ionic Liquid and Chromium(III) Complexes Catalyzed Conversion of Hexose into 5-Hydroxymethylfurfural. *Chin. J. Chem.* **2017**, *35* (11), 1739-1748.
79. Noda, H.; Motokura, K.; Miyaji, A.; Baba, T., Heterogeneous Synergistic Catalysis by a Palladium Complex and an Amine on a Silica Surface for Acceleration of the Tsuji-Trost Reaction. *Angew. Chem. Int. Ed.* **2012**, *51* (32), 8017-8020.
80. Motokura, K.; Saitoh, K.; Noda, H.; Uemura, Y.; Chun, W.-J.; Miyaji, A.; Yamaguchi, S.; Baba, T., Co-Immobilization of a Palladium-Bisphosphine Complex and Strong Organic Base on a Silica Surface for Heterogeneous Synergistic Catalysis. *ChemCatChem* **2016**, *8* (2), 331-335.
81. Motokura, K.; Kawashima, S.; Nambo, M.; Manaka, Y.; Chun, W. J., Accumulation of Active Species in Silica Mesopore: Effect of the Pore Size and Free Base Additives on Pd-catalyzed Allylation using Allylic Alcohol. *ChemCatChem* **2020**, *12* (10), 2783-2791.
82. Chen, Y.; Fan, B.; Lu, N.; Li, R., Aluminum metal-organic framework as a new host for preparation of encapsulated metal complex catalysts. *Catal. Commun.* **2015**, *64*, 91-95.
83. McDonald, A. R.; Dijkstra, H. P., Tethered Pincer Complexes as Recyclable Homogeneous Catalysts. In *The Privileged Pincer-Metal Platform: Coordination Chemistry & Applications*, 2015; pp 335-369.
84. Huang, Z.; Brookhart, M.; Goldman, A. S.; Kundu, S.; Ray, A.; Scott, S. L.; Vicente, B. C., Highly Active and Recyclable Heterogeneous Iridium Pincer Catalysts for Transfer Dehydrogenation of Alkanes. *Adv. Synth. Catal.* **2009**, *351* (1-2), 188-206.
85. Vicente, B. C.; Huang, Z.; Brookhart, M.; Goldman, A. S.; Scott, S. L., Reactions of phosphinites with oxide surfaces: a new method for anchoring organic and organometallic complexes. *Dalton Trans.* **2011**, *40* (16), 4268-74.
86. Rimoldi, M.; Mezzetti, A., Silica-grafted 16-electron hydride pincer complexes of iridium(III) and their soluble analogues: synthesis and reactivity with CO. *Inorg. Chem.* **2014**, *53* (22), 11974-84.
87. Sheludko, B.; Cunningham, M. T.; Goldman, A. S.; Celik, F. E., Continuous-Flow Alkane Dehydrogenation by Supported Pincer-Ligated Iridium Catalysts at Elevated Temperatures. *ACS Catal.* **2018**, *8* (9), 7828-7841.
88. Mäki-Arvela, P.; Hájek, J.; Salmi, T.; Murzin, D. Y., Chemoselective hydrogenation of carbonyl compounds over heterogeneous catalysts. *Appl. Catal. A* **2005**, *292*, 1-49.
89. Tamura, M.; Nakagawa, Y.; Tomishige, K., Recent Developments of Heterogeneous Catalysts for Selective Hydrogenation of Unsaturated Carbonyl Compounds to Unsaturated Alcohols. *J. Jpn. Pet. Inst.* **2019**, *62* (3), 106-119.
90. Delocalized Chemical Bonding. In *March's Advanced Organic Chemistry*, 2006; pp 32-105.

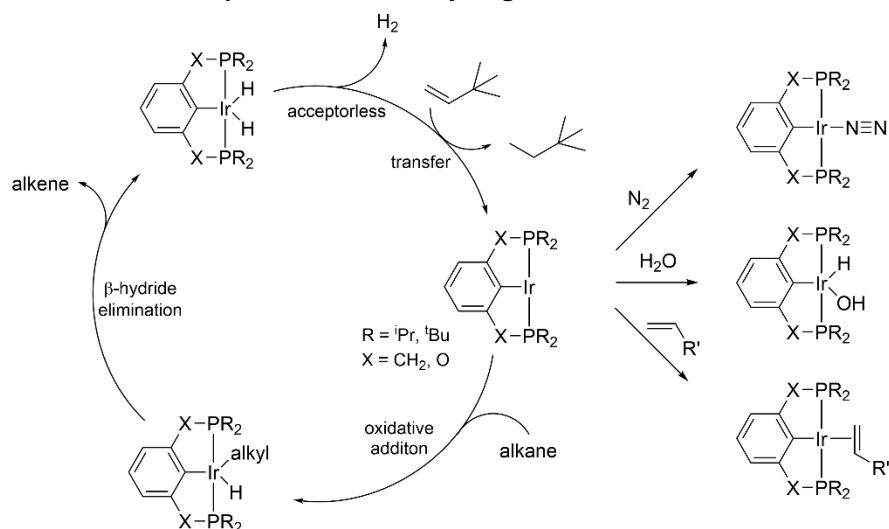
## Chapter 4: Functionalization of Phebox and CCC Ligands for Immobilization on Silica

### 4.1 Introduction

In recent years, the development of shale fracking has provided an abundance of light alkanes and drove the shift away from naphtha-based cracking processes to ethane-based processes. This shift has resulted in a significant decrease in the production of light olefins other than ethylene.<sup>8, 53</sup> In addition, the global demand for light olefins is over hundreds of millions of tons annually,<sup>51</sup> pushing the industry to implement alternative technologies for the production of light olefins such as the direct production of olefins from alkanes via dehydrogenation.<sup>91</sup> Alkane dehydrogenation, however, has an inherent drawback. The reaction requires high temperatures, low pressure, or constant removal of H<sub>2</sub> to drive the reaction forward due to the endothermic nature of the reaction. To overcome the unfavorable thermodynamics, a hydrogen acceptor such as a sacrificial olefin is employed. The use of a sacrificial olefin, however, results in poor atom economy. One strategy to circumvent this drawback is the use of molecular oxygen as the hydrogen acceptor. Cofeeding of the oxygen makes the reaction exothermic, prevents the build-up of coke, and generates environmentally benign H<sub>2</sub>O as the byproduct. The development of oxygen-tolerant transition-metal catalysts for aerobic alkane dehydrogenation is of interest.

Over the past few decades, numerous homogeneous catalytic systems for transfer or acceptorless alkane dehydrogenation with a wide range of pincer ligands were developed.<sup>9, 30</sup> PCP ( $^R\text{PCP} = \kappa^3\text{-C}_6\text{H}_3\text{-2,6-(CH}_2\text{PR}_2)_2$ ) or POCOP ( $^R\text{POCOP} = \kappa^3\text{-C}_6\text{H}_3\text{-2,6-(OPR}_2)_2$ ) ligated complexes were studied extensively for Ir-catalyzed dehydrogenation of alkanes. As depicted in Scheme 4-1, it is proposed that PCP- or POCOP-ligated Ir complexes generate a catalytically active 14-electron Ir(I) species, which undergoes oxidative addition of the alkane substrate to form an Ir(H)(alkyl) species. The Ir(H)(alkyl) species undergoes  $\beta$ -hydride elimination to yield the desired olefin product

**Scheme 4-1. Transfer or acceptorless alkane dehydrogenation via oxidative addition mechanism.**



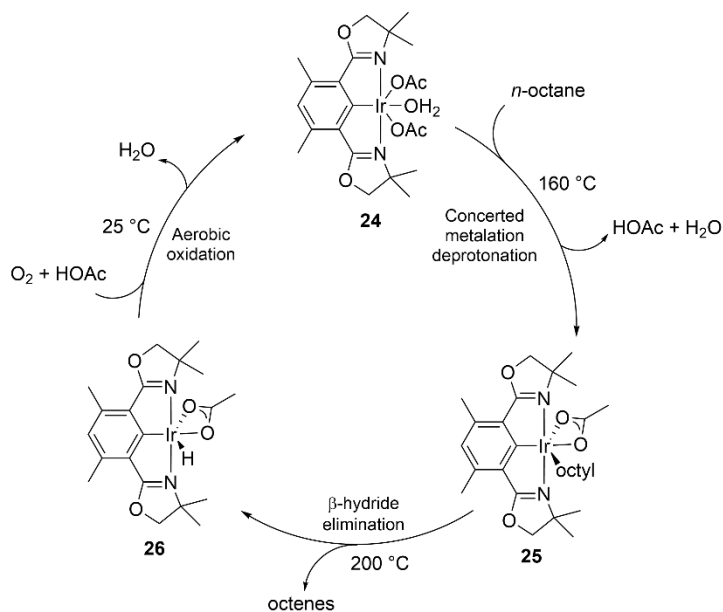
and Ir(H)<sub>2</sub> species. Then the Ir(H)<sub>2</sub> species transfers H<sub>2</sub> to a sacrificial olefin (transfer, shown with *tert*-butyl ethylene in Scheme 4-1) or releases H<sub>2</sub> as a gas (acceptorless) with the regeneration of the 14-electron Ir(I) species. The 14-electron species is very reactive, and its catalytic activity can be inhibited by N<sub>2</sub><sup>58, 92, 93</sup>, H<sub>2</sub>O<sup>94</sup>, and the sacrificial olefin or olefin products<sup>9, 58, 59</sup> by forming an off-cycle species. Furthermore, the binding of O<sub>2</sub> to (<sup>t</sup>BuPCP)Ir species was demonstrated, giving another off-cycle species.<sup>95</sup> The reactivity of the 14-electron Ir(I) intermediate to those off-cycle species rendered the PCP- or POCOP-ligated Ir complexes unsuitable for aerobic alkane dehydrogenation.

Our group focused on the oxazoline-based Ir complex, proposed to undergo a concerted metalation deprotonation (CMD) mechanism, in which the oxidation state of Ir(III) is maintained throughout the dehydrogenation reaction. (<sup>dm</sup>Phebox)Ir(OAc)<sub>2</sub>(OH<sub>2</sub>) (Phebox = 2,6-bis(4,4-dimethyl-oxazolynyl)phenyl) (**24**) was reported for C-H activation of *n*-octane at 160 °C in presence of base, resulting in the formation of acetic acid (HOAc) and (<sup>dm</sup>Phebox)Ir(OAc)(octyl) (**25**).<sup>96</sup> Complex **24** was demonstrated to form (<sup>dm</sup>Phebox)Ir(OAc)(H) (**26**) and octene quantitatively at 200 °C without any base.<sup>97</sup> In contrast to PCP or POCOP complexes, *n*-octane activation by **24** was uninhibited by presence of N<sub>2</sub>, H<sub>2</sub>O, or  $\alpha$ -olefin.<sup>97</sup> The hydride complex **26** converted back to (<sup>dm</sup>Phebox)Ir(OAc)<sub>2</sub>(OH<sub>2</sub>) when allowed to react with O<sub>2</sub> and HOAc.<sup>98</sup> *n*-Octane activation by **24**,  $\beta$ -

hydride elimination from **25** to form octene, and aerobic oxidation of **26** constitute a potential catalytic cycle for the dehydrogenation of alkane with O<sub>2</sub> as a hydrogen acceptor (Scheme 4-2). However, the realization of the catalysis was not achieved because **24** decomposed under O<sub>2</sub> atmosphere at 200 °C. In addition, there was unselective reaction of *n*-octane with O<sub>2</sub> in absence of catalyst.<sup>99</sup> To complete the catalysis, all the steps must occur at lower temperatures.

Gao et al. found that the addition of Lewis acid lowered the temperature required for β-hydride elimination down to 55 °C and the reaction of β-hydride elimination from **25** to form **26** reached the equilibrium at 42% conversion after 3 hours.<sup>100</sup> In the same report, *n*-dodecane was catalytically dehydrogenated by **26** to form dodecenes and H<sub>2</sub> at reflux temperature (bp = 216 °C). The TON with **26** was only 3 after 1 h, but a significant rate enhancement was observed with the addition of NaBARF<sub>24</sub>, increasing TON to 24 under the same conditions. In contrast, after 72 h, the activity leveled off, yielding 78 TON with or without NaBARF<sub>24</sub>. This result is comparable to the results obtained with (A<sup>d</sup>PCP)Ir(H)<sub>2</sub>, the most effective type of homogeneous catalysts for acceptorless alkane dehydrogenation reported to date, which achieves a TON of 71 after 72 h. The similar TONs with these catalysts are attributed to the ineffective removal of H<sub>2</sub> during the reaction. Furthermore,

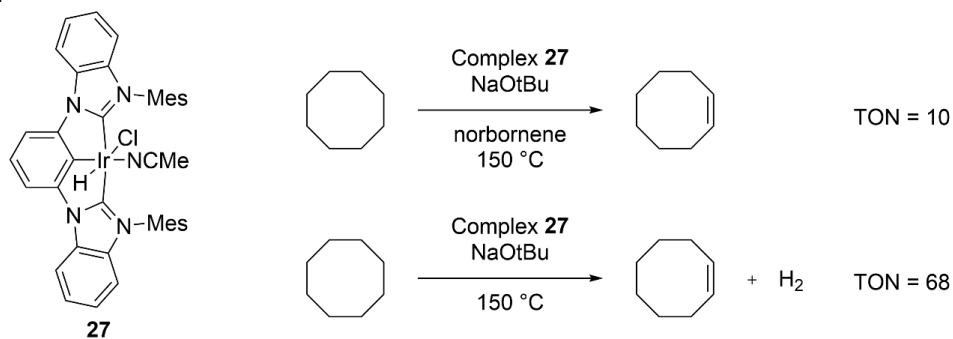
**Scheme 4-2. Stepwise *n*-octane dehydrogenation with O<sub>2</sub> as the hydrogen acceptor.**



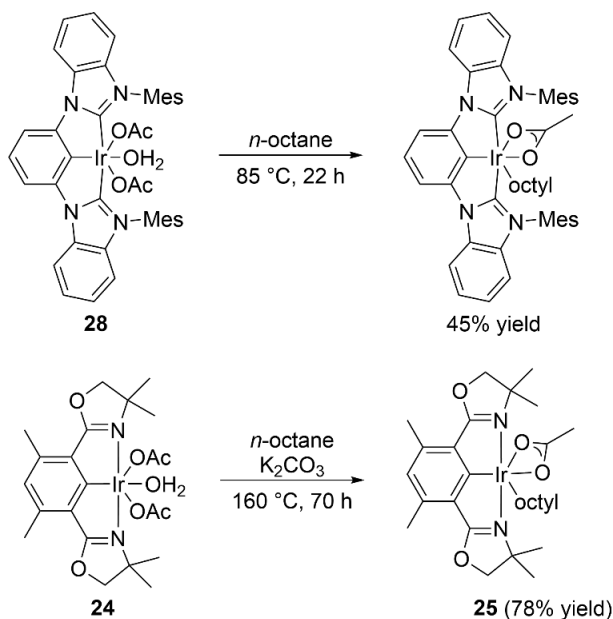
the isomerization of olefin products competes with the dehydrogenation of alkane as the concentration of olefin builds up.<sup>42, 100</sup>

Additionally, the *n*-heterocyclic carbene based (CCC<sup>Mes</sup>)Ir (CCC<sup>Mes</sup> = bis(mesityl-benzimidazol-2-ylidene)phenyl) complexes were examined for alkane dehydrogenation. The CCC-ligated Ir complexes were studied extensively by Chianese and coworkers.<sup>101-103</sup> (CCC<sup>Mes</sup>)Ir(H)(Cl)(NCMe) (**27**) was found to be a reasonable precatalyst for both transfer and acceptorless dehydrogenation of cyclooctane (Scheme 4-3).<sup>101</sup> It was proposed that added base (NaOtBu) promoted the elimination of HCl from **27** to generate a reactive Ir(I) species. An oxidative addition mechanism of C-H activation, analogous to (PCP)Ir or (POCOP)Ir complexes (Scheme 4-1) then occurs.<sup>103</sup> The high thermal stability and air-tolerance indicate that (CCC)Ir complexes may be promising catalysts for aerobic alkane dehydrogenation. Several (CCC)Ir bis-carboxylates were synthesized and examined for activation of C-H bonds. C-H activation for the (CCC)Ir complexes occur by concerted metalation deprotonation (CMD) pathways. (CCC<sup>Mes</sup>)Ir(OAc)<sub>2</sub>(OH<sub>2</sub>) (**28**) was revealed to be highly active for C-H activation of *n*-octane, compared to its Phebox analogue **24**. For example, heating complex **28** in neat *n*-octane at 85 °C resulted in Ir(OAc)(octyl) complex with 45% yield after 22 h while the Phebox analogue **24** required a higher reaction temperature (160 °C) and longer period of heating (70 h) to form the Phebox analogue of Ir(octyl) complex **25** in 78% yield (Scheme 4-4).<sup>96, 104</sup> Similarly, **28** reacted with benzene to generate Ir(phenyl) product at the rate six times faster than that with the Phebox analogue **24**. Based on the hypothesis that the decrease in steric bulk around the metal center would facilitate faster interaction

**Scheme 4-3. Transfer and acceptorless dehydrogenation of cyclooctane by (CCC<sup>Mes</sup>)Ir(H)(Cl) (**27**).**



**Scheme 4-4. *n*-Octane activation by (CCC)Ir(OAc)<sub>2</sub> and (Phebox)Ir(OAc)<sub>2</sub>.**



with benzene, another (CCC)Ir complex was prepared with methyl groups on the benzimidazole rings,  $(^t\text{BuCCC}^{\text{Me}})\text{Ir}(\text{OC}(\text{O})\text{Hex})_2(\text{OH}_2)$  (**29**). Consistent with the hypothesis, the benzene activation by **29** proceeded three times faster than the same reaction by **28**.<sup>104</sup> (CCC)Ir complexes were also shown to have reactivities that make up a potential cycle of aerobic alkane dehydrogenation, analogous to the (Phebox)Ir complexes in Scheme 4-2.<sup>105</sup>

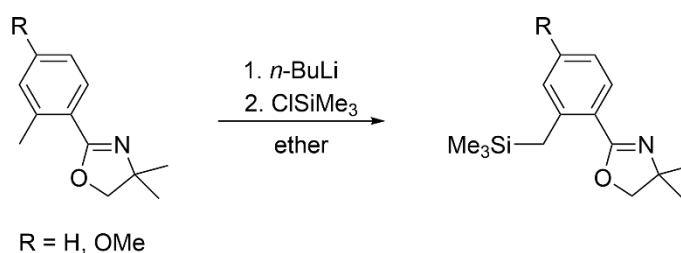
The immobilization of  $(^{\text{dm}}\text{Phebox})\text{Ir}(\text{OAc})_2(\text{OH}_2)$  **24** or  $(\text{CCC}^{\text{Mes}})\text{Ir}(\text{OAc})_2(\text{OH}_2)$  **28** is attractive because the heterogenized catalyst can be used in continuous-flow system, which would alleviate the ineffective removal of H<sub>2</sub> and the isomerization of olefin products. For immobilization of Phebox or CCC complexes, a covalent tethering on silica via trialkoxysilane linker is envisioned because 1) silica is commercially available in various pore sizes and surface areas, 2) silica is superior to titania, magnesia, and alumina in minimizing leaching when bonded with trialkoxysilane,<sup>106</sup> and 3) trialkoxysilane bonds covalently with silica via Si-O-Si linkage, which is superior to C-O-Si linkage.<sup>107</sup> In addition, the chelating nature of Phebox and CCC ligands should reduce leaching of metal. Functionalization of Phebox and CCC ligands with trialkoxysilane is explored in this chapter.

## 4.2 Synthesis and Functionalization of Phebox Ligands

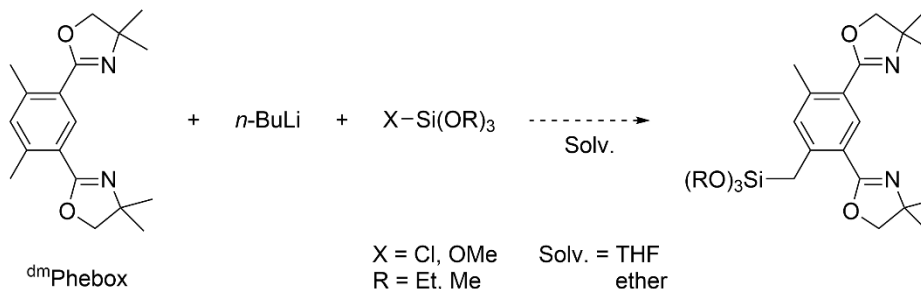
### 4.2.1 Attempted Functionalization of <sup>dm</sup>Phebox

The reactivity of 2-(*o*-tolyl)oxazoline with *n*-butyllithium (*n*-BuLi) and chlorotrimethylsilane (ClSiMe<sub>3</sub>) was reported (Scheme 4-5).<sup>108, 109</sup> Since 2-(*o*-tolyl)oxazoline resembles half of <sup>dm</sup>Phebox ligand, the methyl groups on the ligand backbone of <sup>dm</sup>Phebox may undergo similar silylation (Scheme 4-6). Silane reagents used for the functionalization of <sup>dm</sup>Phebox were chlorotri(ethoxy)silane (ClSi(OEt)<sub>3</sub>) or tetramethoxysilane (Si(OMe)<sub>4</sub>), both of which were used previously to prepare trialkoxysilyl compounds.<sup>110, 111</sup> When *n*-BuLi was added to <sup>dm</sup>Phebox at 0 °C, a deep red color was observed, consistent with previous observations.<sup>108, 109, 112</sup> However, there was no reactivity with silane reagents, indicated by <sup>1</sup>H NMR spectrum showing only <sup>dm</sup>Phebox. To ensure that H<sub>2</sub>O was not present to quench the lithiated species, silane reagents were dried over molecular sieves for two days but experiments still resulted in <sup>dm</sup>Phebox solely. The reactivity of unfunctionalized <sup>H</sup>Phebox with lithium reagents was reported by Harris and coworkers.<sup>113</sup> In their report, <sup>H</sup>Phebox was treated with *n*-BuLi, followed by addition of MeI, to yield a mixture of compounds, including dihydrobenzene as shown in Scheme 4-7 (detailed procedure not reported).

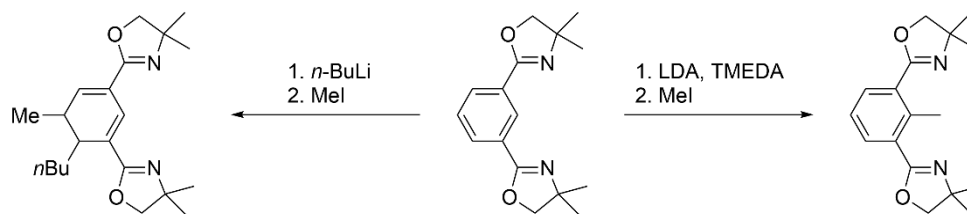
**Scheme 4-5. Silylation of 2-(*o*-tolyl)oxazoline.**<sup>108, 109</sup>



**Scheme 4-6. Proposed synthetic plan to functionalize <sup>dm</sup>Phebox with trialkoxysilane.**



**Scheme 4-7. Reactivity of Phebox with different lithium reagents.**<sup>113</sup>

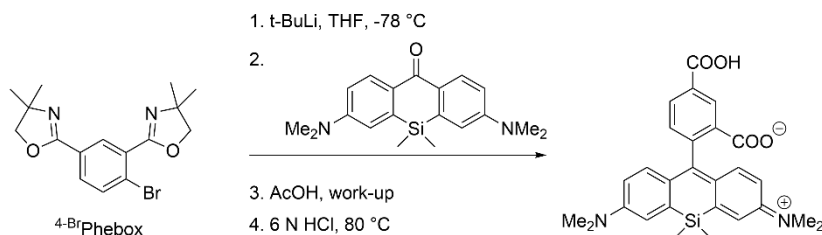


On the other hand, when Phebox reacted with lithium diisopropylamide (LDA) and N,N,N',N'-tetramethylethylenediamine (TMEDA), followed by addition of MeI, the substitution occurred between two oxazolines. In the reactions of <sup>dm</sup>Phebox, no substitution on the benzene ring was observed at all, suggesting that the lithiated species is not very reactive.

#### 4.2.2 Synthesis of <sup>5-Br</sup>Phebox

Since the functionalization of methyl groups of <sup>dm</sup>Phebox was not successful, a method to functionalize the phenyl ring was sought. A selective substitution of bromine-substituted Phebox, <sup>4-Br</sup>Phebox, was reported by Sunbul and Jaschke (Scheme 4-8).<sup>114</sup> In this reaction, *tert*-butyl lithium activated C-Br bond and the resulting lithiated species underwent a nucleophilic substitution at carbonyl compound. Inspired by this report, the synthesis of bromine-substituted Phebox ligands and functionalization of them were carried out. Adapting literature procedures,<sup>114, 115</sup> Phebox ligands with bromine substituted at 4- or 5-position of the benzene ring were synthesized from 4- or 5-bromoisophthalic acid (Scheme 4-9). <sup>4-Br</sup>Phebox was isolated as a yellow oil and its <sup>1</sup>H NMR matched well with the reported <sup>1</sup>H NMR.<sup>114</sup> The reaction product from 5-bromoisophthalic acid was also isolated as a yellow oil. <sup>1</sup>H NMR spectrum (Figure 4-1) showed two aromatic proton signals at 8.39 and 8.19 ppm in 1:2 ratio appeared for two *ortho* and one *para* protons to bromine. One

**Scheme 4-8. Substitution of <sup>4-Br</sup>Phebox.**<sup>114</sup>



#### Scheme 4-9. Synthesis of bromine-substituted Phebox ligands.

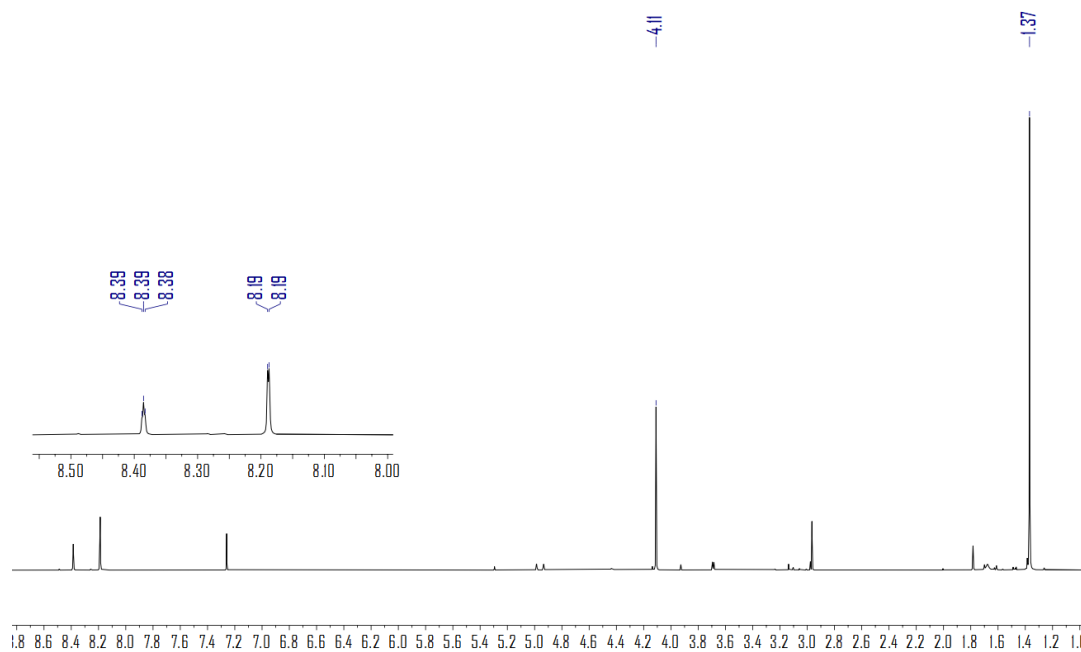
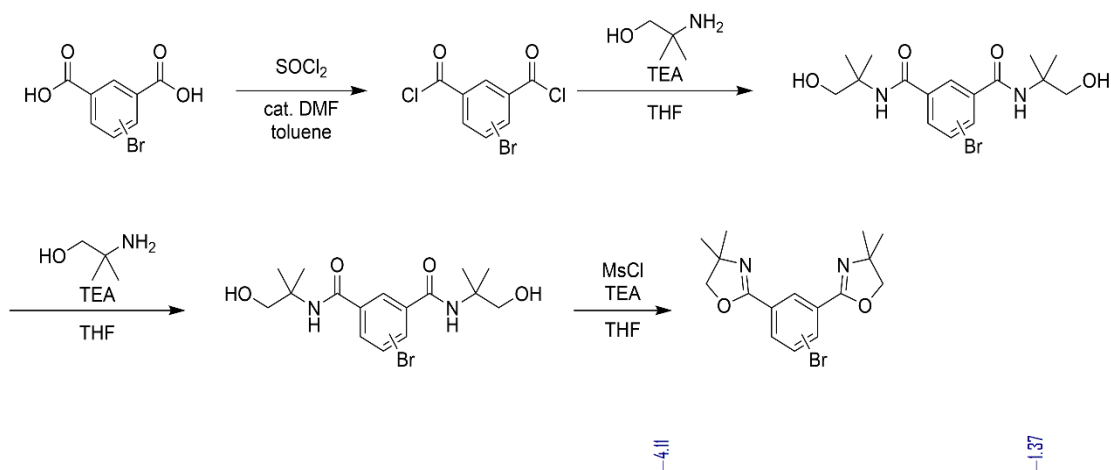


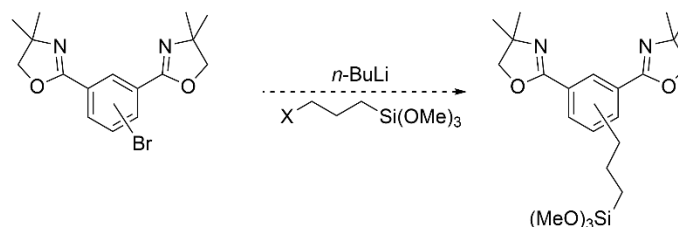
Figure 4-1.  $^1\text{H}$  NMR spectrum of  $5\text{-BrPhebox}$  in  $\text{CDCl}_3$ .

methylene proton signal and one methyl proton signal from oxazolines were observed at 4.11 and 1.37 ppm respectively. Mass spec analysis showed signals at 351 and 353 for  $[\text{M}(^{79}\text{Br})+\text{H}]^+$  and  $[\text{M}(^{81}\text{Br})+\text{H}]^+$ . These NMR and mass spec data verified that the product was  $5\text{-BrPhebox}$ .

#### 4.2.3 Attempted Functionalization of $5\text{-BrPhebox}$ with Trimethoxysilane

Under an Ar atmosphere,  $5\text{-BrPhebox}$  was treated with  $n\text{-BuLi}$  at cold temperatures, followed by addition of trimethoxysilane (Scheme 4-10). The aromatic region of the  $^1\text{H}$  NMR spectrum was the best indicator to determine the number and type of Phebox species. For

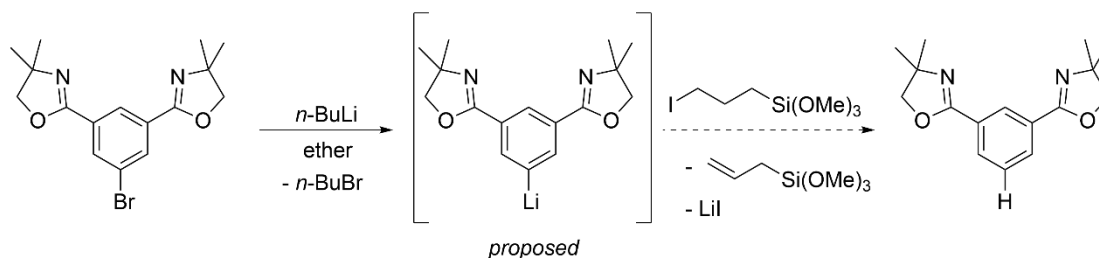
**Scheme 4-10. Functionalization of <sup>Br</sup>Phebox with trimethoxysilane.**



symmetric <sup>5-Br</sup>Phebox, three aromatic protons show up as two signals in 2:1 ratio. For asymmetric <sup>4-Br</sup>Phebox, three aromatic protons result in a total of three signals, one for each proton. The dehalogenated product, 1,3-bis(4,4'-dimethyl-2-oxazolinyloxy)benzene (<sup>H</sup>Phebox), has four aromatic protons that show up as three signals in 1:2:1 ratio. The addition of *n*-BuLi at -78 °C to <sup>5-Br</sup>Phebox resulted in a deep red solution. The color change likely indicates the activation of the C-Br bond of <sup>5-Br</sup>Phebox and formation of a new lithium species. After the reaction with 3-chloropropyltrimethoxysilane, analysis of crude reaction mixture by <sup>1</sup>H NMR spectrum showed <sup>H</sup>Phebox, matching well with the reported <sup>1</sup>H NMR spectral data.<sup>116</sup> To ensure complete reaction of the *n*-BuLi and formation of the lithiated intermediate, the temperature of *n*-BuLi addition was increased to 0 °C, resulting in a deep red solution again. However, the analysis of the reaction mixture after the addition of silane by <sup>1</sup>H NMR revealed that <sup>H</sup>Phebox was again the major product. Similarly, when the *n*-BuLi addition at -78 or 0 °C to <sup>4-Br</sup>Phebox was carried out, after the reaction with 3-chloropropyltrimethoxysilane, <sup>H</sup>Phebox was again determined to be a major product by <sup>1</sup>H NMR spectroscopy. The observation of <sup>H</sup>Phebox product suggests that *n*-BuLi activated C-Br bond of both <sup>4-Br</sup>Phebox and <sup>5-Br</sup>Phebox but the lithiated intermediate did not react with 3-chloropropyltrimethoxysilane.

To promote the reactivity of the lithiated intermediate with trimethoxysilane, chloride was replaced with iodide, a better leaving group than chloride.<sup>117</sup> The lithiated intermediate from <sup>5-Br</sup>Phebox was treated with 3-iodopropyltrimethoxysilane, but again the reaction resulted in predominantly <sup>H</sup>Phebox and no desired product. It is possible that the dehydrohalogenation reaction (Scheme 4-11) occurred with 3-iodopropyltrimethoxysilane to quench the lithiated intermediate and that the dehydrohalogenated product, allyltrimethoxysilane (b.p. = 136 °C)<sup>118</sup>, was

**Scheme 4-11. Potential dehydrohalogenation of 3-iodopropyltrimethoxysilane.**



not observed in  $^1\text{H}$  NMR spectrum because allyltrimethoxysilane evaporated under reduced pressure during work-up.

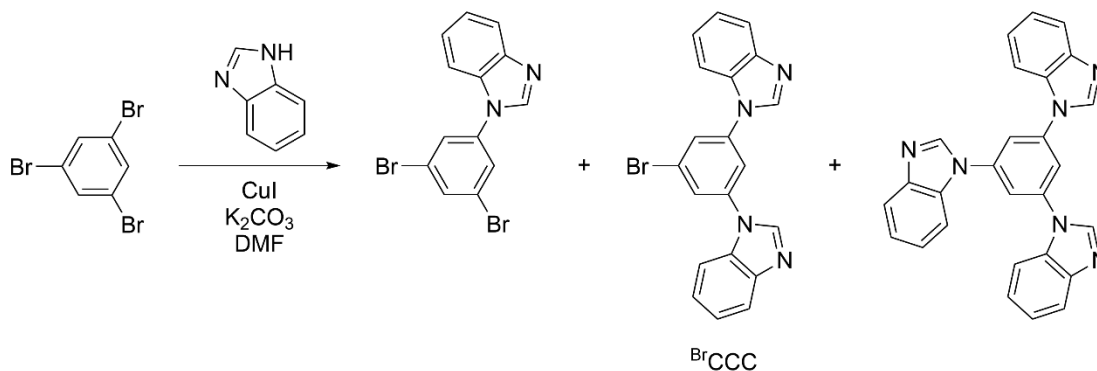
To examine whether dehydrohalogenation occurred, methyl iodide was employed because dehydrogenation is not feasible for methyl iodide.  $^5\text{-BrPhebox}$  was treated with *n*-BuLi at  $-78^\circ\text{C}$ , resulting in a deep red solution, and MeI was added to the red solution. After deep red color dissipated,  $^1\text{H}$  NMR of the crude reaction mixture revealed  $^5\text{HPhexox}$  as a major product. These experiments suggest that the lithiated intermediate is not very reactive. Previous study by Harris and coworkers showed that the identity of lithium reagent gave different outcomes (Scheme 4-7)<sup>113</sup> and may suggest that the desired lithium intermediate forms only when *tert*-butyl lithium is used as in the study by Sunbul and Jaschke (Scheme 4-8).<sup>114</sup>

### 4.3 Synthesis and Functionalization of CCC Ligands and CCC(Ir) Complexes

#### 4.3.1 Synthesis and Metalation of $\text{alkyneCCC}^{\text{Me}}$

A different approach was taken for CCC ligand immobilization, using covalent linkage between azide-functionalized support materials and alkyne-functionalized molecular complexes via click chemistry.<sup>119, 120</sup> Since  $(^t\text{BuCCC}^{\text{Me}})\text{Ir}(\text{OC}(\text{O})\text{Hex})_2(\text{OH}_2)$  (**29**) activated benzene three times faster than  $(\text{CCC}^{\text{Mes}})\text{Ir}(\text{OAc})_2(\text{OH}_2)$  (**28**),<sup>104</sup> we sought to functionalize  $\text{CCC}^{\text{Me}}$  ligand and support the  $(\text{CCC}^{\text{Me}})\text{Ir}$  complex. Adapting from literature procedures,<sup>121, 122</sup>  $\text{BrCCC}$  precursor was synthesized (Scheme 4-12). Its identity was verified by  $^1\text{H}$  NMR spectroscopy, consistent with the

**Scheme 4-12. Synthesis of <sup>Br</sup>CCC precursor.**<sup>121, 122</sup>

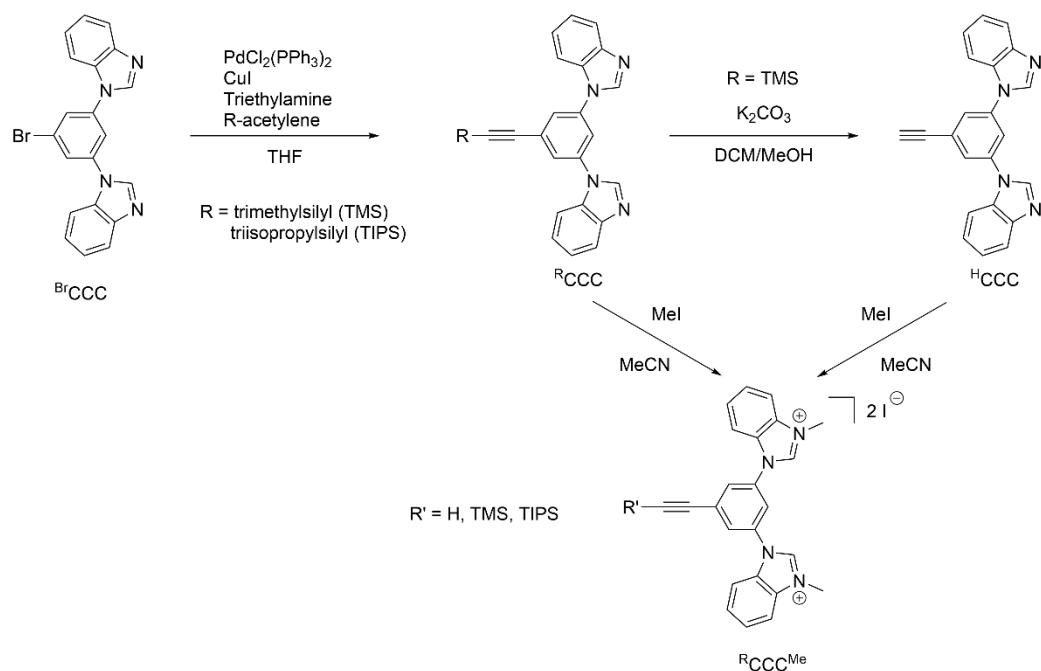


literature,<sup>122</sup> and MS, showing a mono-brominated compound with the signals at 389 and 391 for [M(<sup>79</sup>Br)+H]<sup>+</sup> and [M(<sup>81</sup>Br)+H]<sup>+</sup>.

Sonogashira cross-coupling between <sup>Br</sup>CCC and trimethylsilylacetylene (TMS-acetylene), followed by desilylation with K<sub>2</sub>CO<sub>3</sub>, yielded alkyne functionalized <sup>H</sup>CCC, indicated by the appearance of acetylene proton at 3.40 ppm in the <sup>1</sup>H NMR spectrum (top pathway in Scheme 4-13). The alkylation of benzimidazole arms was also successful in the reaction with MeI. The product <sup>H</sup>CCC<sup>Me</sup> had a poor solubility in CDCl<sub>3</sub> and was characterized by <sup>1</sup>H NMR spectroscopy in DMSO-d<sub>6</sub>. <sup>1</sup>H NMR signals at 4.23 ppm for two methyl groups and at 10.3 ppm for carbene protons were present. The metalation of <sup>H</sup>CCC<sup>Me</sup> ligand with [Ir(μ-Ome)(COD)]<sub>2</sub> gave a light brown solid with no solubility in CDCl<sub>3</sub> in disagreement with the observations of the related complex, which exhibited an orange color and was soluble in CDCl<sub>3</sub>. The metalation is supposed to activate C-H bonds of carbene and ipso-protons, but the <sup>H</sup>CCC<sup>Me</sup> ligand contains an acidic acetylene proton, apparently complicating the metalation reaction. This proposal led us to consider protecting the acetylene group until the CCC<sup>Me</sup> ligand is metalated.

A trimethylsilyl (TMS) group improved the solubility of <sup>TMS</sup>CCC<sup>Me</sup> ligand in the chlorinated solvents, enabling direct comparisons of <sup>1</sup>H NMR spectral data. Upon methylation of benzimidazole arms, the <sup>1</sup>H NMR spectrum of <sup>TMS</sup>CCC<sup>Me</sup> presented a signal at 4.28 ppm for two methyl groups and downfield shift of carbene protons from 8.18 to 11.19 ppm (bottom pathway in Scheme 4-13). A metalation reaction of <sup>TMS</sup>CCC<sup>Me</sup> with [Ir(μ-Ome)(COD)]<sub>2</sub> resulted in an orange solid, but it was

**Scheme 4-13. Synthesis of alkyne-functionalized CCC<sup>Me</sup> ligands.**

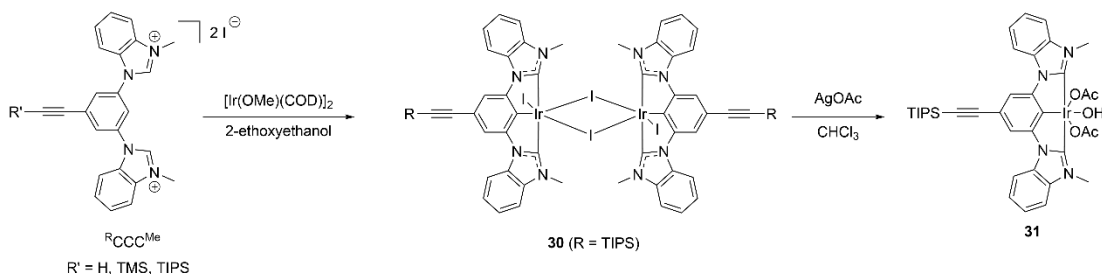


not soluble in  $\text{CDCl}_3$ . Assuming the orange solid was the dimer product, it was heated in refluxing  $\text{MeCN}$  to break up a dimer, a procedure that was performed for a related complex to afford a monomeric complex.<sup>123</sup> After heated in refluxing  $\text{MeCN}$  overnight, much of the solid was left undissolved. In  $^1\text{H}$  NMR spectrum, a broad feature in the aromatic region restricted the identification of number of aromatic  $^1\text{H}$  NMR signals. However, most important is that an intense signal (9H) from the TMS group was not observed, which was expected if the metalation was successful. The TMS protecting group is highly labile in presence of acid or base, and the metalation reaction of  $\text{TMSCCCMe}$  with  $[\text{Ir}(\mu\text{-OMe})(\text{COD})]_2$  contains a methoxide anion that might interact with TMS group, potentially leading to the deprotection of alkyne group.

Instead of TMS group, triisopropylsilyl (TIPS) group was utilized due to its much higher stability to acid and base.<sup>124</sup> Sonogashira cross-coupling reaction between  $\text{BrCCC}$  and TIPS-acetylene afforded  $\text{TIPSCCC}$  cleanly. In the  $^1\text{H}$  NMR spectrum, an intense signal at 1.16 ppm appeared for the 21 protons of TIPS group. Methylation of the benzimidazole arms generated  $\text{TIPSCCCMe}$  with  $^1\text{H}$  NMR signals at 4.28 ppm for the methyl groups and 11.10 ppm for the carbene

protons, comparable to those of  $\text{TMS}^{\text{Me}}\text{CCC}^{\text{Me}}$  (Scheme 4-13). The metalation reaction with  $[\text{Ir}(\mu\text{-OMe})(\text{COD})]_2$  (Scheme 4-14) afforded an orange solid which was soluble in chlorinated solvents. In the  $^1\text{H}$  NMR spectrum ( $\text{CDCl}_3$ ), there were no longer signals for two carbene protons and one ipso-proton disappeared, as would be consistent with the formation of pincer-ligated Ir complex.  $^1\text{H}$  NMR spectrum showed five signals in the aromatic region, one from phenyl-H and four from benzimidazole, a signal for methyl groups at 4.16 ppm and a signal for TIPS at 1.24 ppm. Based on  $^1\text{H}$  NMR data, the orange solid was determined to be the desired dimer **30** (Scheme 4-14). Dimer **30** was treated with silver acetate ( $\text{AgOAc}$ ) to afford  $(\text{TIPS}^{\text{Me}}\text{CCC}^{\text{Me}})\text{Ir}(\text{OAc})_2(\text{OH}_2)$  (**31**), confirmed by appearance of a signal for the acetate groups at 1.46 ppm in  $^1\text{H}$  NMR spectrum.

**Scheme 4-14. Metalation of  $\text{alkyne}^{\text{Me}}\text{CCC}^{\text{Me}}$  ligand with  $[\text{Ir}(\mu\text{-OMe})(\text{COD})]_2$  and synthesis of  $\text{Ir}(\text{OAc})_2$  complex.**



#### 4.3.2 Attempted Desilylation of TIPS Group of Complex **31**

Desilylation of the TIPS group in complex **31** was attempted with tetrabutylammonium fluoride (TBAF) in chloroform or dichloromethane. The reaction was monitored by  $^1\text{H}$  NMR spectroscopy (Figure 4-2). A signal for the TIPS protons at 1.19 ppm disappeared, suggesting that desilylation occurred. Signals for aromatic protons of **31** at 8.09, 7.66, 7.54 and 7.44 ppm disappeared, and a new set of signals at 8.04, 7.69, 7.54 and 7.40 ppm were observed. The observation of a precipitate in the reaction mixture suggested that the desilylated product has lower solubility in chloroform than the starting material **31**. A similar solubility difference was observed with  $\text{alkyne}^{\text{Me}}\text{CCC}^{\text{Me}}$  ligands, where deprotected  $\text{H}^{\text{Me}}\text{CCC}^{\text{Me}}$  ligand had poor solubility in chlorinated

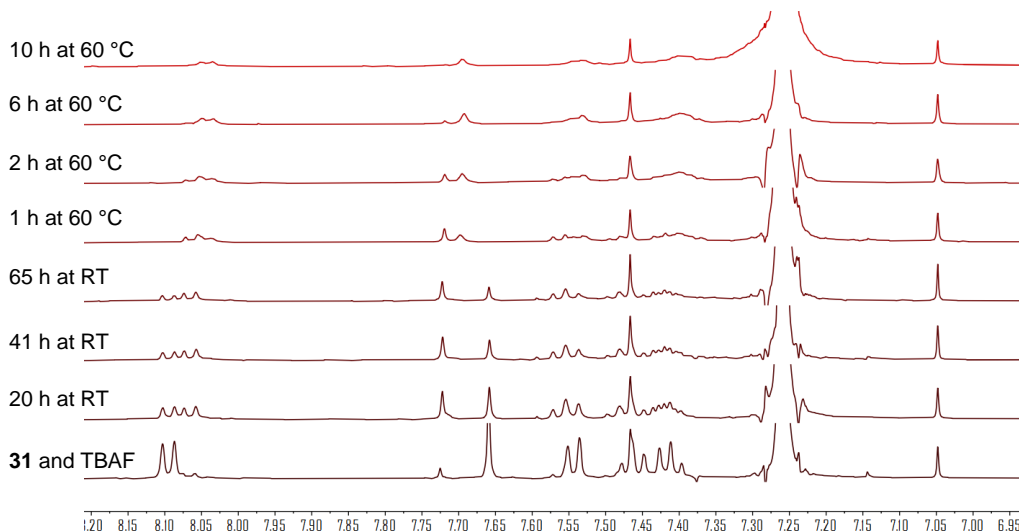


**Figure 4-2.** Desilylation reaction progress of **31** monitored by  $^1\text{H}$  NMR.

solvents and required DMSO for solution-phase characterization, while  $\text{TMS}^{\text{Me}}\text{CCC}^{\text{Me}}$  or  $\text{TIPS}^{\text{Me}}\text{CCC}^{\text{Me}}$  ligands were soluble and could be characterized in chlorinated solvents.

In a separate experiment, **31** was treated with TBAF in  $\text{CDCl}_3$  at  $60\text{ }^\circ\text{C}$  for 24 h, resulting in a darker yellow solution and white precipitate. The chloroform solution was decanted, and the ppt was washed with ethyl acetate. The white ppt did not dissolve in  $\text{H}_2\text{O}$  but was soluble enough in  $\text{CDCl}_3$  to record  $^1\text{H}$  NMR spectrum (Figure 4-3). The number (10H) and splitting patterns of aromatic signals, along with methyl and acetate signals at 4.50 and 1.59 ppm, resembled  $(\text{CCC}^{\text{Me}})\text{Ir}(\text{OAc})_2$  species, similar to **31**, and a signal for TIPS was not observed (Figure 4-3). To remove residual TBAF observed in  $^1\text{H}$  NMR of the ppt, a DCM-aqueous extraction was performed, but the organic extract resulted in a messy  $^1\text{H}$  NMR spectrum. The aromatic region showed new signals that were broad and overlapping each other, making it difficult to accurately determine the number and identity of species in the solution. An optimization of the work-up procedure is likely necessary to isolate the desired product.

A different approach can also be considered to make an immobilized  $(\text{CCC})\text{Ir}$  complex. The desilylated precursor  $^{\text{H}}\text{CCC}$  can be immobilized on azide-functionalized silica via click chemistry. Then the  $(\text{CCC})\text{Ir}$  complex can be constructed on the surface of silica. This method

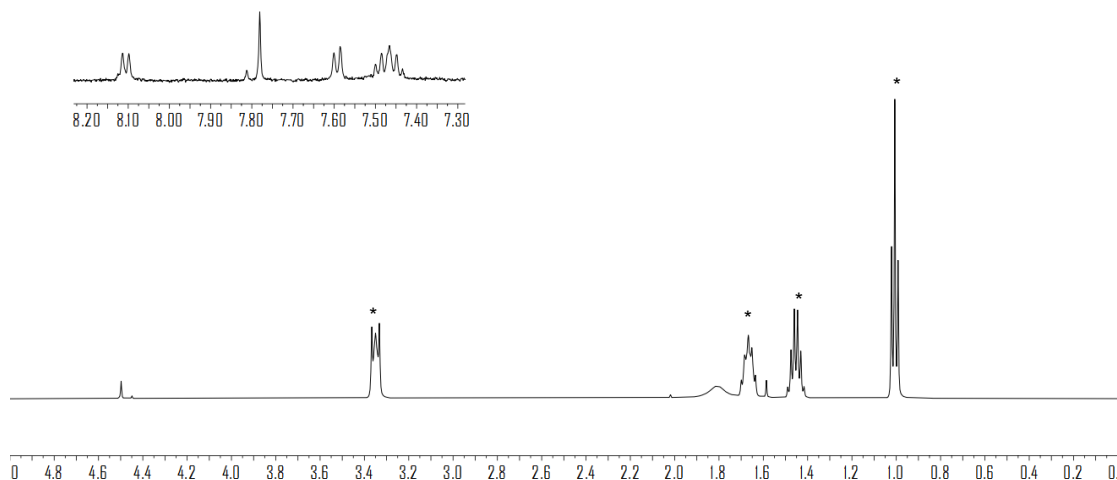


**Figure 4-3.**  $^1\text{H}$  NMR spectrum in  $\text{CDCl}_3$  of white ppt from desilylation reaction. Residual TBAF denoted with \*.

would avoid the complications with desilylation of TIPS group. The silver salt from iodide abstraction is problematic because of its low solubility in organic solvents, but the use of soluble halide abstraction reagents on immobilized complexes have been reported.<sup>125, 126</sup>

#### 4.4 Conclusion

In order to immobilize Phebox or CCC complexes, we sought to install a trialkoxysilyl group on the ligand backbone as the covalent tethering between trialkoxysilyl group and silica via Si-O-Si bridge should be effective in minimizing leaching of the metal complex. The reaction of  $^{\text{dm}}$ Phebox with  $n\text{-BuLi}$  and silane reagents did not yield any silyl functionalized product. To directly functionalize the phenyl ring of Phebox,  $^5\text{-Br}$ Phebox was synthesized and characterized with  $^1\text{H}$  NMR spectroscopy and MS. When  $^5\text{-Br}$ Phebox was treated with  $n\text{-BuLi}$ , followed by the reaction with silane reagents or MeI, the major product was dehalogenated product  $^{\text{H}}$ Phebox, indicating that the C-Br bond of  $^5\text{-Br}$ Phebox was activated but the lithiated intermediate was not reactive. The study by Harris and coworkers showed that the identity of lithium reagents gave different outcomes (Scheme 4-7),<sup>113</sup> suggesting that the desired reaction may only occur with a specific lithium reagent.

For CCC system, a different approach via click chemistry was taken using covalent linkage between azide-functionalized support materials and alkyne-functionalized molecular complexes. The metalation of the  $\text{alkyne-CCC}^{\text{Me}}$  ligand with  $[\text{Ir}(\mu\text{-OMe})(\text{COD})]_2$  and formation of  $(\text{CCC})\text{Ir}(\text{OAc})_2(\text{OH}_2)$  with  $\text{AgOAc}$  were demonstrated when alkyne group on CCC ligand was protected with TIPS group. In the reaction of  $(\text{TIPS-CCC}^{\text{Me}})\text{Ir}(\text{OAc})_2(\text{OH}_2)$  with TBAF to desilylate TIPS group, disappearance of TIPS group was observed.  $^1\text{H}$  NMR spectrum of crude product resembled that of  $(\text{CCC})\text{Ir}(\text{OAc})_2$  complex (Figure 4-3). These preliminary observations were promising, and it is possible that a better work-up procedure can lead to the isolation of the desired complex,  $(\text{HCCC}^{\text{Me}})\text{Ir}(\text{OAc})_2(\text{OH}_2)$ .

## 4.5 Experimental

All experiments and manipulations were performed using standard Schlenk techniques under an argon atmosphere or in a nitrogen-filled glovebox unless otherwise specified. THF, diethyl ether, toluene, DCM, MeOH, MeCN and DMF were passed through columns containing activated alumina and molecular sieves. 2-ethoxyethanol was dried over 4Å sieves and sparged with Ar. All other reagents were used as received. For the purpose of characterization,  $\text{CDCl}_3$  and  $\text{CD}_2\text{Cl}_2$  were used as received.  $^1\text{H}$  and  $^{13}\text{C}\{^1\text{H}\}$  NMR spectra were recorded on Bruker AVII500, UNI500 or NEO600 instruments at ambient temperature and referenced to the residual solvent peak ( $^1\text{H}$ ,  $^{13}\text{C}\{^1\text{H}\}$ ).<sup>44</sup> Nominal mass accuracy ESI-MS data were obtained by use of a Waters Acquity UPLC system equipped with a Waters TUV detector (254 nm) and a Waters SQD single quadrupole mass analyzer with electrospray ionization. Samples were taken up in  $\text{CH}_3\text{CN}$  and introduced via loop injection (0.1% v/v formic acid MeCN carrier).  $^{\text{dm}}\text{Phebox}$ ,<sup>115</sup> 3-iodopropyltrimethoxysilane,<sup>127</sup> and  $[\text{Ir}(\mu\text{-OMe})(\text{COD})]_2$ <sup>128</sup> were synthesized according to literature procedures.

### 4.5.1 Attempted Functionalization of $^{\text{dm}}\text{Phebox}$

*n*-BuLi was titrated against salicylaldehyde phenylhydrazone and its concentration was determined to be 1.43 M in hexane.<sup>129</sup>  $^{\text{dm}}\text{Phebox}$  (50mg, 0.166 mmol) was dissolved in dry THF or

diethyl ether (5 mL) and cooled to 0 °C (in ice-water bath) or -78 °C (in acetone-dry ice bath). *n*-BuLi (0.429 mmol, 1.43 M in hexane, 300  $\mu$ L) was added to the solution via a gas-tight syringe, resulting in a deep red solution. After stirring for 1 h at cold temperatures, Si(OMe)<sub>4</sub> or ClSi(OEt)<sub>3</sub> (2 equiv.) was added via a gas-tight syringe. The reaction mixture was warmed to room temperature and stirred overnight, during which the color of the solution changed from deep red to yellow. The reaction was quenched with H<sub>2</sub>O (5 mL), extracted with DCM (25 mL x 4), and dried over MgSO<sub>4</sub>. The solvents were evaporated under vacuum to isolate a lightly colored solid, identified as <sup>dm</sup>Phebox based on the matching <sup>1</sup>H NMR data with the literature.<sup>115</sup>

#### 4.5.2 Synthesis of Bromine-Substituted Phebox

##### *Synthesis of 2,2'-(5-Bromo-1,3-phenylene)bis(4,4-dimethyl-4,5-dihydrooxazole) (<sup>5-Br</sup>Phebox)*

This procedure was adapted from the literature.<sup>114, 115</sup> 5-bromoisophthalic acid (2 g, 8 mmol) was added to a dry Schlenk flask and cycled with high vacuum/Ar atmosphere three times. Toluene (30 mL) was cannula transferred to the flask, forming a colorless solution. Upon addition of thionyl chloride (6 mL, 82 mmol) and DMF (5 drops) via a gas-tight syringe, a white cloudy mixture formed. After heating at 110 °C for 2.5 h, the volatiles were evaporated under vacuum to yield a yellow oil. This oil was dissolved in dry THF (25 mL). A THF (25 mL) solution of 2-amino-2-methylpropan-1-ol (2 g, 22 mmol) and triethylamine (5 mL, 36 mmol) was cannula transferred at 0 °C. After stirring at room temperature overnight, a THF (20 mL) solution of methanesulfonyl chloride (2 mL, 26 mmol) and triethylamine (5 mL, 36 mmol) was added to the mixture. After stirring further at room temperature overnight, aqueous K<sub>2</sub>CO<sub>3</sub> (1 M, 50 mL) was added, resulting in dissolution of a white solid and formation of two layers. After extraction with ethyl acetate (50 mL x 3), the combined organic layer was washed with H<sub>2</sub>O (100 mL) and sat. brine (100 mL), dried over MgSO<sub>4</sub>, and concentrated. The crude product was purified by column chromatography on silica gel and eluted with hexane/EtOAc (50:50 v/v) to yield a light yellow oil (2.37 g, 83% yield).

<sup>1</sup>H NMR (CDCl<sub>3</sub>, 600 MHz):  $\delta$  8.39 (t, J = 1.5 Hz; 1H; Ar-H), 8.19 (d, J = 1.5 Hz; 2H; Ar-

H), 4.11 (s, 4H; oxazoline), 1.37 (s, 12H; 4 Me).

$^{13}\text{C}\{^1\text{H}\}$  NMR ( $\text{CDCl}_3$ , 150 MHz):  $\delta$  160.5, 133.7, 130.3, 126.7, 122.5, 79.5, 68.1, 28.5.

Nominal mass ESI-MS  $m/z$  = 351.3 [ $\text{M}(^{79}\text{Br})+\text{H}$ ] $^+$  (100%), 353.3 [ $\text{M}(^{81}\text{Br})+\text{H}$ ] $^+$  (98%).

*Synthesis of 2,2'-(4-Bromo-1,3-phenylene)bis(4,4-dimethyl-4,5-dihydrooxazole)*<sup>114</sup> (*<sup>4-Br</sup>Phebox*)

This synthesis followed a procedure of  $^{5-}\text{Br}$ Phebox synthesis except 4-bromoisophthalic acid was used.  $^{4-}\text{Br}$ Phebox was isolated as a light yellow oil (1.5 g, 57% yield).  $^1\text{H}$  NMR and MS data matched the literature data.<sup>114</sup>

#### 4.5.3 Attempted Functionalization of $^{\text{Br}}$ Phebox

$^{4-}\text{Br}$ Phebox or  $^{5-}\text{Br}$ Phebox (250mg, 0.71 mmol) was dissolved in dry THF or diethyl ether (10 mL) and cooled to 0 °C (in ice-water bath) or -78 °C (in acetone-dry ice bath). *n*-BuLi (1.6 M in hexane, 500  $\mu\text{L}$ ) was added to the solution via a gas-tight syringe, resulting in a deep red solution. After stirring for 1 h at cold temperatures, 3-chloro or 3-iodopropyltrimethoxysilane (1 mmol) or methyl iodide (0.80 mmol) was added via a gas-tight syringe. The reaction mixture was warmed to room temperature and stirred for 24 h, during which the color of the solution turned from deep red to yellow. The reaction was quenched with  $\text{H}_2\text{O}$  (20 mL), extracted with DCM (50 mL x 3), and dried over  $\text{MgSO}_4$ . The solvents were evaporated under vacuum to produce a yellow-brown oil. The crude oil was analyzed with  $^1\text{H}$  NMR spectroscopy, and 1,3-bis(4,4'-dimethyl-2-oxazoliny)benzene ( $^{\text{H}}$ Phebox) was identified as the major product.<sup>116</sup>

#### 4.5.4 Synthesis of Alkyne-Substituted CCC Ligands and Ir Complexes

*Synthesis of 1,1'-(5-bromo-1,3-phenylene)bis(1-benzimidazole)*<sup>122</sup> (*<sup>Br</sup>CCC*)

This procedure was adapted from the literature.<sup>121, 122</sup> A Schlenk flask was charged with CuI (0.84 mmol),  $\text{K}_2\text{CO}_3$  (16 mmol), 1,3,5-tribromobenzene (4 mmol), and benzimidazole (8 mmol), and dry DMF (20 mL) was added. The suspension was heated at 150 °C for 17 h under an Ar atmosphere. The reaction mixture was diluted with ethyl acetate (50 mL) and filtered. The ethyl acetate solution was washed with sat. brine (100 mL x 5) to remove DMF and concentrated on the

rotary evaporator to yield a yellow-brown oil. Column chromatography on silica gel, eluted with 0.5% methanol in DCM, separated mono-, di-, tri-substituted products. The desired disubstituted product was washed with hexane and isolated as an off-white solid (359 mg, 23% yield).

$^1\text{H}$  NMR ( $\text{CD}_2\text{Cl}_2$ , 600 MHz):  $\delta$  8.18 (s; 2H; carbene-H), 7.88-7.84 (m; 2H; benzimidazole), 7.83 (d,  $J = 1.9$  Hz; 2H; Ar-H), 7.72 (t,  $J = 1.9$  Hz; 1H; ipso-H), 7.66-7.61 (m; 2H; benzimidazole), 7.42-7.37 (m; 4H; benzimidazole).

$^{13}\text{C}\{^1\text{H}\}$  NMR ( $\text{CD}_2\text{Cl}_2$ , 150 MHz):  $\delta$  144.4, 141.9, 139.0, 133.2, 125.9, 124.6, 124.2, 123.3, 120.8, 117.8, 110.2.

Nominal mass ESI-MS  $m/z = 389.3$  [ $\text{M}(^{79}\text{Br})+\text{H}$ ] $^+$  (100%), 391.3 [ $\text{M}(^{81}\text{Br})+\text{H}$ ] $^+$  (90%).

*Synthesis of 1,1'-(5-(trimethylsilylethynyl)-1,3-phenylene)bis(1-benzimidazole) ( $^{\text{TMS}}$ CCC)*

A Schlenk flask with a Teflon stopcock was charged with  $^{\text{Br}}$ CCC (195 mg, 0.5 mmol), CuI (10 mg, 0.05 mmol), and  $\text{PdCl}_2(\text{PPh}_3)_2$  (17.9 mg, 0.025 mmol). In a nitrogen-atmosphere glovebox, trimethylsilylacetylene (100 mg, 1.01 mmol) and triethylamine (1.5 g, 15 mmol) were added with THF (3 mL). The flask was sealed with a Teflon stopcock, removed from the glovebox, and heated to 80 °C for 16 h. The reaction mixture darkened to an almost black color. After the volatiles were evaporated under vacuum, the crude product was purified by column chromatography on silica gel and eluted with 1% MeOH in DCM to yield a light brown solid (142 mg, 70% yield).

$^1\text{H}$  NMR ( $\text{CD}_2\text{Cl}_2$ , 600 MHz):  $\delta$  8.18 (s; 2H; carbene-H), 7.86-7.84 (m; 2H; benzimidazole), 7.73 (d,  $J = 1.9$  Hz; 2H; Ar-H), 7.70 (t,  $J = 1.9$  Hz; 1H; ipso-H), 7.65-7.63 (m; 2H; benzimidazole), 7.41-7.35 (m; 4H; benzimidazole), 0.29 (s; 9H; TMS).

$^{13}\text{C}\{^1\text{H}\}$  NMR ( $\text{CD}_2\text{Cl}_2$ , 150 MHz):  $\delta$  144.8, 142.4, 138.5, 133.8, 127.6, 126.4, 124.5, 123.5, 121.1, 119.5, 110.7, -0.23.

*Synthesis of 1,1'-(5-(triisopropylsilylethynyl)-1,3-phenylene)bis(1-benzimidazole) ( $^{\text{TIPS}}$ CCC)*

A Schlenk flask with a Teflon stopcock was charged with <sup>Br</sup>CCC (400 mg, 1 mmol), CuI (23 mg, 0.12 mmol), and PdCl<sub>2</sub>(PPh<sub>3</sub>)<sub>2</sub> (36 mg, 0.05 mmol). In a nitrogen-atmosphere glovebox, triisopropylsilylacetylene (377 mg, 2.07 mmol) and triethylamine (437 mg, 4.3 mmol) were added with THF (4 mL). The flask was sealed with a Teflon stopcock, removed from the glovebox, and heated to 80 °C for 21 h. The reaction mixture darkened to an almost black color. After the volatiles were evaporated under vacuum, the crude product was purified by column chromatography on silica gel and eluted with 1% MeOH in DCM to yield a brown oil (515 mg, 76% yield).

<sup>1</sup>H NMR (CD<sub>2</sub>Cl<sub>2</sub>, 600 MHz): δ 8.19 (s; 2H; carbene-H), 7.86-7.84 (m; 2H; benzimidazole), 7.73 (d, J = 2.0 Hz; 2H; Ar-H), 7.71 (t, J = 2.0 Hz; 1H; ipso-H), 7.63-7.62 (m; 2H; benzimidazole), 7.40-7.35 (m; 4H; benzimidazole), 1.16 (m; 21H; TIPS).

*Synthesis of 1,1'-(5-ethynyl-1,3-phenylene)bis(1-benzimidazole) (<sup>H</sup>CCC)*

In a nitrogen-atmosphere glovebox, <sup>TM</sup>SCC (31 mg, 0.076 mmol) and K<sub>2</sub>CO<sub>3</sub> (94.7 mg, 0.685 mmol) were dissolved in DCM (2 mL) and MeOH (7 mL) in a vial. The reaction mixture was stirred at room temperature for 20 h and filtered through a pad of celite and concentrated. The product was extracted with DCM (15 mL), washed with H<sub>2</sub>O (10 mL x 4) and sat. brine (15 mL), and dried over MgSO<sub>4</sub>. Evaporation of solvents produced a white solid (16 mg, 63% yield).

<sup>1</sup>H NMR (CD<sub>2</sub>Cl<sub>2</sub>, 500 MHz): δ 8.18 (s; 2H; carbene-H), 7.86-7.84 (m; 2H; benzimidazole), 7.77-7.75 (m; 3H; Ar-H), 7.65-7.63 (m; 2H; benzimidazole), 7.41-7.36 (m; 4H; benzimidazole), 3.40 (s; 1H; acetylene-H).

*Synthesis of 1,1'-(5-ethynyl-1,3-phenylene)bis(1-benzimidazolium) diiodide (<sup>H</sup>CCC<sup>Me</sup>)*

In a nitrogen-atmosphere glovebox, a Schlenk flask with a Teflon stopcock was charged with <sup>H</sup>CCC (117 mg, 0.35 mmol), MeI (240 mg, 1.69 mmol), and dry MeCN (4 mL) in the dark. The flask was wrapped in aluminum foil and heated at 100 °C for 39 h. After the reaction mixture was cool to room temperature, the volatiles were removed under vacuum. The product was washed

with DCM (20 mL) and hexane (20 mL) and filtered to collect an off-white solid (93.8 mg, 43% yield).

$^1\text{H}$  NMR (dms $o$ -d $_6$ , 600 MHz):  $\delta$  10.28 (s, 2H, carbene-H), 8.44 (t,  $J$  = 2.0 Hz; 1H; Ar-H), 8.29 (d,  $J$  = 2.0 Hz; 2H; Ar-H), 8.20 (d,  $J$  = 8.3 Hz; 2H; benzimidazole), 8.06 (d,  $J$  = 8.3 Hz; 2H; benzimidazole), 7.86 – 7.74 (m, 4H; benzimidazole), 4.78 (s, 1H; acetylene-H), 4.23 (s, 6H; Me).

*Synthesis of 1,1'-(5-(trimethylsilylethynyl)-1,3-phenylene)bis(1-benzimidazolium) diiodide (TMS $^{\text{CCC}}\text{Me}$ )*

In a nitrogen-atmosphere glovebox, a Schlenk flask with a Teflon stopcock was charged with TMS $^{\text{CCC}}$  (421 mg, 1.07 mmol), MeI (390  $\mu\text{L}$ , 6.26 mmol), and dry MeCN (10 mL) in the dark. The flask was wrapped in aluminum foil and heated at 100  $^{\circ}\text{C}$  for 20 h. After the reaction mixture was cool to room temperature, the volatiles were removed under vacuum. The product was further dried under vacuum to produce a light brown solid (483.9 mg, 43% yield).

$^1\text{H}$  NMR (CD $_2$ Cl $_2$ , 500 MHz):  $\delta$  11.19 (s; 2H; carbene-H), 8.96 (t,  $J$  = 2.0 Hz; 1H; Ar-H), 8.13 (d,  $J$  = 2.0 Hz; 2H; Ar-H), 8.07-7.99 (m; 2H; benzimidazole), 7.92-7.85 (m; 2H; benzimidazole), 7.81 – 7.74 (m; 4H; benzimidazole), 4.28 (s; 6H; Me), 0.29 (s; 9H; TMS).

*Synthesis of 1,1'-(5-(triisopropylsilylethynyl)-1,3-phenylene)bis(1-benzimidazolium) diiodide (TIPS $^{\text{CCC}}\text{Me}$ )*

In a nitrogen-atmosphere glovebox, a Schlenk flask with a Teflon stopcock was charged with TIPS $^{\text{CCC}}$  (265 mg, 0.54 mmol), MeI (241  $\mu\text{L}$ , 3.87 mmol), and dry MeCN (6 mL) in the dark. The flask was wrapped in aluminum foil and heated at 100  $^{\circ}\text{C}$  for 20 h. After the reaction mixture was cool to room temperature, the volatiles were removed under vacuum. The product was further dried under vacuum to produce a light brown solid (403.9 mg, 97% yield).

$^1\text{H}$  NMR (CD $_2$ Cl $_2$ , 500 MHz):  $\delta$  11.39 (s; 2H; carbene-H), 8.93 (t,  $J$  = 2.0 Hz; 1H; Ar-H), 8.11 (d,  $J$  = 2.0 Hz; 2H; Ar-H), 8.08-8.05 (m; 2H; benzimidazole), 7.87-7.79 (m; 6H;

benzimidazole), 4.35 (s; 6H; Me), 1.17-1.16 (m; 21H; TIPS).

*Synthesis of dimeric complex [(TIPSCCC<sup>Me</sup>)Ir(I)<sub>2</sub>]<sub>2</sub> (**30**)*

This procedure was adapted from the literature.<sup>123</sup> In a nitrogen-atmosphere glovebox, a Schlenk flask with a Teflon stopcock was charged with TIPSCCC<sup>Me</sup> ligand (100 mg, 0.129 mmol), [Ir(μ-OMe)(COD)]<sub>2</sub> (44.5 mg, 0.067 mmol), NaI (116 mg, 0.773 mmol), and 2-ethoxyethanol (10 mL). The flask was sealed with a Teflon stopcock, removed from the glovebox, and heated at 140 °C for 24 h. An orange precipitate was observed during the reaction. The reaction mixture was cooled to room temperature and diluted with MeOH (50 mL), and filtered through a medium frit. The orange solid on the frit was washed with MeOH (50 mL) and hexane (20 mL). With a different receiving flask, DCM was added to the orange solid on the frit until no more colored solution came off. Evaporation of DCM on rotary evaporator resulted in dimeric complex **30** as an orange solid (82 mg, 66% yield).

<sup>1</sup>H NMR (CDCl<sub>3</sub>, 500 MHz): δ 8.24 (d, *J* = 8.1 Hz; 4H; benzimidazole), 7.84 (s; 4H; Ar-H), 7.61-7.50 (m; 8H; benzimidazole), 7.45-7.42 (m; 4H; benzimidazole), 4.16 (s; 12H; Me), 1.24 (m; 42H; TIPS).

*Synthesis of bis-acetate complex (TIPSCCC<sup>Me</sup>)Ir(OAc)<sub>2</sub>(OH)<sub>2</sub> (**31**)*

In a nitrogen-atmosphere glovebox, a Schlenk flask with a Teflon stopcock was charged with dimer **31** (70 mg, 0.036 mmol), silver acetate (60 mg, 0.36 mmol), and 8 mL of CHCl<sub>3</sub> (dried over CaH<sub>2</sub>, distilled and sparged with N<sub>2</sub>). The flask was sealed with a Teflon stopcock, wrapped in aluminum foil, removed from the glovebox, and heated at 60 °C for 3 h. The reaction mixture was cool to room temperature and filtered through a PTFE syringe filter on the benchtop. Evaporation of solvent from the yellow filtrate resulted in a yellow oil, which solidified upon further drying under vacuum. Yield: 59.3 mg (97% yield).

<sup>1</sup>H NMR (CD<sub>2</sub>Cl<sub>2</sub>, 500 MHz): δ 8.16 (d, *J* = 8 Hz; 2H; benzimidazole), 7.73 (s; 2H; Ar-H), 7.62 (d, *J* = 8 Hz; 2H; benzimidazole), 7.53-7.46 (m; 4H; benzimidazole), 4.49 (s; 6H; Me)

x 2), 1.46 (s; 6H; OAc x 2), 1.24 (m; 21H; TIPS).

#### 4.5.5 Attempted Desilylation of Complex **31** with TBAF

This reaction was set up in a nitrogen-atmosphere glovebox. Complex **31** (5.8 mg, 0.007 mmol) was dispensed into an NMR tube with a J Young style cap. 0.6 mL of CDCl<sub>3</sub> (dried over CaH<sub>2</sub>) was added, making a homogeneous yellow solution. Outside the glovebox, under Ar funnel, tetrabutylammonium fluoride (1M in THF, 70  $\mu$ L, 0.07 mmol) was added via a gas-tight syringe. The NMR tube was sealed and placed in a 60 °C-oil bath for 24 hours, during which the color of the solution darkened, and a white precipitate was observed. The reaction mixture was cooled to room temperature, and the solution was carefully decanted. The white ppt inside the NMR tube was washed with ethyl acetate. This ppt partially dissolved in CDCl<sub>3</sub> and an <sup>1</sup>H NMR spectrum was recorded (Figure 4-2). The white ppt was then suspended in H<sub>2</sub>O (150 mL), extracted with DCM (30 mL x 3), and dried over MgSO<sub>4</sub>. Evaporation of solvent yielded a white solid, whose <sup>1</sup>H NMR spectrum in CDCl<sub>3</sub> was messy and it was difficult to identify the species present in the solution.

## 4.6 References

8. Dong, S.; Altvater, N. R.; Mark, L. O.; Hermans, I., Assessment and comparison of ordered & non-ordered supported metal oxide catalysts for upgrading propane to propylene. *Appl. Catal. A* **2021**, *617*, 118121.
9. Kumar, A.; Bhatti, T. M.; Goldman, A. S., Dehydrogenation of Alkanes and Aliphatic Groups by Pincer-Ligated Metal Complexes. *Chem. Rev.* **2017**, *117* (19), 12357-12384.
30. Choi, J.; MacArthur, A. H.; Brookhart, M.; Goldman, A. S., Dehydrogenation and related reactions catalyzed by iridium pincer complexes. *Chem. Rev.* **2011**, *111* (3), 1761-79.
42. Punji, B.; Emge, T. J.; Goldman, A. S., A Highly Stable Adamantyl-Substituted Pincer-Ligated Iridium Catalyst for Alkane Dehydrogenation. *Organometallics* **2010**, *29* (12), 2702-2709.
44. Fulmer, G. R.; Miller, A. J. M.; Sherden, N. H.; Gottlieb, H. E.; Nudelman, A.; Stoltz, B. M.; Bercaw, J. E.; Goldberg, K. I., NMR Chemical Shifts of Trace Impurities: Common Laboratory Solvents, Organics, and Gases in Deuterated Solvents Relevant to the Organometallic Chemist. *Organometallics* **2010**, *29* (9), 2176-2179.
51. Grant, J. T.; Venegas, J. M.; McDermott, W. P.; Hermans, I., Aerobic Oxidations of Light Alkanes over Solid Metal Oxide Catalysts. *Chem. Rev.* **2018**, *118* (5), 2769-2815.
53. Grant, J. T.; Love, A. M.; Carrero, C. A.; Huang, F.; Panger, J.; Verel, R.;

- Hermans, I., Improved Supported Metal Oxides for the Oxidative Dehydrogenation of Propane. *Top. Catal.* **2016**, *59* (17-18), 1545-1553.
58. Gupta, M.; Hagen, C.; Flesher, R. J.; Kaska, W. C.; Jensen, C. M., A highly active alkane dehydrogenation catalyst: stabilization of dihydrido rhodium and iridium complexes by a P–C–P pincer ligand. *Chem. Commun.* **1996**, (17), 2083-2084.
59. Göttker-Schnetmann, I.; White, P.; Brookhart, M., Iridium Bis(phosphinite) p-XPCP Pincer Complexes: Highly Active Catalysts for the Transfer Dehydrogenation of Alkanes. *J. Am. Chem. Soc.* **2004**, *126* (6), 1804-1811.
91. Docherty, S. R.; Rochlitz, L.; Payard, P.-A.; Copéret, C., Heterogeneous alkane dehydrogenation catalysts investigated via a surface organometallic chemistry approach. *Chem. Soc. Rev.* **2021**, *50* (9), 5806-5822.
92. Lee, D. W.; Kaska, W. C.; Jensen, C. M., Mechanistic Features of Iridium Pincer Complex Catalyzed Hydrocarbon Dehydrogenation Reactions: Inhibition upon Formation of a  $\mu$ -Dinitrogen Complex. *Organometallics* **1998**, *17* (1), 1-3.
93. Ghosh, R.; Kanzelberger, M.; Emge, T. J.; Hall, G. S.; Goldman, A. S., Dinitrogen Complexes of Pincer-Ligated Iridium. *Organometallics* **2006**, *25* (23), 5668-5671.
94. Morales-Morales, D.; Lee, D. W.; Wang, Z.; Jensen, C. M., Oxidative Addition of Water by an Iridium PCP Pincer Complex: Catalytic Dehydrogenation of Alkanes by IrH(OH){C<sub>6</sub>H<sub>3</sub>-2,6-(CH<sub>2</sub>PBut<sub>2</sub>)<sub>2</sub>}. *Organometallics* **2001**, *20* (6), 1144-1147.
95. Bridget Williams, D.; Kaminsky, W.; Mayer, J. M.; Goldberg, K. I., Reactions of iridium hydride pincer complexes with dioxygen: new dioxygen complexes and reversible O<sub>2</sub> binding. *Chem. Commun.* **2008**, (35), 4195.
96. Ito, J.-I.; Kaneda, T.; Nishiyama, H., Intermolecular C–H Bond Activation of Alkanes and Arenes by NCN Pincer Iridium(III) Acetate Complexes Containing Bis(oxazoliny)phenyl Ligands. *Organometallics* **2012**, *31* (12), 4442-4449.
97. Allen, K. E.; Heinekey, D. M.; Goldman, A. S.; Goldberg, K. I., Alkane Dehydrogenation by C–H Activation at Iridium(III). *Organometallics* **2013**, *32* (6), 1579-1582.
98. Allen, K. E.; Heinekey, D. M.; Goldman, A. S.; Goldberg, K. I., Regeneration of an Iridium(III) Complex Active for Alkane Dehydrogenation Using Molecular Oxygen. *Organometallics* **2014**, *33* (6), 1337-1340.
99. Allen, K. E. Synthesis of Electrophilic Rhodium and Iridium Complexes and Investigation of Reactivity for Carbon-Hydrogen Bond Activation and Functionalization. Ph.D., University of Washington, Ann Arbor, 2013.
100. Gao, Y.; Guan, C.; Zhou, M.; Kumar, A.; Emge, T. J.; Wright, A. M.; Goldberg, K. I.; Krogh-Jespersen, K.; Goldman, A. S.,  $\beta$ -Hydride Elimination and C–H Activation by an Iridium Acetate Complex, Catalyzed by Lewis Acids. Alkane Dehydrogenation Cocatalyzed by Lewis Acids and [2,6-Bis(4,4-dimethyloxazoliny)-3,5-dimethylphenyl]iridium. *J. Am. Chem. Soc.* **2017**, *139* (18), 6338-6350.
101. Chianese, A. R.; Mo, A.; Lampland, N. L.; Swartz, R. L.; Bremer, P. T., Iridium Complexes of CCC-Pincer N-Heterocyclic Carbene Ligands: Synthesis and Catalytic C–H Functionalization. *Organometallics* **2010**, *29* (13), 3019-3026.
102. Chianese, A. R.; Shaner, S. E.; Tendler, J. A.; Pudalov, D. M.; Shopov, D. Y.; Kim, D.; Rogers, S. L.; Mo, A., Iridium Complexes of Bulky CCC-Pincer N-Heterocyclic Carbene

Ligands: Steric Control of Coordination Number and Catalytic Alkene Isomerization. *Organometallics* **2012**, *31* (21), 7359-7367.

103. Chianese, A. R.; Drance, M. J.; Jensen, K. H.; Mccollom, S. P.; Yusufova, N.; Shaner, S. E.; Shopov, D. Y.; Tandler, J. A., Acceptorless Alkane Dehydrogenation Catalyzed by Iridium CCC-Pincer Complexes. *Organometallics* **2014**, *33* (2), 457-464.
104. Rubashkin, S. B.; Chu, W.-Y.; Goldberg, K. I., Lowering the Barrier to C–H Activation at Ir(III) through Pincer Ligand Design. *Organometallics* **2021**, *40* (9), 1296-1302.
105. Rubashkin, S. Aerobic Oxidation of Hydrocarbons with Iridium(III) Pincer. Ph.D., University of Pennsylvania, 2021.
106. Merckle, C.; Blümel, J., Bifunctional Phosphines Immobilized on Inorganic Oxides. *Chem. Mater.* **2001**, *13* (10), 3617-3623.
107. Reinhard, S.; Šoba, P.; Rominger, F.; Blümel, J., New Silica-Immobilized Nickel Catalysts for Cyclootrimerizations of Acetylenes. *Adv. Synth. Catal.* **2003**, *345* (5), 589-602.
108. Djuric, S.; Sarkar, T.; Magnus, P., Silicon in synthesis: an exceptionally short synthesis of dl-11.alpha.-hydroxyestrone methyl ether. *J. Am. Chem. Soc.* **1980**, *102* (22), 6885-6886.
109. Ito, Y.; Amino, Y.; Nakatsuka, M.; Saegusa, T., A new approach to asymmetric synthesis of polycycles on the basis of o-quinodimethane generation. *J. Am. Chem. Soc.* **1983**, *105* (6), 1586-1590.
110. Imae, I.; Tokita, D.; Ooyama, Y.; Komaguchi, K.; Ohshita, J.; Harima, Y., Oligothiophenes incorporated in a polysilsesquioxane network: application to tunable transparent conductive films. *J. Mater. Chem.* **2012**, *22* (32), 16407.
111. Yukimoto, M.; Minoura, M., The Synthesis of a Novel Bulky Primary Alkyl Group and Its Application toward the Kinetic Stabilization of a Tetraalkyldisilene. *Bull. Chem. Soc. Jpn.* **2018**, *91* (4), 585-587.
112. Fu, P. P.; Unruh, L. E.; Miller, D. W.; Huang, L. W.; Yang, D. T. C., Synthesis of 3-aryl-3,4-dihydroisocoumarins. *J. Org. Chem.* **1985**, *50* (8), 1259-1261.
113. Harris, T.; Neuschwander, B.; Boekelheide, V., Synthesis of trans-15-n-butyl-16-methylidihydropyrene. Synthetic access to 1,2,3-trisubstituted benzene derivatives via direct alkylation of 1,3-bis(4',4'-dimethyl-2'-oxazoliny)benzene. *The Journal of Organic Chemistry* **1978**, *43* (4), 727-730.
114. Wirth, R.; Gao, P.; Nienhaus, G. U.; Sunbul, M.; Jäschke, A., SiRA: A Silicon Rhodamine-Binding Aptamer for Live-Cell Super-Resolution RNA Imaging. *J. Am. Chem. Soc.* **2019**, *141* (18), 7562-7571.
115. Ito, J. I.; Shiomi, T.; Nishiyama, H., Efficient preparation of new rhodium- and iridium-[bis(oxazoliny)-3,5-dimethylphenyl] complexes by C-H bond activation: Applications in asymmetric synthesis. *Adv. Synth. Catal.* **2006**, *348* (10-11), 1235-1240.
116. Zhao, D.; Krause, J. A.; Connick, W. B., Platinum(II) Monomer and Dimer Complexes with a Bis(oxazoliny)phenyl Pincer Ligand. *Inorg. Chem.* **2015**, *54* (17), 8339-8347.
117. Aliphatic Substitution: Nucleophilic and Organometallic. *March's Advanced Organic Chemistry* **2006**, 425-656.
118. Pola, J.; Jakoubková, M.; Chvalovský, V., The extent of some intramolecular effects in triethoxy- and trimethoxysilanes. *Collection of Czechoslovak Chemical Communications* **1978**, *43*

(12), 3391-3395.

119. Wu, L.; Eberhart, M.; Shan, B.; Nayak, A.; Brennaman, M. K.; Miller, A. J. M.; Shao, J.; Meyer, T. J., Stable Molecular Surface Modification of Nanostructured, Mesoporous Metal Oxide Photoanodes by Silane and Click Chemistry. *ACS Appl. Mater. Interfaces* **2019**, *11* (4), 4560-4567.

120. Bagherzadeh, M.; Hosseini, M.; Mortazavi-Manesh, A., Manganese(III) porphyrin anchored onto magnetic nanoparticles via "Click" reaction: An efficient and reusable catalyst for the heterogeneous oxidation of alkenes and sulfides. *Inorg. Chem. Commun.* **2019**, *107*.

121. Li, C.; Gao, C.; Lan, J.; You, J.; Gao, G., An AIE active Y-shaped diimidazolylbenzene: aggregation and disaggregation for Cd<sup>2+</sup> and Fe<sup>3+</sup> sensing in aqueous solution. *Org. Biomol. Chem.* **2014**, *12* (47), 9524-9527.

122. Brazeau, A. L.; Yuan, K.; Ko, S.-B.; Wyman, I.; Wang, S., Anion Sensing with a Blue Fluorescent Triarylboron-Functionalized Bisbenzimidazole and Its Bisbenzimidazolium Salt. *ACS Omega* **2017**, *2* (12), 8625-8632.

123. Adamovich, V.; Boudreault, P.-L. T.; Esteruelas, M. A.; Gómez-Bautista, D.; López, A. M.; Oñate, E.; Tsai, J.-Y., Preparation via a NHC Dimer Complex, Photophysical Properties, and Device Performance of Heteroleptic Bis(tridentate) Iridium(III) Emitters. *Organometallics* **2019**, *38* (14), 2738-2747.

124. Protection for the Hydroxyl Group, Including 1,2- and 1,3-Diols. *Greene's Protective Groups in Organic Synthesis* **2014**, 17-471.

125. Mehendale, N. C.; Bezemer, C.; Van Walree, C. A.; Klein Gebbink, R. J. M.; Van Koten, G., Novel silica immobilized NCN-pincer palladium(II) and platinum(II) complexes: Application as Lewis acid catalysts. *J. Mol. Catal. A: Chem.* **2006**, *257* (1-2), 167-175.

126. Reiner, B. R.; Mucha, N. T.; Rothstein, A.; Temme, J. S.; Duan, P.; Schmidt-Rohr, K.; Foxman, B. M.; Wade, C. R., Zirconium Metal–Organic Frameworks Assembled from Pd and Pt PNNNP Pincer Complexes: Synthesis, Postsynthetic Modification, and Lewis Acid Catalysis. *Inorg. Chem.* **2018**, *57* (5), 2663-2672.

127. Chen, J.; Hua, L.; Chen, C.; Guo, L.; Zhang, R.; Chen, A.; Xiu, Y.; Liu, X.; Hou, Z., Temperature-Dependent Immobilization of a Tungsten Peroxo Complex That Catalyzes the Hydroxymethoxylation of Olefins. *ChemPlusChem* **2015**, *80* (6), 1029-1037.

128. Pang, Y.; Ishiyama, T.; Kubota, K.; Ito, H., Iridium(I)-Catalyzed C-H Borylation in Air by Using Mechanochemistry. *Chem. Eur. J.* **2019**, *25* (18), 4654-4659.

129. Love, B. E.; Jones, E. G., The Use of Salicylaldehyde Phenylhydrazone as an Indicator for the Titration of Organometallic Reagents. *J. Org. Chem.* **1999**, *64* (10), 3755-3756.

## Appendix A: Crystallographic Information

Data was collected at -173 °C on a Bruker APEX II single crystal X-ray diffractometer, Mo-radiation. Solution by direct methods (SHELXS, SIR97<sup>130, 131</sup>) produced a complete heavy atom phasing model consistent with the proposed structure. The structure was completed by difference Fourier synthesis with SHELXL97.<sup>132-134</sup> Scattering factors are from Waasmair and Kirfel.<sup>135</sup> Hydrogen atoms were placed in geometrically idealized positions and constrained to ride on their parent atoms with C---H distances in the range 0.95-1.00 Angstrom. Isotropic thermal parameters  $U_{eq}$  were fixed such that they were  $1.2U_{eq}$  of their parent atom  $U_{eq}$  for CH's and  $1.5U_{eq}$  of their parent atom  $U_{eq}$  in case of methyl groups. All non-hydrogen atoms were refined anisotropically by full-matrix least-squares.

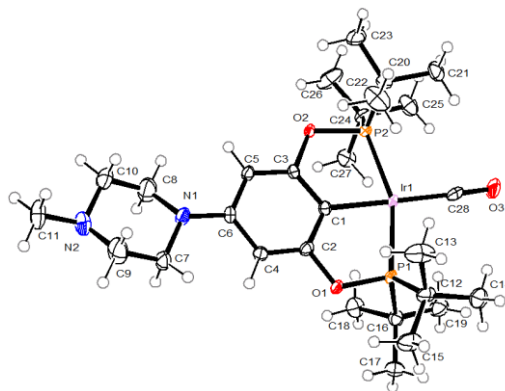
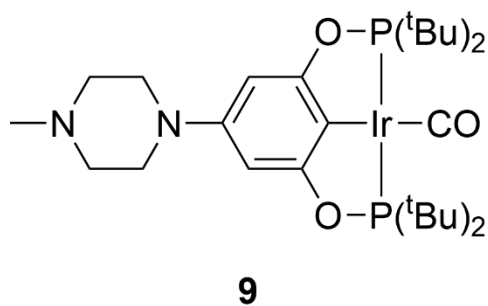


**Figure A-1.** ORTEP of complex 9 with thermal ellipsoids at the 50% probability level. The dichloromethane molecule was removed for clarity.

**Table A-1. Crystal data and structure refinement for complex 9.**

Empirical formula	C <sub>29</sub> H <sub>51</sub> Cl <sub>2</sub> Ir N <sub>2</sub> O <sub>3</sub> P <sub>2</sub>
Formula weight	800.76
Temperature	100(2) K
Wavelength	0.71073 Å
Crystal system	Orthorhombic
Space group	P b c a
Unit cell dimensions	a = 11.5734(5) Å      α = 90°. b = 15.6094(7) Å      β = 90°. c = 38.1996(18) Å     γ = 90°.
Volume	6900.9(5) Å <sup>3</sup>
Z	8
Density (calculated)	1.541 Mg/m <sup>3</sup>
Absorption coefficient	4.148 mm <sup>-1</sup>
F(000)	3232
Crystal size	0.15 x 0.08 x 0.05 mm <sup>3</sup>
Theta range for data collection	2.06 to 25.43°.
Index ranges	-13 ≤ h ≤ 13, -18 ≤ k ≤ 18, -46 ≤ l ≤ 46
Reflections collected	152176
Independent reflections	6355 [R(int) = 0.0824]
Completeness to theta = 25.00°	100.0 %
Absorption correction	Semi-empirical from equivalents
Max. and min. transmission	0.8194 and 0.5750
Refinement method	Full-matrix least-squares on F <sup>2</sup>
Data / restraints / parameters	6355 / 0 / 365
Goodness-of-fit on F <sup>2</sup>	1.073
Final R indices [I > 2σ(I)]	R1 = 0.0291, wR2 = 0.0532
R indices (all data)	R1 = 0.0431, wR2 = 0.0576
Largest diff. peak and hole	1.161 and -1.567 e.Å <sup>-3</sup>

**Table A-2.** Atomic coordinates ( $\times 10^4$ ) and equivalent isotropic displacement parameters ( $\text{\AA}^2 \times 10^3$ ) for complex **9**.  $U(\text{eq})$  is defined as one third of the trace of the orthogonalized  $U^{ij}$  tensor.

	x	y	z	U(eq)
Ir(1)	5148(1)	9578(1)	8304(1)	15(1)
P(1)	6571(1)	10276(1)	8599(1)	16(1)
P(2)	3812(1)	8542(1)	8197(1)	15(1)
Cl(1)	2694(1)	10437(1)	9458(1)	57(1)
O(1)	6752(2)	9762(2)	8975(1)	18(1)
Cl(2)	3537(2)	9508(1)	10062(1)	79(1)
O(2)	3875(2)	7867(2)	8533(1)	17(1)
C(17)	8990(4)	10675(3)	8602(1)	28(1)
O(3)	4732(4)	10777(2)	7700(1)	63(1)
C(1)	5316(3)	8833(2)	8740(1)	16(1)
C(2)	6050(3)	9037(2)	9013(1)	18(1)
C(12)	6247(4)	11369(3)	8764(1)	26(1)
C(15)	7030(4)	11658(3)	9067(1)	36(1)
C(13)	5005(4)	11316(3)	8896(2)	42(1)
C(14)	6316(5)	12006(3)	8457(2)	40(1)
C(16)	8034(4)	10200(3)	8403(1)	21(1)
C(19)	7988(4)	10509(3)	8024(1)	34(1)
C(18)	8305(4)	9232(3)	8400(1)	30(1)
C(4)	6124(4)	8581(3)	9323(1)	18(1)
C(6)	5399(4)	7866(2)	9370(1)	17(1)
N(1)	5368(3)	7418(2)	9689(1)	23(1)
C(7)	6148(4)	7656(3)	9970(1)	28(1)
C(9)	5705(5)	7325(3)	10314(1)	45(1)
N(2)	5468(4)	6433(3)	10316(1)	40(1)
C(10)	4642(5)	6239(4)	10042(1)	43(1)
C(8)	5152(5)	6496(3)	9687(1)	43(1)
C(11)	5044(5)	6143(3)	10657(1)	40(1)
C(5)	4649(3)	7633(2)	9097(1)	17(1)

C(3)	4632(3)	8108(2)	8798(1)	14(1)
C(20)	2271(3)	8878(3)	8230(1)	22(1)
C(23)	1433(4)	8121(3)	8241(2)	49(2)
C(22)	2206(4)	9374(4)	8575(1)	43(1)
C(21)	1948(4)	9482(3)	7929(1)	30(1)
C(24)	4105(4)	7784(3)	7833(1)	20(1)
C(26)	3440(5)	6937(3)	7858(1)	44(2)
C(27)	5398(4)	7588(3)	7862(1)	28(1)
C(25)	3885(4)	8215(3)	7481(1)	34(1)
C(28)	4921(4)	10305(3)	7924(1)	33(1)
C(29)	3181(6)	9446(4)	9618(2)	63(2)

---

**Table A-3.** Bond lengths [Å] and angles [°] for complex **9**.

---

Ir(1)-C(28)	1.862(5)
Ir(1)-C(1)	2.041(4)
Ir(1)-P(2)	2.2741(10)
Ir(1)-P(1)	2.2753(11)
P(1)-O(1)	1.657(3)
P(1)-C(12)	1.855(4)
P(1)-C(16)	1.856(4)
P(2)-O(2)	1.664(3)
P(2)-C(24)	1.855(4)
P(2)-C(20)	1.863(4)
Cl(1)-C(29)	1.756(6)
O(1)-C(2)	1.401(5)
Cl(2)-C(29)	1.750(7)
O(2)-C(3)	1.390(5)
C(17)-C(16)	1.534(6)
C(17)-H(17A)	0.9800
C(17)-H(17B)	0.9800
C(17)-H(17C)	0.9800
O(3)-C(28)	1.149(5)
C(1)-C(2)	1.382(6)
C(1)-C(3)	1.399(5)
C(2)-C(4)	1.385(6)
C(12)-C(13)	1.526(6)
C(12)-C(14)	1.537(7)
C(12)-C(15)	1.539(6)
C(15)-H(15A)	0.9800
C(15)-H(15B)	0.9800
C(15)-H(15C)	0.9800
C(13)-H(13A)	0.9800
C(13)-H(13B)	0.9800
C(13)-H(13C)	0.9800
C(14)-H(14A)	0.9800

C(14)-H(14B)	0.9800
C(14)-H(14C)	0.9800
C(16)-C(19)	1.526(6)
C(16)-C(18)	1.543(6)
C(19)-H(19A)	0.9800
C(19)-H(19B)	0.9800
C(19)-H(19C)	0.9800
C(18)-H(18A)	0.9800
C(18)-H(18B)	0.9800
C(18)-H(18C)	0.9800
C(4)-C(6)	1.408(6)
C(4)-H(4)	0.9500
C(6)-C(5)	1.404(6)
C(6)-N(1)	1.405(5)
N(1)-C(7)	1.450(6)
N(1)-C(8)	1.462(6)
C(7)-C(9)	1.502(7)
C(7)-H(7A)	0.9900
C(7)-H(7B)	0.9900
C(9)-N(2)	1.419(6)
C(9)-H(9A)	0.9900
C(9)-H(9B)	0.9900
N(2)-C(10)	1.452(6)
N(2)-C(11)	1.463(6)
C(10)-C(8)	1.532(7)
C(10)-H(10A)	0.9900
C(10)-H(10B)	0.9900
C(8)-H(8A)	0.9900
C(8)-H(8B)	0.9900
C(11)-H(11A)	0.9800
C(11)-H(11B)	0.9800
C(11)-H(11C)	0.9800
C(5)-C(3)	1.363(5)
C(5)-H(5)	0.9500

C(20)-C(23)	1.529(6)
C(20)-C(22)	1.531(6)
C(20)-C(21)	1.533(6)
C(23)-H(23A)	0.9800
C(23)-H(23B)	0.9800
C(23)-H(23C)	0.9800
C(22)-H(22A)	0.9800
C(22)-H(22B)	0.9800
C(22)-H(22C)	0.9800
C(21)-H(21A)	0.9800
C(21)-H(21B)	0.9800
C(21)-H(21C)	0.9800
C(24)-C(25)	1.527(6)
C(24)-C(27)	1.531(6)
C(24)-C(26)	1.533(6)
C(26)-H(26A)	0.9800
C(26)-H(26B)	0.9800
C(26)-H(26C)	0.9800
C(27)-H(27A)	0.9800
C(27)-H(27B)	0.9800
C(27)-H(27C)	0.9800
C(25)-H(25A)	0.9800
C(25)-H(25B)	0.9800
C(25)-H(25C)	0.9800
C(29)-H(29A)	0.9900
C(29)-H(29B)	0.9900
C(28)-Ir(1)-C(1)	175.96(19)
C(28)-Ir(1)-P(2)	101.37(13)
C(1)-Ir(1)-P(2)	78.87(12)
C(28)-Ir(1)-P(1)	101.38(13)
C(1)-Ir(1)-P(1)	78.38(12)
P(2)-Ir(1)-P(1)	157.23(4)

O(1)-P(1)-C(12)	100.23(19)
O(1)-P(1)-C(16)	101.85(17)
C(12)-P(1)-C(16)	112.3(2)
O(1)-P(1)-Ir(1)	106.82(10)
C(12)-P(1)-Ir(1)	117.47(15)
C(16)-P(1)-Ir(1)	115.39(14)
O(2)-P(2)-C(24)	99.55(17)
O(2)-P(2)-C(20)	99.67(17)
C(24)-P(2)-C(20)	113.9(2)
O(2)-P(2)-Ir(1)	106.33(10)
C(24)-P(2)-Ir(1)	117.65(14)
C(20)-P(2)-Ir(1)	116.01(14)
C(2)-O(1)-P(1)	114.0(2)
C(3)-O(2)-P(2)	114.8(2)
C(16)-C(17)-H(17A)	109.5
C(16)-C(17)-H(17B)	109.5
H(17A)-C(17)-H(17B)	109.5
C(16)-C(17)-H(17C)	109.5
H(17A)-C(17)-H(17C)	109.5
H(17B)-C(17)-H(17C)	109.5
C(2)-C(1)-C(3)	114.5(4)
C(2)-C(1)-Ir(1)	122.9(3)
C(3)-C(1)-Ir(1)	122.4(3)
C(1)-C(2)-C(4)	124.4(4)
C(1)-C(2)-O(1)	117.7(4)
C(4)-C(2)-O(1)	117.9(4)
C(13)-C(12)-C(14)	109.7(4)
C(13)-C(12)-C(15)	108.7(4)
C(14)-C(12)-C(15)	110.6(4)
C(13)-C(12)-P(1)	104.7(3)
C(14)-C(12)-P(1)	109.1(3)
C(15)-C(12)-P(1)	113.9(3)
C(12)-C(15)-H(15A)	109.5
C(12)-C(15)-H(15B)	109.5

H(15A)-C(15)-H(15B)	109.5
C(12)-C(15)-H(15C)	109.5
H(15A)-C(15)-H(15C)	109.5
H(15B)-C(15)-H(15C)	109.5
C(12)-C(13)-H(13A)	109.5
C(12)-C(13)-H(13B)	109.5
H(13A)-C(13)-H(13B)	109.5
C(12)-C(13)-H(13C)	109.5
H(13A)-C(13)-H(13C)	109.5
H(13B)-C(13)-H(13C)	109.5
C(12)-C(14)-H(14A)	109.5
C(12)-C(14)-H(14B)	109.5
H(14A)-C(14)-H(14B)	109.5
C(12)-C(14)-H(14C)	109.5
H(14A)-C(14)-H(14C)	109.5
H(14B)-C(14)-H(14C)	109.5
C(19)-C(16)-C(17)	110.1(4)
C(19)-C(16)-C(18)	108.1(4)
C(17)-C(16)-C(18)	109.2(4)
C(19)-C(16)-P(1)	109.4(3)
C(17)-C(16)-P(1)	115.2(3)
C(18)-C(16)-P(1)	104.5(3)
C(16)-C(19)-H(19A)	109.5
C(16)-C(19)-H(19B)	109.5
H(19A)-C(19)-H(19B)	109.5
C(16)-C(19)-H(19C)	109.5
H(19A)-C(19)-H(19C)	109.5
H(19B)-C(19)-H(19C)	109.5
C(16)-C(18)-H(18A)	109.5
C(16)-C(18)-H(18B)	109.5
H(18A)-C(18)-H(18B)	109.5
C(16)-C(18)-H(18C)	109.5
H(18A)-C(18)-H(18C)	109.5
H(18B)-C(18)-H(18C)	109.5

C(2)-C(4)-C(6)	118.7(4)
C(2)-C(4)-H(4)	120.7
C(6)-C(4)-H(4)	120.7
C(5)-C(6)-N(1)	120.0(4)
C(5)-C(6)-C(4)	118.6(4)
N(1)-C(6)-C(4)	121.3(4)
C(6)-N(1)-C(7)	119.9(3)
C(6)-N(1)-C(8)	119.2(4)
C(7)-N(1)-C(8)	111.3(4)
N(1)-C(7)-C(9)	110.2(4)
N(1)-C(7)-H(7A)	109.6
C(9)-C(7)-H(7A)	109.6
N(1)-C(7)-H(7B)	109.6
C(9)-C(7)-H(7B)	109.6
H(7A)-C(7)-H(7B)	108.1
N(2)-C(9)-C(7)	114.2(4)
N(2)-C(9)-H(9A)	108.7
C(7)-C(9)-H(9A)	108.7
N(2)-C(9)-H(9B)	108.7
C(7)-C(9)-H(9B)	108.7
H(9A)-C(9)-H(9B)	107.6
C(9)-N(2)-C(10)	109.1(4)
C(9)-N(2)-C(11)	112.0(4)
C(10)-N(2)-C(11)	111.0(4)
N(2)-C(10)-C(8)	109.3(4)
N(2)-C(10)-H(10A)	109.8
C(8)-C(10)-H(10A)	109.8
N(2)-C(10)-H(10B)	109.8
C(8)-C(10)-H(10B)	109.8
H(10A)-C(10)-H(10B)	108.3
N(1)-C(8)-C(10)	108.5(4)
N(1)-C(8)-H(8A)	110.0
C(10)-C(8)-H(8A)	110.0
N(1)-C(8)-H(8B)	110.0

C(10)-C(8)-H(8B)	110.0
H(8A)-C(8)-H(8B)	108.4
N(2)-C(11)-H(11A)	109.5
N(2)-C(11)-H(11B)	109.5
H(11A)-C(11)-H(11B)	109.5
N(2)-C(11)-H(11C)	109.5
H(11A)-C(11)-H(11C)	109.5
H(11B)-C(11)-H(11C)	109.5
C(3)-C(5)-C(6)	119.4(4)
C(3)-C(5)-H(5)	120.3
C(6)-C(5)-H(5)	120.3
C(5)-C(3)-O(2)	118.2(3)
C(5)-C(3)-C(1)	124.3(4)
O(2)-C(3)-C(1)	117.4(3)
C(23)-C(20)-C(22)	109.6(4)
C(23)-C(20)-C(21)	110.0(4)
C(22)-C(20)-C(21)	108.8(4)
C(23)-C(20)-P(2)	113.1(3)
C(22)-C(20)-P(2)	104.3(3)
C(21)-C(20)-P(2)	110.8(3)
C(20)-C(23)-H(23A)	109.5
C(20)-C(23)-H(23B)	109.5
H(23A)-C(23)-H(23B)	109.5
C(20)-C(23)-H(23C)	109.5
H(23A)-C(23)-H(23C)	109.5
H(23B)-C(23)-H(23C)	109.5
C(20)-C(22)-H(22A)	109.5
C(20)-C(22)-H(22B)	109.5
H(22A)-C(22)-H(22B)	109.5
C(20)-C(22)-H(22C)	109.5
H(22A)-C(22)-H(22C)	109.5
H(22B)-C(22)-H(22C)	109.5
C(20)-C(21)-H(21A)	109.5
C(20)-C(21)-H(21B)	109.5

H(21A)-C(21)-H(21B)	109.5
C(20)-C(21)-H(21C)	109.5
H(21A)-C(21)-H(21C)	109.5
H(21B)-C(21)-H(21C)	109.5
C(25)-C(24)-C(27)	108.3(4)
C(25)-C(24)-C(26)	110.6(4)
C(27)-C(24)-C(26)	108.3(4)
C(25)-C(24)-P(2)	110.4(3)
C(27)-C(24)-P(2)	104.6(3)
C(26)-C(24)-P(2)	114.3(3)
C(24)-C(26)-H(26A)	109.5
C(24)-C(26)-H(26B)	109.5
H(26A)-C(26)-H(26B)	109.5
C(24)-C(26)-H(26C)	109.5
H(26A)-C(26)-H(26C)	109.5
H(26B)-C(26)-H(26C)	109.5
C(24)-C(27)-H(27A)	109.5
C(24)-C(27)-H(27B)	109.5
H(27A)-C(27)-H(27B)	109.5
C(24)-C(27)-H(27C)	109.5
H(27A)-C(27)-H(27C)	109.5
H(27B)-C(27)-H(27C)	109.5
C(24)-C(25)-H(25A)	109.5
C(24)-C(25)-H(25B)	109.5
H(25A)-C(25)-H(25B)	109.5
C(24)-C(25)-H(25C)	109.5
H(25A)-C(25)-H(25C)	109.5
H(25B)-C(25)-H(25C)	109.5
O(3)-C(28)-Ir(1)	176.0(5)
Cl(2)-C(29)-Cl(1)	111.4(3)
Cl(2)-C(29)-H(29A)	109.3
Cl(1)-C(29)-H(29A)	109.3
Cl(2)-C(29)-H(29B)	109.3
Cl(1)-C(29)-H(29B)	109.3



**Table A-4.** Anisotropic displacement parameters ( $\text{\AA}^2 \times 10^3$ ) for complex **9**. The anisotropic displacement factor exponent takes the form:  $-2\pi^2 [ h^2 a^{*2} U^{11} + \dots + 2 h k a^* b^* U^{12} ]$

	U <sup>11</sup>	U <sup>22</sup>	U <sup>33</sup>	U <sup>23</sup>	U <sup>13</sup>	U <sup>12</sup>
Ir(1)	17(1)	10(1)	18(1)	3(1)	-3(1)	-2(1)
P(1)	17(1)	8(1)	22(1)	1(1)	-2(1)	-1(1)
P(2)	15(1)	13(1)	17(1)	2(1)	-1(1)	-2(1)
Cl(1)	60(1)	46(1)	65(1)	-12(1)	16(1)	-4(1)
O(1)	24(2)	14(2)	17(2)	4(1)	-4(1)	-7(1)
Cl(2)	84(1)	88(1)	66(1)	-2(1)	-18(1)	-26(1)
O(2)	21(2)	14(1)	16(2)	6(1)	-4(1)	-6(1)
C(17)	17(2)	34(3)	34(3)	1(2)	-1(2)	-2(2)
O(3)	77(3)	51(2)	60(3)	43(2)	-43(2)	-39(2)
C(1)	17(2)	12(2)	19(2)	1(2)	0(2)	2(2)
C(2)	17(2)	12(2)	24(3)	0(2)	2(2)	-1(2)
C(12)	22(2)	13(2)	43(3)	-7(2)	-4(2)	0(2)
C(15)	33(3)	21(2)	53(4)	-16(2)	-5(3)	0(2)
C(13)	25(3)	35(3)	66(4)	-28(3)	3(3)	5(2)
C(14)	42(3)	14(2)	64(4)	1(2)	-16(3)	1(2)
C(16)	23(2)	19(2)	23(3)	1(2)	0(2)	1(2)
C(19)	31(3)	38(3)	31(3)	4(2)	3(2)	-10(2)
C(18)	32(3)	24(2)	35(3)	-4(2)	3(2)	9(2)
C(4)	21(2)	17(2)	16(2)	-1(2)	-2(2)	-2(2)
C(6)	23(2)	15(2)	14(2)	3(2)	1(2)	3(2)
N(1)	31(2)	17(2)	20(2)	2(2)	0(2)	-5(2)
C(7)	38(3)	26(2)	19(3)	4(2)	-5(2)	-7(2)
C(9)	73(4)	42(3)	21(3)	0(2)	-8(3)	-8(3)
N(2)	49(3)	45(3)	27(2)	15(2)	-5(2)	-4(2)
C(10)	50(3)	46(3)	34(3)	19(3)	-5(3)	-19(3)
C(8)	62(4)	31(3)	35(3)	3(2)	-6(3)	-7(3)
C(11)	60(4)	37(3)	24(3)	13(2)	11(3)	9(3)
C(5)	20(2)	13(2)	18(2)	2(2)	0(2)	-2(2)
C(3)	16(2)	14(2)	14(2)	0(2)	0(2)	2(2)

C(20)	15(2)	24(2)	26(3)	2(2)	-1(2)	1(2)
C(23)	14(2)	38(3)	94(5)	27(3)	-3(3)	-2(2)
C(22)	33(3)	67(4)	30(3)	-5(3)	8(2)	19(3)
C(21)	26(2)	25(2)	37(3)	6(2)	-1(2)	11(2)
C(24)	22(2)	18(2)	20(2)	-1(2)	2(2)	-5(2)
C(26)	55(4)	34(3)	41(3)	-20(3)	15(3)	-23(3)
C(27)	29(3)	23(2)	33(3)	-8(2)	-1(2)	7(2)
C(25)	35(3)	43(3)	24(3)	-2(2)	-2(2)	11(2)
C(28)	32(3)	26(2)	41(3)	9(2)	-12(2)	-18(2)
C(29)	79(5)	49(4)	62(5)	-16(3)	8(4)	6(3)

---

## References

130. Altomare, A.; Cascarano, G.; Giacovazzo, C.; Guagliardi, A., Completion and refinement of crystal structures with SIR92. *Journal of Applied Crystallography* **1993**, *26* (3), 343-350.
131. Altomare, A.; Burla, M. C.; Camalli, M.; Cascarano, G. L.; Giacovazzo, C.; Guagliardi, A.; Moliterni, A. G. G.; Polidori, G.; Spagna, R., SIR97: a new tool for crystal structure determination and refinement. *Journal of Applied Crystallography* **1999**, *32* (1), 115-119.
132. Sheldrick, G. M., Crystal structure refinement with SHELXL. *Acta Crystallographica Section C Structural Chemistry* **2015**, *71* (1), 3-8.
133. Sheldrick, G. M. *SHELXS-97, Program for crystal structure solution*, University of Göttingen, Göttingen, Germany, 1997.
134. Mackay, S.; Edwards, C.; Henderson, A.; Gilmore, C.; Stewart, N.; Shankland, K.; Donald, A. *MaXus: a computer program for the solution and refinement of crystal structures from diffraction data*, University of Glasgow, Scotland, 1997.
135. Waasmaier, D.; Kirfel, A., New analytical scattering-factor functions for free atoms and ions. *Acta Crystallographica Section A Foundations of Crystallography* **1995**, *51* (3), 416-431.

## Bibliography

1. Anastas, P.; Eghbali, N., Green Chemistry: Principles and Practice. *Chem. Soc. Rev.* **2010**, 39 (1), 301-312.
2. Energy Information Administration U.S. energy facts explained. <https://www.eia.gov/energyexplained/us-energy-facts/> (accessed Dec 19, 2021).
3. Quispe, C. A. G.; Coronado, C. J. R.; Carvalho Jr, J. A., Glycerol: Production, consumption, prices, characterization and new trends in combustion. *Renew. Sustain. Energy Rev.* **2013**, 27, 475-493.
4. Johnson, D. T.; Taconi, K. A., The glycerin glut: Options for the value-added conversion of crude glycerol resulting from biodiesel production. *Environ. Prog.* **2007**, 26 (4), 338-348.
5. Anitha, M.; Kamarudin, S. K.; Kofli, N. T., The potential of glycerol as a value-added commodity. *Chem. Eng. J.* **2016**, 295, 119-130.
6. Vivek, N.; Pandey, A.; Binod, P., Production and Applications of 1,3-Propanediol. In *Curr. Dev. Biotechnol. Bioeng.: Prod., Isol. Purif. Ind. Prod.*, 2017; pp 719-738.
7. Sattler, J. J. H. B.; Ruiz-Martinez, J.; Santillan-Jimenez, E.; Weckhuysen, B. M., Catalytic Dehydrogenation of Light Alkanes on Metals and Metal Oxides. *Chem. Rev.* **2014**, 114 (20), 10613-10653.
8. Dong, S.; Altvater, N. R.; Mark, L. O.; Hermans, I., Assessment and comparison of ordered & non-ordered supported metal oxide catalysts for upgrading propane to propylene. *Appl. Catal. A* **2021**, 617, 118121.
9. Kumar, A.; Bhatti, T. M.; Goldman, A. S., Dehydrogenation of Alkanes and Aliphatic Groups by Pincer-Ligated Metal Complexes. *Chem. Rev.* **2017**, 117 (19), 12357-12384.
10. Kozuch, S.; Martin, J. M. L., "Turning Over" Definitions in Catalytic Cycles. *ACS Catal.* **2012**, 2 (12), 2787-2794.
11. OECD/FAO, *OECD-FAO Agricultural Outlook (Edition 2020)*, <https://www.oecd-ilibrary.org/content/data/4919645f-en> (accessed 2021-09-19).
12. *Top Value Added Chemicals from Biomass: Volume I -- Results of Screening for Potential Candidates from Sugars and Synthesis Gas*, U.S. Department of Energy: Energy Efficiency and Renewable Energy, United States, 2004.
13. Zhou, C. H.; Beltramini, J. N.; Fan, Y. X.; Lu, G. Q., Chemoselective catalytic conversion of glycerol as a biorenewable source to valuable commodity chemicals. *Chem. Soc. Rev.* **2008**, 37 (3), 527-49.
14. Nakamura, C. E.; Whited, G. M., Metabolic engineering for the microbial production of 1,3-propanediol. *Curr. Opin. Biotechnol.* **2003**, 14 (5), 454-459.
15. Saxena, R. K.; Anand, P.; Saran, S.; Isar, J., Microbial production of 1,3-propanediol: Recent developments and emerging opportunities. *Biotechnol. Adv.* **2009**, 27 (6), 895-913.
16. Celinska, E., Debottlenecking the 1,3-propanediol pathway by metabolic engineering. *Biotechnol. Adv.* **2010**, 28 (4), 519-30.
17. Maervoet, V. E. T.; De Mey, M.; Beauprez, J.; De Maeseneire, S.; Soetaert, W. K., Enhancing the Microbial Conversion of Glycerol to 1,3-Propanediol Using Metabolic Engineering.

*Org. Process Res. Dev.* **2011**, *15* (1), 189-202.

18. Frazao, C. J. R.; Trichez, D.; Serrano-Bataille, H.; Dagkesamanskaia, A.; Topham, C. M.; Walther, T.; Francois, J. M., Construction of a synthetic pathway for the production of 1,3-propanediol from glucose. *Sci. Rep.* **2019**, *9* (1), 11576.
19. Ju, J. H.; Wang, D.; Heo, S. Y.; Kim, M. S.; Seo, J. W.; Kim, Y. M.; Kim, D. H.; Kang, S. A.; Kim, C. H.; Oh, B. R., Enhancement of 1,3-propanediol production from industrial by-product by *Lactobacillus reuteri* CH53. *Microb. Cell Fact.* **2020**, *19* (1), 6.
20. Schlaf, M., Selective deoxygenation of sugar polyols to alpha,omega-diols and other oxygen content reduced materials--a new challenge to homogeneous ionic hydrogenation and hydrogenolysis catalysis. *Dalton Trans.* **2006**, (39), 4645-53.
21. Bhowmik, S.; Darbha, S., Advances in solid catalysts for selective hydrogenolysis of glycerol to 1,3-propanediol. *Catal. Rev.* **2020**, 1-65.
22. Arundhathi, R.; Mizugaki, T.; Mitsudome, T.; Jitsukawa, K.; Kaneda, K., Highly Selective Hydrogenolysis of Glycerol to 1,3-Propanediol over a Boehmite-Supported Platinum/Tungsten Catalyst. *ChemSusChem* **2013**, *6* (8), 1345-1347.
23. Che, T. M. Production of propanediols. US4642394A, 1987.
24. Drent, E.; Jager, W. w. Hydrogenolysis of glycerol. US6080898A, 2000.
25. Braca, G.; Raspolli Galletti, A. M.; Sbrana, G., Anionic ruthenium iodocarbonyl complexes as selective dehydroxylation catalysts in aqueous solution. *J. Organomet. Chem.* **1991**, *417* (1-2), 41-49.
26. Dykeman, R. R.; Luska, K. L.; Thibault, M. E.; Jones, M. D.; Schlaf, M.; Khanfar, M.; Taylor, N. J.; Britten, J. F.; Harrington, L., Catalytic deoxygenation of terminal-diols under acidic aqueous conditions by the ruthenium complexes  $[(\eta^6\text{-arene})\text{Ru}(\text{X})(\text{N}\cap\text{N})](\text{OTf})_n$ ,  $\text{X}=\text{H}_2\text{O}$ ,  $\text{H}$ ,  $\eta^6\text{-arene}=\text{p-Me-iPr-C}_6\text{H}_4$ ,  $\text{C}_6\text{Me}_6$ ,  $\text{N}\cap\text{N}=\text{bipy}$ ,  $\text{phen}$ ,  $6,6'$ -diamino-bipy,  $2,9$ -diamino-phen,  $n=1, 2$ ). *J. Mol. Catal. A: Chem.* **2007**, *277* (1-2), 233-251.
27. Taher, D.; Thibault, M. E.; Di Mondo, D.; Jennings, M.; Schlaf, M., Acid-, water- and high-temperature-stable ruthenium complexes for the total catalytic deoxygenation of glycerol to propane. *Chem. Eur. J.* **2009**, *15* (39), 10132-43.
28. Thibault, M. E.; DiMondo, D. V.; Jennings, M.; Abdelnur, P. V.; Eberlin, M. N.; Schlaf, M., Cyclopentadienyl and pentamethylcyclopentadienyl ruthenium complexes as catalysts for the total deoxygenation of 1,2-hexanediol and glycerol. *Green Chem.* **2011**, *13* (2), 357-366.
29. Ahmed Foskey, T. J.; Heinekey, D. M.; Goldberg, K. I., Partial Deoxygenation of 1,2-Propanediol Catalyzed by Iridium Pincer Complexes. *ACS Catal.* **2012**, *2* (6), 1285-1289.
30. Choi, J.; MacArthur, A. H.; Brookhart, M.; Goldman, A. S., Dehydrogenation and related reactions catalyzed by iridium pincer complexes. *Chem. Rev.* **2011**, *111* (3), 1761-79.
31. Göttker-Schnetmann, I.; White, P.; Brookhart, M., Iridium Bis(phosphinite)p-XPCP Pincer Complexes: Highly Active Catalysts for the Transfer Dehydrogenation of Alkanes. *J. Am. Chem. Soc.* **2004**, *126* (6), 1804-1811.
32. Lao, D. B.; Owens, A. C. E.; Heinekey, D. M.; Goldberg, K. I., Partial Deoxygenation of Glycerol Catalyzed by Iridium Pincer Complexes. *ACS Catal.* **2013**, *3* (10), 2391-2396.
33. Goldberg, J. M.; Wong, G. W.; Brastow, K. E.; Kaminsky, W.; Goldberg, K. I.;

Heinekey, D. M., The Importance of Steric Factors in Iridium Pincer Complexes. *Organometallics* **2015**, *34* (4), 753-762.

34. Goldberg, J. M.; Goldberg, K. I.; Heinekey, D. M.; Burgess, S. A.; Lao, D. B.; Linehan, J. C., Detection of an Iridium-Dihydrogen Complex: A Proposed Intermediate in Ionic Hydrogenation. *J. Am. Chem. Soc.* **2017**, *139* (36), 12638-12646.

35. Finn, M.; Ridenour, J. A.; Heltzel, J.; Cahill, C.; Voutchkova-Kostal, A., Next-Generation Water-Soluble Homogeneous Catalysts for Conversion of Glycerol to Lactic Acid. *Organometallics* **2018**, *37* (9), 1400-1409.

36. Walsh, J. J.; Neri, G.; Smith, C. L.; Cowan, A. J., Water-Soluble Manganese Complex for Selective Electrocatalytic CO<sub>2</sub> Reduction to CO. *Organometallics* **2018**, *38* (6), 1224-1229.

37. Kang, P.; Meyer, T. J.; Brookhart, M., Selective electrocatalytic reduction of carbon dioxide to formate by a water-soluble iridium pincer catalyst. *Chem. Sci.* **2013**, *4* (9), 3497-3502.

38. Kang, P.; Cheng, C.; Chen, Z.; Schauer, C. K.; Meyer, T. J.; Brookhart, M., Selective electrocatalytic reduction of CO<sub>2</sub> to formate by water-stable iridium dihydride pincer complexes. *J. Am. Chem. Soc.* **2012**, *134* (12), 5500-3.

39. Göttker-Schnetmann, I.; White, P. S.; Brookhart, M., Synthesis and Properties of Iridium Bis(phosphinite) Pincer Complexes (p-XPCP)IrH<sub>2</sub>, (p-XPCP)Ir(CO), (p-XPCP)Ir(H)(aryl), and {(p-XPCP)Ir}<sub>2</sub>{μ-N<sub>2</sub>} and Their Relevance in Alkane Transfer Dehydrogenation. *Organometallics* **2004**, *23* (8), 1766-1776.

40. Hansch, C.; Leo, A.; Taft, R. W., A Survey of Hammett Substituent Constants and Resonance and Field Parameters. *Chem. Rev.* **1991**, *91* (2), 165-195.

41. Gitnes, R. M.; Wang, M.; Bao, Y.; Scheuermann, M. L., In Situ Generation of Catalytically Relevant Nanoparticles from a Molecular Pincer Iridium Precatalyst during Polyol Deoxygenation. *ACS Catal.* **2021**, *11* (2), 495-501.

42. Punji, B.; Emge, T. J.; Goldman, A. S., A Highly Stable Adamantyl-Substituted Pincer-Ligated Iridium Catalyst for Alkane Dehydrogenation. *Organometallics* **2010**, *29* (12), 2702-2709.

43. Goldberg, J. M.; Cherry, S. D. T.; Guard, L. M.; Kaminsky, W.; Goldberg, K. I.; Heinekey, D. M., Hydrogen Addition to (pincer)Ir(CO) Complexes: The Importance of Steric and Electronic Factors. *Organometallics* **2016**, *35* (20), 3546-3556.

44. Fulmer, G. R.; Miller, A. J. M.; Sherden, N. H.; Gottlieb, H. E.; Nudelman, A.; Stoltz, B. M.; Bercaw, J. E.; Goldberg, K. I., NMR Chemical Shifts of Trace Impurities: Common Laboratory Solvents, Organics, and Gases in Deuterated Solvents Relevant to the Organometallic Chemist. *Organometallics* **2010**, *29* (9), 2176-2179.

45. Roberto, D.; Cariati, E.; Psaro, R.; Ugo, R., Formation of [Ir(CO)<sub>2</sub>Cl]<sub>x</sub> (x = 2, n) Species by Mild Carbonylation of [Ir(cyclooctene)<sub>2</sub>Cl]<sub>2</sub> Supported on Silica or in Solution: A New Convenient Material for the Synthesis of Iridium(I) Carbonyl Complexes. *Organometallics* **1994**, *13* (11), 4227-4231.

46. Najari, S.; Saeidi, S.; Concepcion, P.; Dionysiou, D. D.; Bhargava, S. K.; Lee, A. F.; Wilson, K., Oxidative dehydrogenation of ethane: catalytic and mechanistic aspects and future trends. *Chem. Soc. Rev.* **2021**, *50* (7), 4564-4605.

47. Zhang, Z.; Jimenez-Izal, E.; Hermans, I.; Alexandrova, A. N., Dynamic Phase Diagram of Catalytic Surface of Hexagonal Boron Nitride under Conditions of Oxidative

Dehydrogenation of Propane. *J. Phys. Chem. Lett.* **2019**, *10* (1), 20-25.

48. Venegas, J. M.; McDermott, W. P.; Hermans, I., Serendipity in Catalysis Research: Boron-Based Materials for Alkane Oxidative Dehydrogenation. *Acc. Chem. Res.* **2018**, *51* (10), 2556-2564.
49. Van Goethem, M. W. M.; Barendregt, S.; Grievink, J.; Moulijn, J. A.; Verheijen, P. J. T., Ideal Chemical Conversion Concept for the Industrial Production of Ethene from Hydrocarbons. *Ind. Eng. Chem. Res.* **2007**, *46* (12), 4045-4062.
50. Amghizar, I.; Vandewalle, L. A.; Van Geem, K. M.; Marin, G. B., New Trends in Olefin Production. *Engineering* **2017**, *3* (2), 171-178.
51. Grant, J. T.; Venegas, J. M.; McDermott, W. P.; Hermans, I., Aerobic Oxidations of Light Alkanes over Solid Metal Oxide Catalysts. *Chem. Rev.* **2018**, *118* (5), 2769-2815.
52. Sundaram, K. M.; Shreehan, M. M.; Olszewski, E. F., Ethylene. In *Kirk-Othmer Encyclopedia of Chemical Technology*, John Wiley & Sons, Inc.: 2010.
53. Grant, J. T.; Love, A. M.; Carrero, C. A.; Huang, F.; Panger, J.; Verel, R.; Hermans, I., Improved Supported Metal Oxides for the Oxidative Dehydrogenation of Propane. *Top. Catal.* **2016**, *59* (17-18), 1545-1553.
54. Nawaz, Z., Light alkane dehydrogenation to light olefin technologies: a comprehensive review. *Rev. Chem. Eng.* **2015**, *31* (5), 413-436.
55. Crabtree, R. H.; Mihelcic, J. M.; Quirk, J. M., Iridium complexes in alkane dehydrogenation. *J. Am. Chem. Soc.* **1979**, *101* (26), 7738-7740.
56. Baudry, D.; Ephritikhine, M.; Felkin, H.; Holmes-Smith, R., The selective catalytic conversion of cycloalkanes into cycloalkenes using a soluble rhenium polyhydride system. *J. Chem. Soc., Chem. Commun.* **1983**, (14), 788-789.
57. Burk, M. J.; Crabtree, R. H.; Parnell, C. P.; Uriarte, R. J., Selective stoichiometric and catalytic carbon-hydrogen bond cleavage reactions in hydrocarbons by iridium complexes. *Organometallics* **1984**, *3* (5), 816-817.
58. Gupta, M.; Hagen, C.; Flesher, R. J.; Kaska, W. C.; Jensen, C. M., A highly active alkane dehydrogenation catalyst: stabilization of dihydrido rhodium and iridium complexes by a P-C-P pincer ligand. *Chem. Commun.* **1996**, (17), 2083-2084.
59. Göttker-Schnetmann, I.; White, P.; Brookhart, M., Iridium Bis(phosphinite) p-XPCP Pincer Complexes: Highly Active Catalysts for the Transfer Dehydrogenation of Alkanes. *J. Am. Chem. Soc.* **2004**, *126* (6), 1804-1811.
60. Xu, W.-W.; Rosini, G. P.; Krogh-Jespersen, K.; Goldman, A. S.; Gupta, M.; Jensen, C. M.; Kaska, W. C., Thermochemical alkane dehydrogenation catalyzed in solution without the use of a hydrogen acceptor. *Chem. Commun.* **1997**, (23), 2273-2274.
61. Liu, F.; Goldman, A. S., Efficient thermochemical alkane dehydrogenation and isomerization catalyzed by an iridium pincer complex. *Chem. Commun.* **1999**, (7), 655-656.
62. Kumar, A.; Zhou, T.; Emge, T. J.; Mironov, O.; Saxton, R. J.; Krogh-Jespersen, K.; Goldman, A. S., Dehydrogenation of n-Alkanes by Solid-Phase Molecular Pincer-Iridium Catalysts. High Yields of  $\alpha$ -Olefin Product. *J. Am. Chem. Soc.* **2015**, *137* (31), 9894-9911.
63. Védrine, J. C., Metal Oxides in Heterogeneous Oxidation Catalysis: State of the Art and Challenges for a More Sustainable World. *ChemSusChem* **2019**, *12* (3), 577-588.

64. Phan, N. T. S.; Van Der Sluys, M.; Jones, C. W., On the Nature of the Active Species in Palladium Catalyzed Mizoroki–Heck and Suzuki–Miyaura Couplings – Homogeneous or Heterogeneous Catalysis, A Critical Review. *Adv. Synth. Catal.* **2006**, *348* (6), 609-679.
65. Richardson, J.; Jones, C., Strong evidence of solution-phase catalysis associated with palladium leaching from immobilized thiols during Heck and Suzuki coupling of aryl iodides, bromides, and chlorides. *J. Catal.* **2007**, *251* (1), 80-93.
66. Kingsbury, J. S.; Hoveyda, A. H., Regarding the Mechanism of Olefin Metathesis with Sol–Gel-Supported Ru-Based Complexes Bearing a Bidentate Carbene Ligand. Spectroscopic Evidence for Return of the Propagating Ru Carbene. *J. Am. Chem. Soc.* **2005**, *127* (12), 4510-4517.
67. Bieniek, M.; Michrowska, A.; Usanov, D. L.; Grela, K., In an Attempt to Provide a User's Guide to the Galaxy of Benzylidene, Alkoxybenzylidene, and Indenylidene Ruthenium Olefin Metathesis Catalysts. *Chem. Eur. J.* **2008**, *14* (3), 806-818.
68. Bates, J. M.; Lummiss, J. A. M.; Bailey, G. A.; Fogg, D. E., Operation of the Boomerang Mechanism in Olefin Metathesis Reactions Promoted by the Second-Generation Hoveyda Catalyst. *ACS Catal.* **2014**, *4* (7), 2387-2394.
69. Rimoldi, M.; Nakamura, A.; Vermeulen, N. A.; Henkelis, J. J.; Blackburn, A. K.; Hupp, J. T.; Stoddart, J. F.; Farha, O. K., A metal-organic framework immobilised iridium pincer complex. *Chem. Sci.* **2016**, *7* (8), 4980-4984.
70. Burgess, S. A.; Kassie, A.; Baranowski, S. A.; Fritzsching, K. J.; Schmidt-Rohr, K.; Brown, C. M.; Wade, C. R., Improved Catalytic Activity and Stability of a Palladium Pincer Complex by Incorporation into a Metal–Organic Framework. *J. Am. Chem. Soc.* **2016**, *138* (6), 1780-1783.
71. Syed, Z. H.; Kaphan, D. M.; Perras, F. A.; Pruski, M.; Ferrandon, M. S.; Wegener, E. C.; Celik, G.; Wen, J.; Liu, C.; Dogan, F.; Goldberg, K. I.; Delferro, M., Electrophilic Organoiridium(III) Pincer Complexes on Sulfated Zirconia for Hydrocarbon Activation and Functionalization. *J. Am. Chem. Soc.* **2019**, *141* (15), 6325-6337.
72. Hübner, S.; de Vries, J. G.; Farina, V., Why Does Industry Not Use Immobilized Transition Metal Complexes as Catalysts? *Adv. Synth. Catal.* **2016**, *358* (1), 3-25.
73. Wang, P.-W.; Fox, M. A., A Polymer-Bound Bidentate-Phosphine-Palladium Complex as a Catalyst in the Heck Arylation. *J. Org. Chem.* **1994**, *59* (18), 5358-5364.
74. Allen, D. P.; Van Wingerden, M. M.; Grubbs, R. H., Well-Defined Silica-Supported Olefin Metathesis Catalysts. *Org. Lett.* **2009**, *11* (6), 1261-1264.
75. Waki, M.; Maegawa, Y.; Hara, K.; Goto, Y.; Shirai, S.; Yamada, Y.; Mizoshita, N.; Tani, T.; Chun, W.-J.; Muratsugu, S.; Tada, M.; Fukuoka, A.; Inagaki, S., A Solid Chelating Ligand: Periodic Mesoporous Organosilica Containing 2,2'-Bipyridine within the Pore Walls. *J. Am. Chem. Soc.* **2014**, *136* (10), 4003-4011.
76. Zeidan, R. K.; Hwang, S.-J.; Davis, M. E., Multifunctional Heterogeneous Catalysts: SBA-15-Containing Primary Amines and Sulfonic Acids. *Angew. Chem. Int. Ed.* **2006**, *45* (38), 6332-6335.
77. Wang, Y.; Gu, Z.; Liu, W.; Yao, Y.; Wang, H.; Xia, X.-F.; Li, W., Conversion of glucose into 5-hydroxymethylfurfural catalyzed by chromium(III) Schiff base complexes and acidic ionic liquids immobilized on mesoporous silica. *RSC Adv.* **2015**, *5* (75), 60736-60744.

78. Yuan, W.; Huang, Y.; Wu, C.; Liu, X.; Xia, Y.; Wang, H., MCM-41 Immobilized Acidic Functional Ionic Liquid and Chromium(III) Complexes Catalyzed Conversion of Hexose into 5-Hydroxymethylfurfural. *Chin. J. Chem.* **2017**, *35* (11), 1739-1748.
79. Noda, H.; Motokura, K.; Miyaji, A.; Baba, T., Heterogeneous Synergistic Catalysis by a Palladium Complex and an Amine on a Silica Surface for Acceleration of the Tsuji-Trost Reaction. *Angew. Chem. Int. Ed.* **2012**, *51* (32), 8017-8020.
80. Motokura, K.; Saitoh, K.; Noda, H.; Uemura, Y.; Chun, W.-J.; Miyaji, A.; Yamaguchi, S.; Baba, T., Co-Immobilization of a Palladium-Bisphosphine Complex and Strong Organic Base on a Silica Surface for Heterogeneous Synergistic Catalysis. *ChemCatChem* **2016**, *8* (2), 331-335.
81. Motokura, K.; Kawashima, S.; Nambo, M.; Manaka, Y.; Chun, W. J., Accumulation of Active Species in Silica Mesopore: Effect of the Pore Size and Free Base Additives on Pd-catalyzed Allylation using Allylic Alcohol. *ChemCatChem* **2020**, *12* (10), 2783-2791.
82. Chen, Y.; Fan, B.; Lu, N.; Li, R., Aluminum metal-organic framework as a new host for preparation of encapsulated metal complex catalysts. *Catal. Commun.* **2015**, *64*, 91-95.
83. McDonald, A. R.; Dijkstra, H. P., Tethered Pincer Complexes as Recyclable Homogeneous Catalysts. In *The Privileged Pincer-Metal Platform: Coordination Chemistry & Applications*, 2015; pp 335-369.
84. Huang, Z.; Brookhart, M.; Goldman, A. S.; Kundu, S.; Ray, A.; Scott, S. L.; Vicente, B. C., Highly Active and Recyclable Heterogeneous Iridium Pincer Catalysts for Transfer Dehydrogenation of Alkanes. *Adv. Synth. Catal.* **2009**, *351* (1-2), 188-206.
85. Vicente, B. C.; Huang, Z.; Brookhart, M.; Goldman, A. S.; Scott, S. L., Reactions of phosphinites with oxide surfaces: a new method for anchoring organic and organometallic complexes. *Dalton Trans.* **2011**, *40* (16), 4268-74.
86. Rimoldi, M.; Mezzetti, A., Silica-grafted 16-electron hydride pincer complexes of iridium(III) and their soluble analogues: synthesis and reactivity with CO. *Inorg. Chem.* **2014**, *53* (22), 11974-84.
87. Sheludko, B.; Cunningham, M. T.; Goldman, A. S.; Celik, F. E., Continuous-Flow Alkane Dehydrogenation by Supported Pincer-Ligated Iridium Catalysts at Elevated Temperatures. *ACS Catal.* **2018**, *8* (9), 7828-7841.
88. Mäki-Arvela, P.; Hájek, J.; Salmi, T.; Murzin, D. Y., Chemoselective hydrogenation of carbonyl compounds over heterogeneous catalysts. *Appl. Catal. A* **2005**, *292*, 1-49.
89. Tamura, M.; Nakagawa, Y.; Tomishige, K., Recent Developments of Heterogeneous Catalysts for Selective Hydrogenation of Unsaturated Carbonyl Compounds to Unsaturated Alcohols. *J. Jpn. Pet. Inst.* **2019**, *62* (3), 106-119.
90. Delocalized Chemical Bonding. In *March's Advanced Organic Chemistry*, 2006; pp 32-105.
91. Docherty, S. R.; Rochlitz, L.; Payard, P.-A.; Copéret, C., Heterogeneous alkane dehydrogenation catalysts investigated via a surface organometallic chemistry approach. *Chem. Soc. Rev.* **2021**, *50* (9), 5806-5822.
92. Lee, D. W.; Kaska, W. C.; Jensen, C. M., Mechanistic Features of Iridium Pincer Complex Catalyzed Hydrocarbon Dehydrogenation Reactions: Inhibition upon Formation of a  $\mu$ -Dinitrogen Complex. *Organometallics* **1998**, *17* (1), 1-3.

93. Ghosh, R.; Kanzelberger, M.; Emge, T. J.; Hall, G. S.; Goldman, A. S., Dinitrogen Complexes of Pincer-Ligated Iridium. *Organometallics* **2006**, *25* (23), 5668-5671.
94. Morales-Morales, D.; Lee, D. W.; Wang, Z.; Jensen, C. M., Oxidative Addition of Water by an Iridium PCP Pincer Complex: Catalytic Dehydrogenation of Alkanes by IrH(OH){C<sub>6</sub>H<sub>3</sub>-2,6-(CH<sub>2</sub>PBut<sub>2</sub>)<sub>2</sub>}. *Organometallics* **2001**, *20* (6), 1144-1147.
95. Bridget Williams, D.; Kaminsky, W.; Mayer, J. M.; Goldberg, K. I., Reactions of iridium hydride pincer complexes with dioxygen: new dioxygen complexes and reversible O<sub>2</sub> binding. *Chem. Commun.* **2008**, (35), 4195.
96. Ito, J.-I.; Kaneda, T.; Nishiyama, H., Intermolecular C–H Bond Activation of Alkanes and Arenes by NCN Pincer Iridium(III) Acetate Complexes Containing Bis(oxazolinyl)phenyl Ligands. *Organometallics* **2012**, *31* (12), 4442-4449.
97. Allen, K. E.; Heinekey, D. M.; Goldman, A. S.; Goldberg, K. I., Alkane Dehydrogenation by C–H Activation at Iridium(III). *Organometallics* **2013**, *32* (6), 1579-1582.
98. Allen, K. E.; Heinekey, D. M.; Goldman, A. S.; Goldberg, K. I., Regeneration of an Iridium(III) Complex Active for Alkane Dehydrogenation Using Molecular Oxygen. *Organometallics* **2014**, *33* (6), 1337-1340.
99. Allen, K. E. Synthesis of Electrophilic Rhodium and Iridium Complexes and Investigation of Reactivity for Carbon-Hydrogen Bond Activation and Functionalization. Ph.D., University of Washington, Ann Arbor, 2013.
100. Gao, Y.; Guan, C.; Zhou, M.; Kumar, A.; Emge, T. J.; Wright, A. M.; Goldberg, K. I.; Krogh-Jespersen, K.; Goldman, A. S.,  $\beta$ -Hydride Elimination and C–H Activation by an Iridium Acetate Complex, Catalyzed by Lewis Acids. Alkane Dehydrogenation Cocatalyzed by Lewis Acids and [2,6-Bis(4,4-dimethyloxazoliny)-3,5-dimethylphenyl]iridium. *J. Am. Chem. Soc.* **2017**, *139* (18), 6338-6350.
101. Chianese, A. R.; Mo, A.; Lampland, N. L.; Swartz, R. L.; Bremer, P. T., Iridium Complexes of CCC-Pincer N-Heterocyclic Carbene Ligands: Synthesis and Catalytic C–H Functionalization. *Organometallics* **2010**, *29* (13), 3019-3026.
102. Chianese, A. R.; Shaner, S. E.; Tandler, J. A.; Pudalov, D. M.; Shopov, D. Y.; Kim, D.; Rogers, S. L.; Mo, A., Iridium Complexes of Bulky CCC-Pincer N-Heterocyclic Carbene Ligands: Steric Control of Coordination Number and Catalytic Alkene Isomerization. *Organometallics* **2012**, *31* (21), 7359-7367.
103. Chianese, A. R.; Drance, M. J.; Jensen, K. H.; Mccollom, S. P.; Yusufova, N.; Shaner, S. E.; Shopov, D. Y.; Tandler, J. A., Acceptorless Alkane Dehydrogenation Catalyzed by Iridium CCC-Pincer Complexes. *Organometallics* **2014**, *33* (2), 457-464.
104. Rubashkin, S. B.; Chu, W.-Y.; Goldberg, K. I., Lowering the Barrier to C–H Activation at Ir(III) through Pincer Ligand Design. *Organometallics* **2021**, *40* (9), 1296-1302.
105. Rubashkin, S. Aerobic Oxidation of Hydrocarbons with Iridium(III) Pincer. Ph.D., University of Pennsylvania, 2021.
106. Merckle, C.; Blümel, J., Bifunctional Phosphines Immobilized on Inorganic Oxides. *Chem. Mater.* **2001**, *13* (10), 3617-3623.
107. Reinhard, S.; Šoba, P.; Rominger, F.; Blümel, J., New Silica-Immobilized Nickel Catalysts for Cyclotrimerizations of Acetylenes. *Adv. Synth. Catal.* **2003**, *345* (5), 589-602.

108. Djuric, S.; Sarkar, T.; Magnus, P., Silicon in synthesis: an exceptionally short synthesis of dl-11.alpha.-hydroxyestrone methyl ether. *J. Am. Chem. Soc.* **1980**, *102* (22), 6885-6886.
109. Ito, Y.; Amino, Y.; Nakatsuka, M.; Saegusa, T., A new approach to asymmetric synthesis of polycycles on the basis of o-quinodimethane generation. *J. Am. Chem. Soc.* **1983**, *105* (6), 1586-1590.
110. Imae, I.; Tokita, D.; Ooyama, Y.; Komaguchi, K.; Ohshita, J.; Harima, Y., Oligothiophenes incorporated in a polysilsesquioxane network: application to tunable transparent conductive films. *J. Mater. Chem.* **2012**, *22* (32), 16407.
111. Yukimoto, M.; Minoura, M., The Synthesis of a Novel Bulky Primary Alkyl Group and Its Application toward the Kinetic Stabilization of a Tetraalkyldisilene. *Bull. Chem. Soc. Jpn.* **2018**, *91* (4), 585-587.
112. Fu, P. P.; Unruh, L. E.; Miller, D. W.; Huang, L. W.; Yang, D. T. C., Synthesis of 3-aryl-3,4-dihydroisocoumarins. *J. Org. Chem.* **1985**, *50* (8), 1259-1261.
113. Harris, T.; Neuschwander, B.; Boekelheide, V., Synthesis of trans-15-n-butyl-16-methyldihydropyrene. Synthetic access to 1,2,3-trisubstituted benzene derivatives via direct alkylation of 1,3-bis(4',4'-dimethyl-2'-oxazoliny)benzene. *The Journal of Organic Chemistry* **1978**, *43* (4), 727-730.
114. Wirth, R.; Gao, P.; Nienhaus, G. U.; Sunbul, M.; Jäschke, A., SiRA: A Silicon Rhodamine-Binding Aptamer for Live-Cell Super-Resolution RNA Imaging. *J. Am. Chem. Soc.* **2019**, *141* (18), 7562-7571.
115. Ito, J. I.; Shiomi, T.; Nishiyama, H., Efficient preparation of new rhodium- and iridium-[bis(oxazoliny)-3,5-dimethylphenyl] complexes by C-H bond activation: Applications in asymmetric synthesis. *Adv. Synth. Catal.* **2006**, *348* (10-11), 1235-1240.
116. Zhao, D.; Krause, J. A.; Connick, W. B., Platinum(II) Monomer and Dimer Complexes with a Bis(oxazoliny)phenyl Pincer Ligand. *Inorg. Chem.* **2015**, *54* (17), 8339-8347.
117. Aliphatic Substitution: Nucleophilic and Organometallic. *March's Advanced Organic Chemistry* **2006**, 425-656.
118. Pola, J.; Jakoubková, M.; Chvalovský, V., The extent of some intramolecular effects in triethoxy- and trimethoxysilanes. *Collection of Czechoslovak Chemical Communications* **1978**, *43* (12), 3391-3395.
119. Wu, L.; Eberhart, M.; Shan, B.; Nayak, A.; Brennaman, M. K.; Miller, A. J. M.; Shao, J.; Meyer, T. J., Stable Molecular Surface Modification of Nanostructured, Mesoporous Metal Oxide Photoanodes by Silane and Click Chemistry. *ACS Appl. Mater. Interfaces* **2019**, *11* (4), 4560-4567.
120. Bagherzadeh, M.; Hosseini, M.; Mortazavi-Manesh, A., Manganese(III) porphyrin anchored onto magnetic nanoparticles via "Click" reaction: An efficient and reusable catalyst for the heterogeneous oxidation of alkenes and sulfides. *Inorg. Chem. Commun.* **2019**, 107.
121. Li, C.; Gao, C.; Lan, J.; You, J.; Gao, G., An AIE active Y-shaped diimidazolylbenzene: aggregation and disaggregation for Cd<sup>2+</sup> and Fe<sup>3+</sup> sensing in aqueous solution. *Org. Biomol. Chem.* **2014**, *12* (47), 9524-9527.
122. Brazeau, A. L.; Yuan, K.; Ko, S.-B.; Wyman, I.; Wang, S., Anion Sensing with a Blue Fluorescent Triarylboron-Functionalized Bisbenzimidazole and Its Bisbenzimidazolium Salt. *ACS Omega* **2017**, *2* (12), 8625-8632.

123. Adamovich, V.; Boudreault, P.-L. T.; Esteruelas, M. A.; Gómez-Bautista, D.; López, A. M.; Oñate, E.; Tsai, J.-Y., Preparation via a NHC Dimer Complex, Photophysical Properties, and Device Performance of Heteroleptic Bis(tridentate) Iridium(III) Emitters. *Organometallics* **2019**, *38* (14), 2738-2747.
124. Protection for the Hydroxyl Group, Including 1,2- and 1,3-Diols. *Greene's Protective Groups in Organic Synthesis* **2014**, 17-471.
125. Mehendale, N. C.; Bezemer, C.; Van Walree, C. A.; Klein Gebbink, R. J. M.; Van Koten, G., Novel silica immobilized NCN-pincer palladium(II) and platinum(II) complexes: Application as Lewis acid catalysts. *J. Mol. Catal. A: Chem.* **2006**, *257* (1-2), 167-175.
126. Reiner, B. R.; Mucha, N. T.; Rothstein, A.; Temme, J. S.; Duan, P.; Schmidt-Rohr, K.; Foxman, B. M.; Wade, C. R., Zirconium Metal–Organic Frameworks Assembled from Pd and Pt PNNNP Pincer Complexes: Synthesis, Postsynthetic Modification, and Lewis Acid Catalysis. *Inorg. Chem.* **2018**, *57* (5), 2663-2672.
127. Chen, J.; Hua, L.; Chen, C.; Guo, L.; Zhang, R.; Chen, A.; Xiu, Y.; Liu, X.; Hou, Z., Temperature-Dependent Immobilization of a Tungsten Peroxo Complex That Catalyzes the Hydroxymethoxylation of Olefins. *ChemPlusChem* **2015**, *80* (6), 1029-1037.
128. Pang, Y.; Ishiyama, T.; Kubota, K.; Ito, H., Iridium(I)-Catalyzed C-H Borylation in Air by Using Mechanochemistry. *Chem. Eur. J.* **2019**, *25* (18), 4654-4659.
129. Love, B. E.; Jones, E. G., The Use of Salicylaldehyde Phenylhydrazone as an Indicator for the Titration of Organometallic Reagents. *J. Org. Chem.* **1999**, *64* (10), 3755-3756.
130. Altomare, A.; Cascarano, G.; Giacovazzo, C.; Guagliardi, A., Completion and refinement of crystal structures with SIR92. *Journal of Applied Crystallography* **1993**, *26* (3), 343-350.
131. Altomare, A.; Burla, M. C.; Camalli, M.; Cascarano, G. L.; Giacovazzo, C.; Guagliardi, A.; Moliterni, A. G. G.; Polidori, G.; Spagna, R., SIR97: a new tool for crystal structure determination and refinement. *Journal of Applied Crystallography* **1999**, *32* (1), 115-119.
132. Sheldrick, G. M., Crystal structure refinement with SHELXL. *Acta Crystallographica Section C Structural Chemistry* **2015**, *71* (1), 3-8.
133. Sheldrick, G. M. *SHELXS-97, Program for crystal structure solution*, University of Göttingen, Göttingen, Germany, 1997.
134. Mackay, S.; Edwards, C.; Henderson, A.; Gilmore, C.; Stewart, N.; Shankland, K.; Donald, A. *MaXus: a computer program for the solution and refinement of crystal structures from diffraction data*, University of Glasgow, Scotland, 1997.
135. Waasmaier, D.; Kirfel, A., New analytical scattering-factor functions for free atoms and ions. *Acta Crystallographica Section A Foundations of Crystallography* **1995**, *51* (3), 416-431.